Structural and functional studies on Nod Like Receptors:

insights into NAIP/NLRC4 inflammasome formation

Elise Frederike Halff

Cover design: Tirza Kampert en Els Halff
Printed by: Proefschriftmaken.nl || Uitgeverij BOXPress
Published by: Uitgeverij BOXPress, 's-Hertogenbosch

ISBN: 978-90-8891-729-5

Structural and functional studies on Nod Like Receptors:

insights into NAIP/NLRC4 inflammasome formation

Structurele en functionele studies aan Nod gerelateerde receptoren:
inzichten in NAIP/NLRC4 inflammasoom formatie
(met een samenvatting in het Nederlands)

Proefschrift

ter verkrijging van de graad van doctor aan de Universiteit Utrecht op gezag van de rector magnificus, prof.dr. G.J. van der Zwaan, ingevolge het besluit van het college voor promoties in het openbaar te verdedigen op vrijdag 22 november 2013 des middags te 12.45 uur

door

Elise Frederike Halff

geboren op 24 september 1983 te Ede

Promotor: Prof.dr. P. Gros
Co-promotor: Dr. E.G. Huizinga

The research described in this thesis was financially supported by the Dutch Top Institute Pharma, and was performed within the framework of project D1-101

How marvellous are Your works, GOD!
In wisdom You have made them all;
the earth is full of Your creatures.

King David (Psalm 104:24)

Table of contents

Chapter 1:	General Introduction	9
Chapter 2:	Optimization of Recombinant Protein Production in Transiently Transfected HEK293-EBNA1 cells by Plasmid Titration: a case study for NLRs	33
Chapter 3:	Formation and Structure of a NAIP5-NLRC4 Inflammasome Induced by Direct Interactions with Conserved N- and C-terminal Regions of Flagellin	49
Chapter 4:	Structural Modeling of NAIP5/NLRC4 Helical Complexes Based on Cryo-Electron Tomography	71
Chapter 5:	General discussion	91
	Summary	105
	Samenvatting	109
	Dankwoord	113
	Curriculum Vitae	117
	List of publications	117
	Shortlist of frequently used abbreviations	118

Chapter **1**

1

General Introduction

Els F. Halff

Crystal and Structural Chemistry, Bijvoet Center for Biomolecular Research, Department of Chemistry, Faculty of Science, Utrecht University, The Netherlands

General Introduction

1.1 Nod like Receptors and their Role in the Immune System

The Innate and Adaptive Immune System

Staying alive entails a constant battle against invading microorganisms. Our immune system enables this combat by providing mechanisms both for recognition and destruction of harmful microorganisms. The vertebrate immune system is composed of two branches: innate and adaptive immunity (Figure 1). Innate immunity provides the first line of defense and ensures a rapid but non-specific and short-lived response, involving for instance the release of antimicrobial peptides, activation of the complement system, and the secretion of cytokines that induce inflammation and attract phagocytes. Moreover, innate immune cells stimulate the activation of the long-lasting adaptive immune response, among others by the presentation of pathogen-derived peptides (antigens). Adaptive immunity entails the *de novo* generation of antibodies by maturation of B-cells and activation of antigen-specific cytotoxic T-lymphocytes. This results in the specific recognition and clearance of invading microorganisms and the elimination of infected cells[1].

Signaling by the immune system requires tight regulation. Failure to activate the innate defense mechanism in response to pathogens (immunodeficiency), often due to a defect in one of the components, leads to uninhibited proliferation of the infectious agent. On the other hand, failure of control leads to constituent activation of the system (sustained inflammation or auto-inflammation) and damage to the host. Uncontrolled activation of the adaptive immune system gives rise to autoimmune disorders and allergies. The hallmark of autoimmune disorders is a failure to distinguish self from non-self, resulting in the raising of antigen-specific T cells and antibodies against auto-antigens, *i.e.* the body's own molecular constituents. Allergies on the other hand arise from an aberrant response to the presence of harmless non-self molecules and microbes such as food constituents and commensal bacteria in the gut, respectively[1-3].

Receptors of the Innate Immune System: TLRs and NLRs

The activation of the innate immune system relies on the recognition of microbial-specific motifs known as pathogen associated molecular patterns (PAMPs) by dedicated microbial sensors of the host called pattern recognition receptors (PRRs)[4]. PAMPs are conserved structures essential for the survival of the microorganism that are non-existent in the host. They constitute a wide

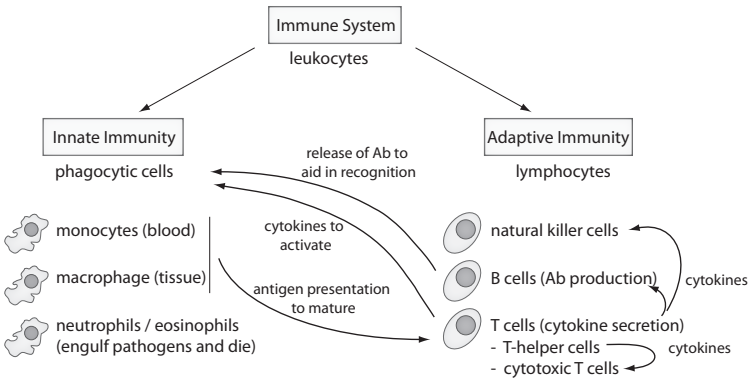

Figure 1: Cell types of the innate and adaptive immune system and their crosstalk. Overview of selected cell types of the innate and adaptive immune system. The arrows indicate examples of crosstalk between the different cell types. Abbreviations: Ab, antibody. The figure was derived from I.M. Roitt et al. (ref. 1)

Table 1: Overview of the human TLRs

Protein name	Cellular location	Pathogenic ligands	Synthetic ligands
TLR1	Cell surface	Peptidoglycan, lipoproteins	Pam_3Cys
TLR2	Cell surface	Peptidoglycan, lipoproteins, LTA	
TLR3	Endosomes	Viral dsRNA	Poly I:C
TLR4	Cell surface	LPS, viral proteins	Lipid A derivatives
TLR5	Cell surface	Flagellin	
TLR6	Cell surface	LTA, lipoproteins	
TLR7	Endosomes	Viral ssRNA	Imidazoquinoline
TLR8	Endosomes	Viral ssRNA	Imidazoquinoline
TLR9	Endosomes	Unmethylated CpG DNA	
TLR10	Cell surface	unknown	

Abbreviations: LPS, lipopolysaccharide; LTA, lipoteichoic acid.
The table was adapted from S. Akira *et al*., Nat.Rev.Imm. 2004 (ref. 68).

variety of molecules such as bacterial cell wall components (e.g. lipopolysaccharides and peptidoglycans), pathogen-specific proteins, and nucleic acid structures derived from bacteria and viruses such as unmethylated CpG motifs and dsRNA respectively[2, 5-7].

Among the first described PRRs were the membrane spanning Toll-like receptors (TLRs), discovered as recent as in 1994, which sense PAMPs in the extracellular environment as well as in endosomes[8-9] (Table 1, Figure 2). TLRs are primarily expressed in immune cells, such as macrophages, monocytes, B-lymphocytes, and dendritic cells. Only just over a decade ago, the cytosolic Nod-like receptors (NLRs) were discovered as a novel class of PRRs, complementing the function of TLRs by their intracellular localization[2, 10]. They were named after Nod1 (nucleotide binding oligomerization domain containing 1), the first family member to be discovered[11], but are by convention also called nucleotide binding domain and leucine rich repeat containing receptors[12]. NLRs are primarily expressed in immune cells and epithelial cells. Not only do they sense invasive PAMPs but also endogenous danger associated molecular patterns (DAMPs). DAMPs comprise signals that indicate the existence of internal errors, such as reactive oxygen species (ROS) or a change in intracellular ion levels, as well as molecules that are released by dying and injured cells such as ATP[13-15]. Currently, in humans 22 NLRs have been identified (Table 2).

As the NLRs were discovered only recently, the field is currently very dynamic. The volume of literature on putative agonists, interaction partners, and signaling pathways is rapidly expanding. Additionally, different studies may report contradicting outcomes. Thus, many aspects related to the role of NLRs are not fully understood at present and much work remains to be done.

NLR-Activating Ligands

NLRs detect a wide variety of ligands (Table 2). Detection of ligands by the cytosolic receptors requires their uptake into the cell. The peptidoglycan cell wall fragments that activate NOD1, NOD2, and NLRP1 supposedly enter the cell by endocytosis or phagocytosis, followed by internalization via acidification of the vacuole[16-17]. The NOD2 and NLRP1 ligand muramyl dipeptide (MDP) was, however, also reported to be actively and selectively transported into the cell[18-19]. Flagellin, the target protein recognized by NLRC4, is accidentally injected into the cell via the bacterial pathogenity island type III secretion system (T3SS), possibly due to its homology to proteins of this system[20].

NLRP3 responds to multiple stimuli, including products of bacteria and viruses, endogenous products signaling internal errors such as monosodium urate crystals

Table 2: Overview of the human NLRs

Protein name	Domain structure (not drawn to scale)	Signaling pathway	Tissue/cell types that express the NLR	Ligand
NOD1		NF-κB	Heart, skeletal muscle, spleen, ovary, placenta, lung, pancreas, testis, epithelium	iE-DAP, Tri-DAP
NOD2		NF-κB	Intestinal epithelium, Paneth cells, monocytes, DCs, granulocytes,	MDP
NLRC3		Inhibits NF-κB	Thymus, myeloid, uterus, kidney, T-cells, B-cells, NK-cells,	
NLRC4		Caspase-1	Colon, kidney, liver, placenta, lung, bone marrow, intestine, spleen, macrophage	Flagellin, T3SS, T4SS
NLRC5		Transcription regulation of MHCI	Lymphocytes	
NLRP1		Caspase-1	Heart, thymus, spleen, kidney, liver, lung, stomach, gut, neurons, testis, monocytes, PBLs, DCs, B-cells, T-cells,	MDP, anthrax lethal toxin
NLRP2		Caspase-1	Thymus, placenta, lung	
NLRP3		Caspase-1	PBLs, monocytes, T-cells, DCs, oropharynx, esophagus, ectocervix	ATP, amyloid, RNA, MSU, toxins, lysins, asbestos, silica
NLRP4		Inhibits NF-κB by binding IKKα	Spleen, kidney, lung, liver, placenta, thymus, pancreas	
NLRP5			Oocytes	
NLRP6		NF-κB, Caspase-1	Epithelium, granulocytes, monocytes, T-cells, B-cells, eosinophils	
NLRP7		Inflammasome regulator	Thymus, spleen, bone marrow, testis, nervous system, PBLs	
NLRP8				
NLRP9				
NLRP10		Inhibits inflammasome, enhances NF-κB	Brain, heart, skeletal muscle, kidney, testis, colon epithelium, skin, macrophages, monocytes, DCs, T-cells, B-cells	
NLRP11				
NLRP12		Caspase-1, inhibits NF-κB	Macrophages, DCs, monocytes, granulocytes, PBLs, eosinophils	
NLRP13				
NLRP14			Testis	
NAIP			Brain, lung, spleen, intestine, liver, macrophage	Flagellin
CIITA		Transcription regulation of MHCII	Lymphocytes, monocytes, DCs, APCs	
NLRX1			Mitochondria	Viral RNA

Abbreviations: AD, acidic domain; APC, antigen presenting cell; BIR, baculovirus inhibitor of apoptosis repeat; CARD, caspase activation and recruitment domain; DAP, diaminopimelic acid; DC, dendritic cell; FIIND, function to find; LRR, leucine-rich repeat; NK-cells, natural killer cells; NACHT, NAIP, CIITA, HET-E, and TP-1; MDP, muramyl dipeptide; MHCI/II, major histocompatibility complex type I/II; MSU, monosodium urate; PBL, peripheral blood lymphocytes; PYD, Pyrin domain; T3(4)SS, Type III (IV) secretion system. Information for this table was derived from ref. 10, 83, 160-163.

(MSU), ATP, and amyloids, and xenogenous compounds such as silica and asbestos (reviewed in ref. 14-15, 21-22). In view of the structural diversity of these activators, it is unlikely that all activators bind NLRP3 directly. This lead to the hypothesis that NLRP3 must respond to a common endogenous cellular mechanism that is induced by the presence of these signals [13,23]. Several models were proposed. The channel model hypothesizes that NLRP3 is activated by cellular ion dysregulation. For instance, extracellular ATP released by dying cells activates the receptor $P2X_7$, which induces the efflux of intracellular potassium ions. Likewise, bacterial pore forming toxins lead to alterations in the intracellular osmolarity[24-26]. The lysosomal rupture model proposes that pathogenic material taken up by phagocytosis causes destabilization of the lysosomes, leading to the escape of lysosomal enzymes such as cathepsin B into the cytosol, which then activate NLRP3[27]. Finally, the ROS model proposes that release of reactive oxygen species from the mitochondria, which is a cellular stress alarm, triggers formation of NLRP3 inflammasomes. This potentially involves interaction with thioredoxin-interacting protein (TXNIP), a protein released upon increase of intracellular ROS[21, 28].

For most of the NLRs, direct interaction with their activating ligands has not yet been shown. Interestingly, for plant resistance proteins (R-proteins), the structural and functional plant homologues of NLRs[29-30], some of the ligands were found to bind their target R-protein directly[31-33], whereas other R-proteins recognize modifications in host factors which in turn are targets of the pathogenic effector[34-35]. This lead to the formulation of the 'guardian model' where the R-protein monitors, or guards, the host factor, or 'guardee', that is targeted by the pathogen. Association with the guardee both keeps the R-protein in its inactive state but also primes the R-protein for action: binding of the pathogenic effector to the guardee induces a conformational change that immediately sets the R-protein to action[36-37]. Except for the potential binding of NLRP3 to TXNIP, a similar mechanism for mammalian NLRs has not yet been identified, but also cannot be excluded.

NLR Signaling Pathways

Ligand recognition by NLRs is thought to induce their multimerization, which subsequently leads to the activation of downstream effectors. The best characterized signaling pathways downstream of NLR activation are the induction of the NF-κB pathway and activation of caspase-1 (Figure 2). Which of these pathways is activated depends on the NLR family member (Table 2). The transcription factor NF-κB controls inflammatory and innate immune responses by upregulating the production of a wide range pro-inflammatory cytokines including the interleukins pro-IL-1β and pro-IL-18[38]. These interleukins require processing by caspase-1 to be secreted into the extracellular environment, where they can exert their function. Caspase-1 in turn also needs to be activated by proteolytic cleavage. Secreted IL-1β and IL-18 exert a wide range of inflammatory effects including the stimulation of fever and a drop in blood pressure, the maturation of lymphocytes to develop an adaptive immune response, directing phagocytes to the site of infection, and activating natural killer cell activity (Figure 1)[3, 39-42].

NLR-Mediated Activation of NF-κB

The primary role of the NLRs NOD1 and NOD2 is to activate NF-κB[11,43]. In the absence of a trigger, the transcription factor NF-κB is retained in the cytosol by binding to its inhibitory factor IκB. Activation and translocation of NF-κB to the nucleus requires IκB to be

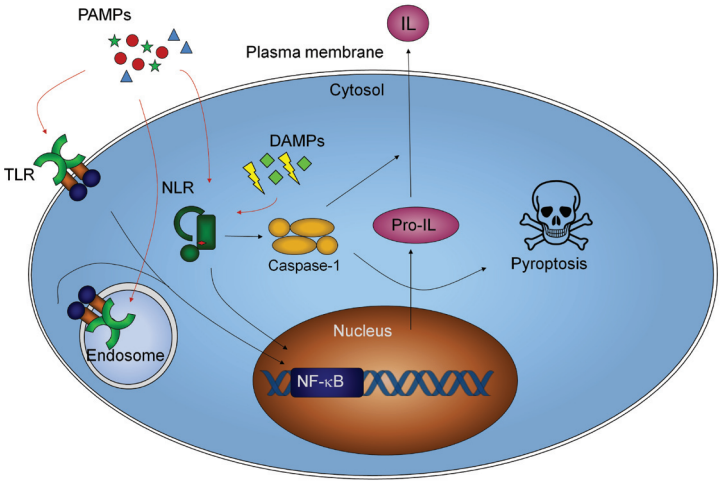

Figure 2: Signaling pathways induced by TLR and NLR activation, and their crosstalk. Schematic representation of the cell showing the signaling pathways induced by NLR and TLR activation.

phosphorylated, polyubiquitylated and subsequently degraded by the proteasome. Phosphorylation of IκB is exhibited by the IκB kinase (IKK) complex. This complex consists of the catalytic subunits IKKα and IKKβ and the regulatory subunit IKKγ or NEMO (for NF-κB essential modulator). NEMO recruits upstream activators that phosporylate IKKβ. The various cellular pathways that induce NF-κB activation all converge at the phosphorylation of the IKK complex[44].

Ligand detection by NOD1 and NOD2 mediates the recruitment of receptor-interacting protein 2 (RIP2, previously called RICK)[11,43,45]. RIP2 then mediates the polyubiquitylation of NEMO, which in turn causes recruitment of the TAK1 complex that phosphorylates IKKβ[46-47].

Caspase-1 Activation by Inflammasomes

For the majority of the NLRs, namely NLRC4 and the NLRPs, ligand recognition is thought to induce their homotypic multimerization into a large complex called inflammasome that induces the proteolytic processing and activation of caspase-1[41, 48-50]. Caspases are cysteine proteases that initiate or execute cellular programs related to inflammation or cell death. They are synthesized as inactive zymogens (procaspases) that contain an N-terminal caspase activation and recruitment domain (CARD) as prodomain, a large subunit (p20) containing the catalytic site and a smaller subunit (p10) that harbors a substrate binding site[51]. Maturation into the active form requires proteolytic removal of the prodomain, dimerization of the p10/20 fragment, and autocleavage of the p10-p20 intersubunit linker. Thus, the final active complex is a tetramer. Effector caspases, which cleave cellular protein substrates, are present as inactive dimers and are activated upon proteolytic cleavage by initiator caspases. Initiator caspases such as caspase-1 on the other hand exist as monomers in the cell. Their activation is thought to be mediated by enforced dimerization and auto-cleavage on procaspase-recruiting platforms such as the inflammasome, a hypothesis called the induced proximity model[52].

Activated caspase-1 is not only required for the processing and secretion of IL-1β and IL-18 as described, but also induces a specific inflammatory cell death called pyroptosis. This type of cell death is distinct from apoptosis and is characterized by plasma membrane rupture via pore formation, followed by osmotic lysis, and finally a release of intracellular contents[42,53]. Pyroptosis is thought to contribute to host defense by preventing replication of the invading microorganism in infected immune cells, by inducing the presentation of intracellular microbial antigens to the adaptive immune system, and by the

release of danger signals (DAMPs) from the dying cells[3]. Interestingly, for the NLRC4-containing inflammasome it was observed that processing of pro-IL-18 and pro-IL-1β required both the helper protein ASC and proteolytic cleavage of procaspase-1. The induction of pyroptosis on the other hand was independent of procaspase-1 processing and ASC, but not independent of procaspase-1 dimerization. This suggests that these two distinct pathways employ different mechanisms[54-55].

Non-Canonical Signaling Pathways

Two of the NLRs, namely NLRC5 and CIITA, appear to have an atypical role, as they localize to the nucleus upon activation, where they regulate transcription of the major histocompatibility complex (MHC) class I and II related genes respectively[56]. The function of several other NLRs has not been elucidated yet (see Table 2). Even for the NLRs that participate in the canonical pathways of NF-κB activation and inflammasome formation new signaling pathways are rapidly being discovered, although in many cases these functions have not yet been well established. For instance, detection of MDP by NOD2 also induces the mitogen-activated protein kinase (MAPK) pathway and the generation of bactericidal ROS[46,57]. Both NOD1 and NOD2 have recently been implicated in autophagy, a cellular process responsible for the degradation of damaged organelles. This mechanism is also utilized as a defense against intracellular bacteria[58-59]. Whereas NOD1 was reported to be able to activate caspase-1[11, 60], NLRP3 can also activate NF-κB[61]. Interestingly, the NLRPs 2, 4, 6, 7, 10, and 12 appear to play a role not only in caspase-1 activation but also in inhibiting the NF-κB pathway[56, 62]. Several NLRs, including NLRP 2, 5, 7, and 14 were found to be expressed only or mainly in gametes and during early embryonal development, suggesting that their role is limited to reproduction[56].

(Putative) Regulators of NLR Activation and Signaling

Both R-proteins and several mammalian NLRs were found to be specifically and functionally associated with the molecular chaperone HSP90 and its *bona fide* helper protein Suppressor of G2 allele of SKP1 homolog (SGT1)[63]. SGT1 was previously suggested to assist in protein maturation by shuttling proteins from HSP70 to HSP90. As HSP70 was also found to associate with NOD1[64], a possible function of the interaction between NLRs and SGT1 plus chaperones may be to contribute to NLR maturation.

Alternatively, the association with these chaperones was suggested to retain the NLR in its inactive conformation or to stabilize a signaling competent state[63]. Silencing of SGT1 or inhibition of HSP90 led to abrogation of signaling by NOD1, NOD2, and NLRP3[65-66]. SGT1 and HSP90 no longer associated with NLRP3 once it was incorporated in the inflammasome, and HSP90 released NOD2 in the presence of MDP[65,67], suggesting a role upstream of ligand detection.

Apart from the general NLR-regulators HSP90 and SGT1, an increasing number of NLR-specific regulators is being discovered, although their roles are often not yet well established (see reviews 38, 46, and 57 for some examples). This multitude of putative binding partners, each with a dedicated function, appear to regulate a variety of processes such as enhancing or inhibiting interaction with downstream signaling partners, stabilizing NLRs in a signaling competent conformation, or preventing them from premature activation. The existence of these putative binding partners further increases the complexity of understanding the role of NLRs in the immune system.

TLR/NLR Crosstalk and Vaccine Development

Activation of TLRs initiates signaling

cascades that induce several inflammatory gene regulators, including the NF-κB pathway, albeit via different signaling routes than NLRs[6,68]. Thus, TLR activation also leads to among others the transcription of the pro-inflammatory cytokines pro-IL-1β and pro-IL-18. To establish a functional immune response mediated by secreted interleukins, TLRs require the simultaneous activation of the caspase-1 activating NLRs (Figure 2). This crosstalk possibly provides a safeguard against aberrant activation as only virulent pathogens that enter the cell, but not harmless microbes, will be able to activate TLRs and NLRs simultaneously[69-70].

As the secreted interleukins contribute to the development of long-lasting adaptive immunity, a particularly important application of TLR/NLR crosstalk is in the development of vaccine adjuvants. The immunostimulatory effect of some of the adjuvants that were developed before the discovery of PRRs, was later shown to be mediated by NLR and TLR activation. For instance, aluminium hydroxide (alum), an adjuvant that absorbs the antigen used for immunization, was shown to activate the NLRP3 inflammasome[27,71-74]. Complete Freund's Adjuvant contains fragments of the bacterial peptidoglycan cell wall that induce the activation of NOD1 and NOD2[4, 75-78] as well as lipoproteins and lipopolysaccharides that mediate an enhancing response via TLRs[6]. Additionally, synthetic TLR agonists mimicking their ligands also improve the immunostimulatory effect of adjuvants[79] (Table 1).

NLR-Associated Disorders

Mutations in NLRs have been associated with a broad range of chronic inflammatory disorders[5,78,80]. These disorders may arise from the inappropriate activation of an immune response in the absence of a stimulus, as well as from a failure to respond to pathogens, and thus the inability to prevent microbial infection. As both loss-of-function and gain-of-function mutations may lead to the same clinical features, defining the mechanisms behind NLR-associated diseases is not always straightforward.

The inflammatory diseases related to mutations in NLRP3 include Muckle-Wells syndrome (MWS), Familial Cold Autoinflammatory Syndrome (FCAS), and neonatal onset multisystem inflammatory disease (NOMID). These diseases are all characterized by recurrent episodes of inflammatory attacks in the absence of infection, including fever, skin rashes, and joint pain. These symptoms are probably caused by spontaneous inflammasome formation, resulting in increased caspase-1 activation and IL-1β secretion. Excessive activation of the NLRP3-inflammasomes also occurs in gout, where the deposition of MSU crystals in the joints leads to acute severe inflammation[81].

The hallmark of Crohn's Disease (CD), associated with various mutations in the *Nod2* gene, is a defective balance between response to commensal bacteria and bacteria that cause inflammation in the gut. Related symptoms include abdominal pain, diarrhea, growth retardation, and anemia[2]. Although the mechanism is yet unclear, the major hypothesis is that irresponsiveness of NOD2 to infection leads to microbial overgrowth, facilitated entry into the epithelial layer, and chronic inflammation. Other NOD2-related diseases are Blau syndrome (BS) and Early onset Sarcoidosis (EOS), which result from increased NF-κB activation in the absence of microbes[2]. Mutations in NOD1 have been associated with asthma and ectopic eczema and likewise exhibit increased spontaneous activation of NF-κB[82].

Mutations in the NLR CIITA, a regulator of expression of the MHC type II in antigen presenting cells (APCs), lead to bare lymphocyte syndrome and other immune deficiency diseases. Reduced expression

of MHC leads to frequent infections in the gastrointestinal and respiratory tract. Additionally, mutations in the promoter region of CIITA are linked to rheumatoid arthritis, multiple sclerosis, and myocardial infection[5,62]. Mutations in the promoter and coding region of NLRP1 associate with among others type I diabetes[3].

1.2 Structural Insights into NLRs and their Activation Mechanism

NLR Domains and their Structures

NLRs typically consist of three functional units. The C-terminal leucine rich repeat (LRR) domain is thought to be responsible for ligand sensing and stabilizing an auto-inhibited state. The N-terminal effector binding domain (EBD) ensures interaction with downstream signaling partners; the identity of the EBD differs between the individual NLRs. NOD1, NOD2, and NLRC4 contain one (NOD1, NLRC4) or two (NOD2) caspase activation and recruitment domains (CARD). NLRP1-14 contain an N-terminal pyrin domain (PYD); NAIP contains three baculoviral inhibitor of apoptosis repeat (BIR) domains. Additional to a CARD-like domain, CIITA contains an acidic domain (AD) involved in DNA binding[10, 83-84] (Table 2). The EBDs of the remaining NLRs have no detectable homology to known domains but in the case of NLRX1 and NLRC5 they do possess a sequence motif that targets the protein to the mitochondrion or nucleus respectively[85-87]. The central and highly conserved NACHT domain (for NAIP, CIITA, HET-E, and TP-1, the first proteins in which this domain was identified[88], also termed NOD for nucleotide-binding oligomerization domain) harbors a number of conserved sequence motifs putatively involved in nucleotide binding and/or hydrolysis. This domain moreover is expected to promote the self-association of NLRs upon activation[89].

The tripartite domain build-up and the presence of the NACHT module define NLRs as a subclass of the family of signal transduction ATPases with numerous domains (STAND) proteins. Proteins belonging to this family are multi-domain proteins that typically function as signaling hubs that integrate incoming signals and, in response, activate other proteins[90-91]. In STAND proteins, the C-terminal end of the NACHT domain is linked, often via an arm region, to a sensor domain that binds the inducer. STAND proteins also contain one or more EBDs involved in downstream signaling[91].

STAND proteins that are functionally related to the NLRs are the R-proteins responsible for the immune defense in plants[30], and the apoptosis-inducing proteins Apaf-1, Dark, and CED-4 in mammals, *Drosophila*, and *C. elegans* respectively[89]. Their domain build-up is comparable to that of NLRs, although they may employ different effector binding or sensor domains (Figure 3). As no structural data on a full length NLR exists, and the available structures of separate NLR domains are sparse, most structural insights derive from these homologous proteins.

Effector Binding Domains

Most of the NLRs harbor an N-terminal CARD or PYD as effector binding domain. CARDs and PYDs belong to the death

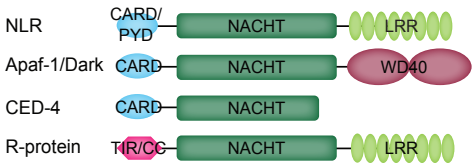

Figure 3: Domain organization of selected STAND proteins homologous to NLRs. Schematic representation of the domain organization of the STAND proteins that are both in structure and function homologous to NLRs. Abbreviations: CARD, caspase activation and recruitment domain; CC, coiled-coil; NACHT, NAIP, CIITA, HET-E, and TP-1; LRR, leucine-rich repeat domain; TIR, Toll/Interleukin-1 receptor homology domain; WD40, WD40 repeats

domain (DD) superfamily and are typically about 100 amino acids (10 kDa) in size. Despite low sequence similarity, the structural similarity of proteins within this class is high. Characteristic of this family is an amphipatic anti-parallel six-helical bundle that surrounds a hydrophobic patch in a structural fold termed the Greek key topology organization (Figure 4A)[92-94]. The structures of NLR EBDs currently available comprise the crystal and NMR structures of the CARD domain of NOD1[95-97] and the PYD domains of NLRP 1, 3, 4, 7, and 12[98-102]. Characteristic of CARDs compared to other DD-folds is an interruption in the first α-helix (Figure 4B)[103]. The defining feature of PYDs is a shorter third helix that is preceded by a flexible loop (Figure 4C)[93-94]. CARDs and PYDs are predominantly involved in homotypic interactions that are thought to occur primarily via electrostatic interaction[93, 96, 104].

BIR domains are slightly smaller, generally about 70 residues, zinc-binding domains. They typically display a fold in which a central three stranded anti-parallel β-sheet is surrounded by 2 or 3 α-helices on both the N- and C-terminal side (Figure 4D)[105-106]. BIR domains are often, but not exclusively, found in proteins that inhibit apoptosis, as they are able to recruit apoptosis effector caspases, thereby removing them from the apoptotic pathway[105, 107-108].

Leucine Rich Repeats

The LRR is a structural motif often found to be involved in protein-protein interaction or ligand sensing. They consist of repeats of 20-29 amino acids in length that contain the consensus sequence $LxxLxLxx^{N}/_{C}xL$ where x can be any amino acid and L can also be Val, Ile, or Phe. LRRs typically form a curved solenoid (horseshoe-like) structure, where the inner circumference (concave side) invariably consists of parallel β-sheets, connected by loops to the outer (convex) surface that, depending on the LRR subtype and the length of the repeat, generally forms an α-helix or a 3_{10}-helix (Figure 5A,B). At their N- and C-terminal end, LRRs contain a flanking region, or cap, that prevents exposure of the hydrophobic core[109].

In NLRs the repeats are generally 27-29 amino acids long and are predicted to contain mainly α-helices at their convex side, which classifies them as members of the 'RI-like' subclass (Figure 5A,B)[11, 43, 110]. The length of the LRR domain differs for each family member, ranging from 6 to over 20 predicted repeats. The only exception is NLRP10, which lacks the LRR domain. The exact number of repeats in each NLR is, however, hard to define as many deviations from the consensus sequence occur. It is yet unclear whether these are atypical repeats, or insertions that possibly contribute to ligand-specificity.

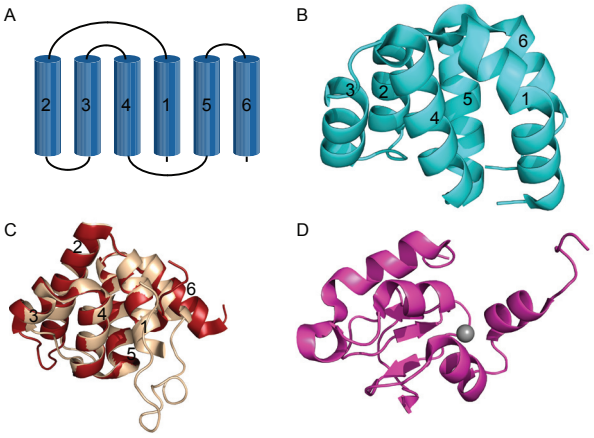

Figure 4: Structures of NLR effector binding domains. *A.* Schematic representation of the Greek key topology, the fold employed by the death domain superfamily. Cylinders represent an α-helix. *B,C.* Cartoon representation of (B) the Apaf-1 CARD domain crystal structure (PDB ID 1Z6T) and (C) the superposed PYD domain crystal structures of NLRP3 (salmon; PDB ID 3QF2) and NLRP4 (dark red; PDB ID 4EWI). Numbers indicate the order or the helices. *D.* Cartoon representation of the human NAIP BIR2 domain crystal structure (PDB ID 2VM5) binding a zinc ion. Panel B, C, and D were created using PyMOL.

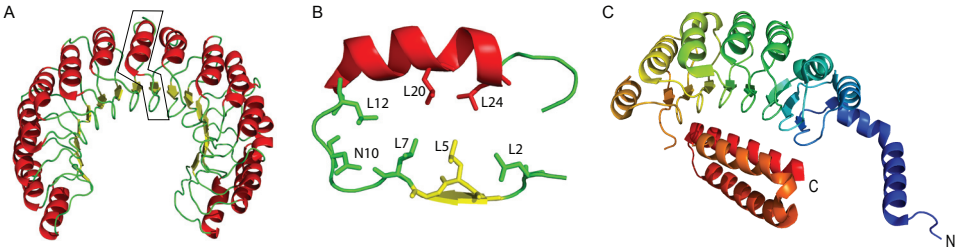

Figure 5: Structures of leucine rich repeat domains. *A.* Cartoon representation of the Ribonuclease Inhibitor crystal structure (PDB ID 3DFJ). The box indicates a single repeat. The α-helical convex side is shown in red, the concave side composed of β-sheets in yellow, and the connecting loops in green. *B.* An isolated repeat from the Ribonuclease Inhibitor crystal structure, showing the consensus sequence and locations of conserved residues typical of the RI-like subclass. Color coding of secondary structure elements corresponds to panel A. *C.* Cartoon representation of the NLRX1 LRR domain crystal structure (PDB ID 3UN9). The N and C termini are indicated. The figure was created using PyMOL.

The NLRs are thought to interact with their ligands via the LRR. Recently, the first crystal structure to be determined of an NLR-LRR was that of NLRX1. The structure revealed an unexpected C-terminal α-helical flanking region (Figure 5C) and gave implications for an RNA binding site[111]. For most of the NLRs, however, it is currently unknown whether direct ligand binding occurs at all due to a lack of both structural data as well as biochemical evidence for direct interaction between NLR-LRRs and their elicitors.

The NACHT Domain

In Apaf-1 and CED-4 it was shown for the first time that the NACHT domain mediates homo-oligomerization in a nucleotide-binding dependent way and that this oligomerization is critical for their functionality[112-114]. The crystal structures of these proteins reveal that, structurally, the NACHT domain is composed of four subdomains (Figure 6A)[115-116]. The first subdomain contains the nucleotide binding site and displays a three-layered α/β Rossmann fold consisting of a five-stranded β-sheet in the center sandwiched by four α-helices on each side, a fold that is characteristic of NTPases. This nucleotide binding domain (NBD) is followed by a short helical domain (HD1) containing four α-helices, and a winged-helix domain (WHD) that contains a core of α-helices and β-sheets surrounded by two non-ordered 'wings'. This latter domain is often found in DNA-binding proteins such as transcription factors. Finally, the NACHT domain of Apaf-1 also displays an extended helical domain (HD2) composed of eight α-helices; in CED-4 this region is slightly shorter and not well resolved in the structure, but predicted to be α-helical as well. In Apaf-1 the HD2 functions as an arm domain, or structural spacer, to accommodate the bulky WD40 sensor domain, and as a hinge region for conformational rearrangements. The NACHT domain of NLRs aligns well with the region in Apaf-1 that is comprised by NBD-HD1-WHD. The arm region preceding the LRRs, sometimes termed NACHT-associated domain (NAD), has no detectable sequence homology to any known structure, but secondary structure prediction suggests that, like the HD2, for most NLRs this region is also composed of eight α-helices in a superhelical arrangement[117].

The region comprised by the α/β Rossmann fold and short helical domain is both in sequence and structure closely related to the family of AAA+ ATPases (ATPases associated with various cellular activities)[118]. AAA+ proteins generally form a ring-shaped hexamer as active unit and possess the highly conserved Walker A and Walker B motifs that contribute to nucleotide binding and hydrolysis[88-89, 119]. In monomeric Apaf-1,

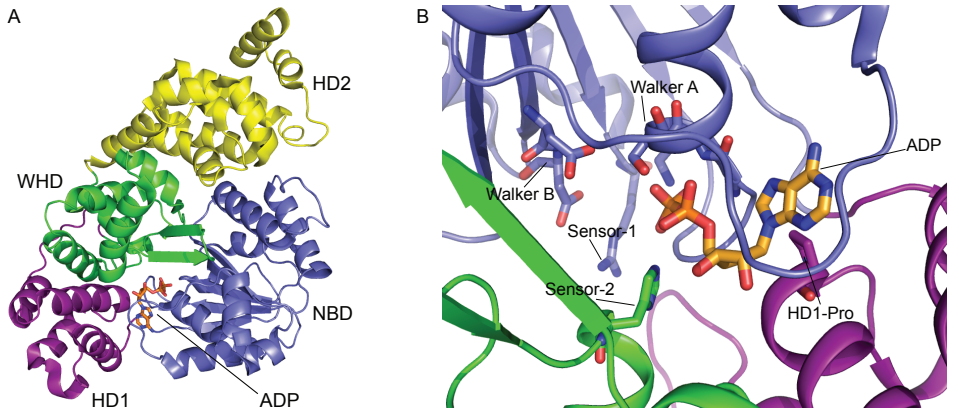

Figure 6: Structure of the Apaf-1 NACHT domain and conserved nucleotide binding site. *A.* Cartoon representation of the Apaf-1 NACHT domain crystal structure in WD40-deleted ADP-bound Apaf-1 (PDB ID 1Z6T) with each of the subdomains in a different color. The nucleotide binding site and position of the subdomains are indicated. *B.* Detailed view of the nucleotide binding site of Apaf-1, indicating the conserved residues that contribute to nucleotide binding and hydrolysis. Color coding for the subdomains corresponds to panel A. The figure was created using PyMOL.

ADP interacts not only with motifs in the α/β-fold and HD1, but is also coordinated by the WHD (Figure 6B)[115, 120]. As in AAA+ proteins, the Walker A motif of Apaf-1, also called P-loop, with consensus sequence GxxxxGK[T/S], directly interacts with a phosphate moiety of the nucleotide via its lysine. The consensus sequence of the Walker B motif is hhhhD[D/E], where h is a hydrophobic residue. This motif is essential for nucleotide hydrolysis through coordination of an Mg^{2+} ion as well as a water molecule. Additionally, both AAA+ proteins and STAND proteins contain a conserved arginine, termed sensor-1 that contacts the γ-phosphate of the nucleotide and thus discerns between ADP and ATP. Sensor-1 is also thought to be involved in coordinating hydrolysis and conformational changes between NACHT subunits. AAA+ proteins, but not STAND proteins, possess a 'sensor-2' residue, often an arginine or lysine, involved in nucleotide binding and hydrolysis[117,119]. In Apaf-1, the sensor-2 motif is replaced by a histidine in the WHD that coordinates the β-phosphate[115]. This histidine is conserved in most NLRs and therefore thought to be involved in nucleotide coordination in NLRs as well[117].

Although NLRs contain most of these highly conserved motifs, they also display unique features. NLRs possess an alternative Walker B motif hhhhD[G/A/S]hDE, a conserved sequence motif FxHxxQEhxA that contains the WHD histidine replacing sensor-2, a unique conserved proline in HD1 predicted to contact the adenine moiety of ATP, and a cysteine-rich region with sequence VCWxVCT, likewise in HD1, that appears to play a role in nucleotide recognition[117]. In the absence of a structure and sufficient biochemical data, it is unknown what the implications of these deviations are for the capacity of NLRs to bind and hydrolyze nucleotides.

A Hypothetical Model for NLR Activation

From Auto-inhibited to Activated Conformation

Like other STAND proteins, NLRs are expected to undergo a series of conformational changes upon activation to facilitate their multimerization and signal transduction. Biochemical and mutational studies on R-proteins, which have been studied for about a decade longer than NLRs, revealed that in dormant R-proteins the EBD and the LRR physically interact with

the NACHT domain, which is in an ADP-bound 'off' state or closed conformation. This interaction is abrogated in the presence of the elicitor[121]. Sensing of the elicitor was moreover required for the protein to bind ATP and interact with downstream effectors; mutants that could no longer hydrolyze ATP were found to be constitutively active[122-123]. These data suggest an activation model for R-proteins in which recognition of the elicitor releases binding of the LRR to the NACHT domain, allowing exchange of ADP for ATP. This in turn disrupts interaction with the EBD, thus exposing the EBD and allowing it to bind and activate downstream signaling partners[91, 124].

Upon activation the apoptosis-inducing proteins Apaf-1, Dark, and CED-4 form a ring-shaped oligomer called apoptosome[125]. The availability of the crystal structure of monomeric Apaf-1 as well as the EM structure of its activated, complex-incorporated conformation in the apoptosome allows for a more detailed structural view of the activation mechanism of STAND proteins, and can serve as a hypothetical model for NLR activation. In monomeric ADP-bound Apaf-1 the WD40 sensor domain interacts with the NBD to maintain the protein in an inactive state. Additionally, the CARD stacks against the NBD and WHD, occluding its binding site for the downstream effector caspase-9 and at the same time limiting the access to the nucleotide binding site (Figure 7A)[115,120]. Apaf-1 is activated by mitochondrial release of cytochrome *c* to bind dATP and undergo structural rearrangement and formation of a heptameric ring-like apoptosome[126-128]. Comparison of the structure of monomeric Apaf-1 to its conformation in the apoptosome shows that cytochrome *c* binding interferes with the interaction between the WD40 domain and the NBD (Figure 7A,B). Ligand binding enforces a large conformational change within the NACHT domain: a rotation of about 180° by the WHD causes the WHD-HD2-WD40 fragment to swing outwards, thereby uncovering the nucleotide binding site, while the interdomain interactions between the NBD and HD1 remain intact[128-130] (Figure 7B). The CARD that is tightly packed against the NACHT domain in monomeric Apaf-1, is flexibly linked in the Apaf-1 apoptosome[131].

Biochemical studies suggest that the activation mechanism of NLRs is comparable to that of these STAND proteins (Figure 7C). As removal of the LRR domain renders the NLR constitutively active, *i.e.* spontaneous activation in the absence of ligand occurs[43, 132-133], the LRR is likely to play a role in maintaining an auto-inhibited state of the protein. The auto-inhibited conformation is thought to be abrogated by binding of the NLR ligands to the LRR domain. Mutations in the LRR domains of NOD2 have been associated with unresponsiveness to the ligand[117, 134-135], suggesting a role for the LRR in ligand binding. These mutations could, however, also stabilize the auto-inhibited form of the NLR, thereby reducing its responsiveness to the agonist. In Apaf-1, the auto-inhibited conformation is furthermore stabilized by interaction between the WHD and CARD. The residues in the WHD and CARD that stabilize this interaction in the dormant conformation of Apaf-1 are conserved in NLRs, suggesting a similar mechanism[117].

Contradicting reports exist on the role of nucleotide binding and hydrolysis in NLR activation. For NLRC4 and the NLRPs 3, 10, and 12, an intact nucleotide binding site was found to be required for oligomerization and downstream signaling, but so far only NLRP3 and NLRP12 were shown to be able to hydrolyze ATP[136-139]. In contrast to the observation in R-proteins that mutations that lock the protein in an ATP-bound state render the protein constitutively active, homologous mutations in NOD1 and NOD2 exhibit a loss-of-function phenotype[140].

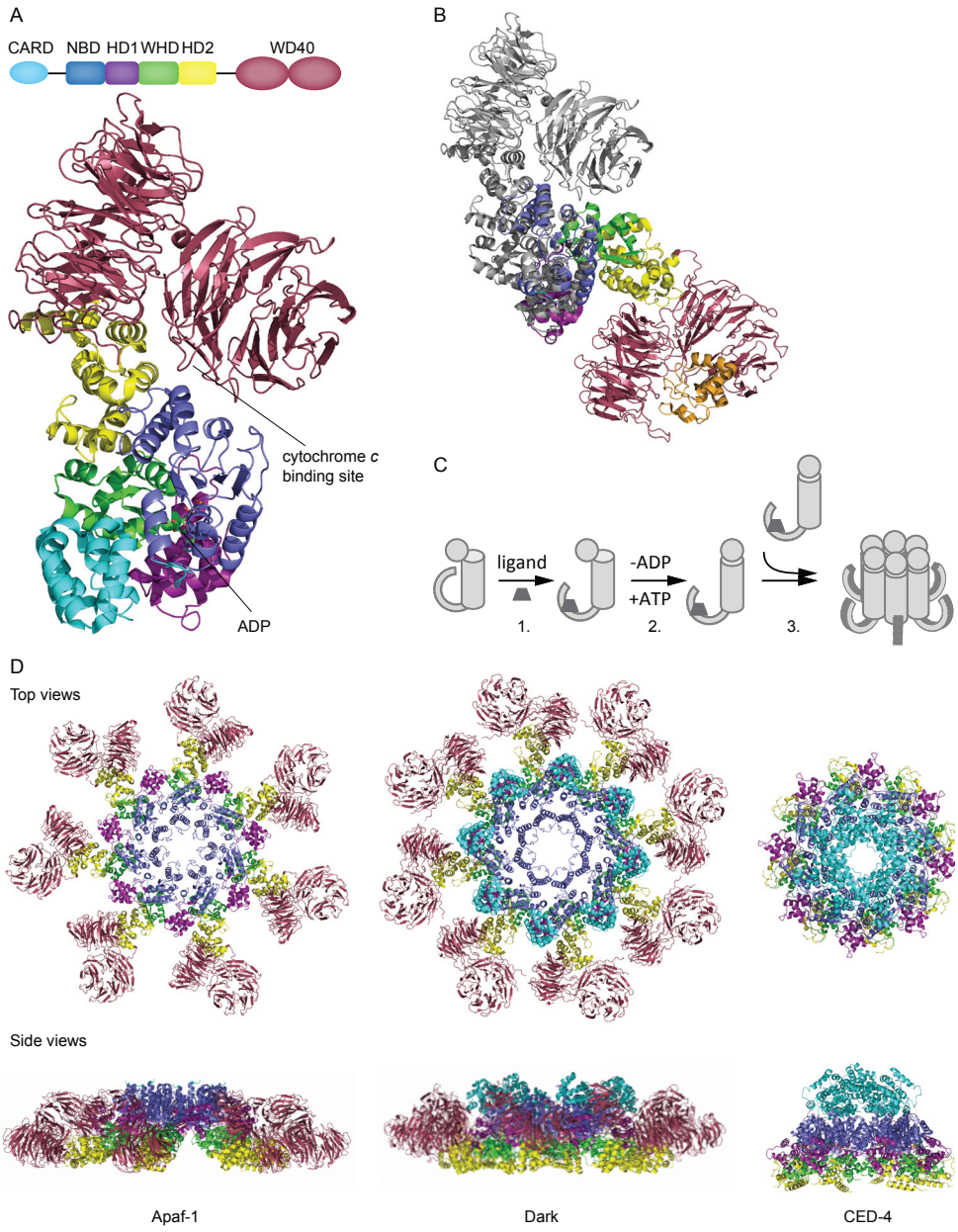

Figure 7: Conformational changes involved in apoptosome and inflammasome formation. *A.* Cartoon representation of the monomeric Apaf-1 crystal structure (PDB ID 3SFZ). The nucleotide binding site and cytochrome *c* binding site are indicated. The location of the CARD is derived from the crystal structure of WD40-deleted Apaf-1 (PDB ID 1Z6T). Color coding of the subdomains is indicated at the top. *B.* Superposition of the Apaf-1 monomer (gray, PDB ID 3SFZ) and apoptosome-incorporated Apaf-1 bound to cytochrome *c* (PDB ID 3J2T) showing the structural rearrangements involved in activation. The structures were superposed on the NACHT subdomains NBD-HD1. Color coding of Apaf-1 subdomans in the apoptosome-incorporated conformations corresponds to panel A; cytochrome *c* is shown in orange. *C.* Schematic representation of the hypothetical model for inflammasome formation based on the mechanism proposed for activation of R-proteins and apoptosome-forming proteins. Ligand binding to the LRR domain induces a conformational change (1), which allows access

to the nucleotide binding site and nucleotide exchange (2). Activated NLR molecules multimerize to form a ring-shaped inflammasome (3). The LRR domains are depicted as arches, NACHT domains as cylinders, and CARDs as spheres. *D.* Cartoon representation of the EM structures of the Apaf-1 apoptosome (left, PDB ID 3IZA) and the Dark apoptosome (middle, PDB ID 3IZ8), and the crystal structure of the CED-4 apoptosome (right, PDB ID 3LQQ). Color coding of the subdomains corresponds to panel A. Panel A, B, and D were created using PyMOL.

Interestingly, homologous mutations in NOD1 and NOD2 in conserved sequences such as the Walker B motif and WHD-histidine lead to inactivation of NOD1 but auto-activation of NOD2[140].

The exact order of events occurring in NLR activation is also unclear. *In vitro* reconstitution of the NLRP1 inflammasome showed that detection of the ligand MDP precedes ATP binding and subsequent oligomerization[141]. Purified NOD1, however, binds ATP in the absence of a ligand[142]. Experiments with purified NOD2 even suggested that pre-incubation with ATPγS enhances binding to MDP and oligomerization of NOD2[143]. The contradicting outcomes of these biochemical studies as well as the previously described deviations in the conserved motifs within the NACHT domain of NLRs, both compared to other STAND proteins as well as within the NLR family, suggest that individual NLR family members may employ different activation mechanisms[117, 144].

Inflammasomes and Nodosomes: Molecular Platforms for Recruiting Downstream Effectors

Most NLRs are thought to oligomerize upon activation and to form a ring-shaped complex stabilized by intermolecular interactions in the NACHT domain, similar to the apoptosomes. This provides a platform for recruitment of downstream effector molecules with high affinity[89]. In apoptosomes the central hub is stabilized by interactions that comprise the NBD, HD1, and the WHD. This central ring comprises a top layer, or inner ring, formed by the NBDs, while the HD1 and WHD form a lower outer ring . The HD2 and sensor domains protrude to the sides (Figure 7D)[130-131, 145]. Whereas in the Dark apoptosome the CARDs extend outward[131], the CARDs in the CED-4 apoptosome cluster together at the top, although this region appears to be more flexible than the rest of the oligomer[146]. The Apaf-1 apoptosome in complex with procasapse-9 displays a dome-like density where the CARDs and procaspase-9 are expected, suggesting that they are flexibly tethered to the ring[130, 147].

Multimerization of NOD1 and NOD2 leads to formation of the Nodosome, or NOD signalosome[45], that exposes its CARD domains for recruitment of RIP2 via homotypic interaction between their CARD domains[11,43]. Mutational analysis suggested that the CARD-CARD interaction between NOD1/2 and RIP2 is mediated by electrostatic interaction, although it is still debated which residues are involved[96,134,148-149]. The charged area of the NLR-CARDs interacting with RIP2 is likely hidden in the auto-inactive conformation of the NLRs.

Formation of an NLRC4 inflammasome likewise exposes a CARD platform. Whereas the NLRC4-inflammasome can therefore directly associate with the CARD of procaspase-1[133, 150], inflammasomes formed by the NLRPs, which harbor an N-terminal PYD domain, require the adapter protein ASC, which consists of an N-terminal PYD and C-terminal CARD, to bridge the NLR to caspase-1[48-50,151]. NLRP-Inflammasome formation thus causes clustering of ASC, consequently exposing a platform of CARD domains. The CARD platform is expected to have a higher affinity for procaspase-1 than isolated NLR subunits do[152-153]. It thereby enforces a high local concentration of procaspase-1, facilitating dimerization of the inactive zymogen, removal of its prodomain, and formation of the active caspase-1 p10/20 tetramer[41, 51, 154].

The first structural insight in inflammasomes was obtained from NLRP1, which oligomerizes into ring-shaped multimers containing either 5 or 7 protomers[141]. On the basis of homology with the heptameric Apaf-1 apoptosome, the hexameric AAA+ complexes, and the octameric CED-4 and Dark apoptosomes[128-130,146,155-156], inflammasomes are generally expected to consist of 5 to 8 protomers (Figure 7C).

A Structural View on Disease-associated Mutations

Understanding the NLR activation mechanism helps to predict the mechanism underlying the diseases on the basis of the location of the mutations.

Mutations linked to Crohn's disease are primarily located in the LRRs, including a frameshift mutation that introduces a premature stop codon and a truncated LRR domain. These mutations show reduced basal NF-κB activation as well as a lack of response to MDP, corresponding to the assumption that CD arises from loss-of-function mutations and that the LRR is responsible for ligand binding[84,157]. In contrast, a mutation in the LRR of NOD1 was associated with increased aspecific NF-κB activation in asthma, suggesting destabilization of the auto-inhibited conformation[82].

Most mutations involved in NLRP3-related diseases (FCAS, MWS, NOMID) are located in the central NACHT domain, although some reside in the NAD. The constitutive activation of the inflammasome, characteristic for these diseases, may well result from stabilization of the active conformation or destabilization of the inactive conformation of NLRP3 by altering the interactions between NACHT subdomains, or by making nucleotide exchange or hydrolysis independent of the inducer[2,5,80,91,157-158]. These auto-active mutants in the NACHT domain of NLRP3 correspond to constitutive active mutants of R-proteins[30,159] and NOD2[80,84,157-158], suggesting a similar mechanism. In patients suffering from BS and EOS, these mutations in NOD2 result in increased MDP-independent basal NF-κB activation[84]. Based on homology modeling many of these mutations in NLRP3 and NOD2 are expected to map near conserved residues involved in nucleotide binding and hydrolysis[157]. Interestingly, none of the disease-associated mutations involves one of the essential conserved residues, suggesting that important functions of the NLRs, such as nucleotide binding, can be impaired but never abolished completely[2,157].

1.3 Scope of this Thesis

The involvement of NLRs in the recognition of a very diverse set of ligands as well as their emerging involvement in an increasing number of pathways makes them an intriguing family of proteins. At the start of this thesis research, many important questions in the NLR field still had to be solved. These questions included: How does each NLR recognize its ligand(s)? Does direct binding occur, or are there intermediate factors involved? And what are the structural rearrangements involved in NLR activation and formation of the inflammasome? We aimed to contribute to solving these questions by structural and functional studies on a selected set of NLRs and their ligands.

Structural and functional characterization of proteins *in vitro* requires their purification in sufficient amounts. NLRs are, however, notoriously hard to purify due to their instability. The first published attempts to purify full length NLRs report severe aggregation of the purified sample and the failure to obtain a homogenous sample, thereby hampering *in vitro* studies. Final

reported yields, if any, were very low, and in most cases purified protein of sufficient quality for biochemical studies could only be obtained by using partial constructs fused to solubility tags[136-138, 141].

In this thesis we present our efforts to purify and characterize a subset of the NLRs, namely human NOD1, NOD2, NLRP3, and NLRC4, as well as murine NLRC4 and NAIP5. These are among the most intensively studied NLRs. NOD1, NOD2, and NLRP3 are associated with a range of diseases, which makes them an important target for study. NLRC4 and NAIP5, on the other hand, are most intensively studied in the context of inflammasome formation.

In **Chapter 2** we present a novel method coined plasmid titration that we developed to improve the recombinant expression of NLRs in suspension growing HEK293E cells. We show how standard transfection methods leads to high total but low soluble production of NLRs, and that reducing expression by plasmid titration shifts the balance from protein aggregation to increasing amounts of soluble protein. This gives a slight improvement in initial yields of purified NLRs. **Chapter 3** provides the first proof for direct interaction between the conserved D0 domain of flagellin and NAIP5, and shows how this interaction induces the formation of a caspase-1 activating hetero-oligomeric NAIP5/NLRC4 inflammasome. Furthermore, this chapter provides the first structural insight into this inflammasome, revealing a disc-shaped structure that contains 11-12 protomers, the majority of which is NLRC4. Images obtained by negative stain EM suggest that this complex has a ring-like arrangement, in which NAIP5 and NLRC4 appear to occupy equivalent positions. To further our understanding of inflammasome structure and formation, in particular to determine the position and role of NAIP5 in the hetero-oligomeric complex, we investigated its structure in closer detail by cryo-electron tomography. The results of these efforts are described in **Chapter 4.** Here we show how we obtained an EM map of a helical NAIP5/NLRC4 complex in which NAIP5 is fused to PKG to discriminate NAIP5 from NLRC4. On the basis of this map we built a model of complex-incorporated NLRC4 that gives insight into conformational changes occurring upon inflammasome formation. In the general discussion (**Chapter 5**), all data is summarized and the impact of our findings is evaluated in the light of recent publications. Finally, the general discussion describes how the insights that we obtained from studying the selected subset of NLRs contribute to unraveling the structure, function, and mechanism of inflammasome formation of other NLR family members.

References

1. Roitt, I.M., J. Brostoff, and D.K. Male, *Immunology*. 4 ed. 1996: Times Mirror International Publishers Limited.
2. Rosenstiel, P., A. Till, and S. Schreiber, *NOD-like receptors and human diseases.* Microbes Infect, 2007. **9**(5): p. 648-57.
3. Lamkanfi, M., L.V. Walle, and T.D. Kanneganti, *Deregulated inflammasome signaling in disease.* Immunol Rev, 2011. **243**(1): p. 163-73.
4. Eisenbarth, S.C. and R.A. Flavell, *Innate instruction of adaptive immunity revisited: the inflammasome.* EMBO Mol Med, 2009. **1**(2): p. 92-8.
5. Fritz, J.H., et al., *Nod-like proteins in immunity, inflammation and disease.* Nat Immunol, 2006. **7**(12): p. 1250-7.
6. Akira, S., S. Uematsu, and O. Takeuchi, *Pathogen recognition and innate immunity.* Cell, 2006. **124**(4): p. 783-801.
7. Philpott, D.J. and S.E. Girardin, *The role of Toll-like receptors and Nod proteins in bacterial infection.* Mol Immunol, 2004. **41**(11): p. 1099-108.

8. Nomura, N., et al., *Prediction of the coding sequences of unidentified human genes. I. The coding sequences of 40 new genes (KIAA0001-KIAA0040) deduced by analysis of randomly sampled cDNA clones from human immature myeloid cell line KG-1.* DNA Res, 1994. **1**(1): p. 27-35.
9. Janeway, C.A., Jr. and R. Medzhitov, *Innate immune recognition.* Annu Rev Immunol, 2002. **20**: p. 197-216.
10. Chen, G., et al., *NOD-like receptors: role in innate immunity and inflammatory disease.* Annu Rev Pathol, 2009. **4**: p. 365-98.
11. Inohara, N., et al., *Nod1, an Apaf-1-like activator of caspase-9 and nuclear factor-kappaB.* J Biol Chem, 1999. **274**(21): p. 14560-7.
12. Ting, J.P., et al., *The NLR gene family: a standard nomenclature.* Immunity, 2008. **28**(3): p. 285-7.
13. Vladimer, G.I., et al., *Inflammasomes and host defenses against bacterial infections.* Curr Opin Microbiol, 2013.
14. Benko, S., D.J. Philpott, and S.E. Girardin, *The microbial and danger signals that activate Nod-like receptors.* Cytokine, 2008. **43**(3): p. 368-73.
15. Franchi, L., R. Munoz-Planillo, and G. Nunez, *Sensing and reacting to microbes through the inflammasomes.* Nat Immunol, 2012. **13**(4): p. 325-32.
16. Lee, J., et al., *pH-dependent internalization of muramyl peptides from early endosomes enables Nod1 and Nod2 signaling.* J Biol Chem, 2009. **284**(35): p. 23818-29.
17. Marina-Garcia, N., et al., *Clathrin- and dynamin-dependent endocytic pathway regulates muramyl dipeptide internalization and NOD2 activation.* J Immunol, 2009. **182**(7): p. 4321-7.
18. Charrier, L. and D. Merlin, *The oligopeptide transporter hPepT1: gateway to the innate immune response.* Lab Invest, 2006. **86**(6): p. 538-46.
19. Ismair, M.G., et al., *hPepT1 selectively transports muramyl dipeptide but not Nod1-activating muramyl peptides.* Can J Physiol Pharmacol, 2006. **84**(12): p. 1313-9.
20. Sun, Y.H., H.G. Rolan, and R.M. Tsolis, *Injection of flagellin into the host cell cytosol by Salmonella enterica serotype Typhimurium.* J Biol Chem, 2007. **282**(47): p. 33897-901.
21. Schroder, K., R. Zhou, and J. Tschopp, *The NLRP3 inflammasome: a sensor for metabolic danger?* Science, 2010. **327**(5963): p. 296-300.
22. Davis, B.K., H. Wen, and J.P. Ting, *The Inflammasome NLRs in Immunity, Inflammation, and Associated Diseases.* Annu Rev Immunol, 2010.
23. Leemans, J.C., S.L. Cassel, and F.S. Sutterwala, *Sensing damage by the NLRP3 inflammasome.* Immunol Rev, 2011. **243**(1): p. 152-62.
24. Petrilli, V., et al., *Activation of the NALP3 inflammasome is triggered by low intracellular potassium concentration.* Cell Death Differ, 2007. **14**(9): p. 1583-9.
25. Mariathasan, S., et al., *Cryopyrin activates the inflammasome in response to toxins and ATP.* Nature, 2006. **440**(7081): p. 228-32.
26. Piccini, A., et al., *ATP is released by monocytes stimulated with pathogen-sensing receptor ligands and induces IL-1beta and IL-18 secretion in an autocrine way.* Proc Natl Acad Sci U S A, 2008. **105**(23): p. 8067-72.
27. Hornung, V., et al., *Silica crystals and aluminum salts activate the NALP3 inflammasome through phagosomal destabilization.* Nat Immunol, 2008. **9**(8): p. 847-56.
28. Zhou, R., et al., *Thioredoxin-interacting protein links oxidative stress to inflammasome activation.* Nat Immunol, 2010. **11**(2): p. 136-40.
29. Rairdan, G. and P. Moffett, *Brothers in arms? Common and contrasting themes in pathogen perception by plant NB-LRR and animal NACHT-LRR proteins.* Microbes Infect, 2007. **9**(5): p. 677-86.
30. Albrecht, M. and F.L. Takken, *Update on the domain architectures of NLRs and R proteins.* Biochem Biophys Res Commun, 2006. **339**(2): p. 459-62.
31. Deslandes, L., et al., *Physical interaction between RRS1-R, a protein conferring resistance to bacterial wilt, and PopP2, a type III effector targeted to the plant nucleus.* Proc Natl Acad Sci U S A, 2003. **100**(13): p. 8024-9.
32. Krasileva, K.V., D. Dahlbeck, and B.J.

Staskawicz, *Activation of an Arabidopsis resistance protein is specified by the in planta association of its leucine-rich repeat domain with the cognate oomycete effector.* Plant Cell, 2010. **22**(7): p. 2444-58.
33. Dodds, P.N., et al., *Direct protein interaction underlies gene-for-gene specificity and coevolution of the flax resistance genes and flax rust avirulence genes.* Proc Natl Acad Sci U S A, 2006. **103**(23): p. 8888-93.
34. Mackey, D., et al., *RIN4 interacts with Pseudomonas syringae type III effector molecules and is required for RPM1-mediated resistance in Arabidopsis.* Cell, 2002. **108**(6): p. 743-54.
35. Mackey, D., et al., *Arabidopsis RIN4 is a target of the type III virulence effector AvrRpt2 and modulates RPS2-mediated resistance.* Cell, 2003. **112**(3): p. 379-89.
36. Collier, S.M. and P. Moffett, *NB-LRRs work a "bait and switch" on pathogens.* Trends Plant Sci, 2009. **14**(10): p. 521-9.
37. DeYoung, B.J. and R.W. Innes, *Plant NBS-LRR proteins in pathogen sensing and host defense.* Nat Immunol, 2006. **7**(12): p. 1243-9.
38. Tattoli, I., et al., *The Nodosome: Nod1 and Nod2 control bacterial infections and inflammation.* Semin Immunopathol, 2007. **29**(3): p. 289-301.
39. Dinarello, C.A., *Interleukin-1 beta, interleukin-18, and the interleukin-1 beta converting enzyme.* Ann N Y Acad Sci, 1998. **856**: p. 1-11.
40. Martinon, F. and J. Tschopp, *Inflammatory caspases and inflammasomes: master switches of inflammation.* Cell Death Differ, 2007. **14**(1): p. 10-22.
41. Schroder, K. and J. Tschopp, *The inflammasomes.* Cell, 2010. **140**(6): p. 821-32.
42. Bergsbaken, T., S.L. Fink, and B.T. Cookson, *Pyroptosis: host cell death and inflammation.* Nat Rev Microbiol, 2009. **7**(2): p. 99-109.
43. Ogura, Y., et al., *Nod2, a Nod1/Apaf-1 family member that is restricted to monocytes and activates NF-kappaB.* J Biol Chem, 2001. **276**(7): p. 4812-8.
44. Karin, M., *The beginning of the end: IkappaB kinase (IKK) and NF-kappaB activation.* J Biol Chem, 1999. **274**(39): p. 27339-42.
45. Inohara, N., et al., *An induced proximity model for NF-kappa B activation in the Nod1/RICK and RIP signaling pathways.* J Biol Chem, 2000. **275**(36): p. 27823-31.
46. Lecat, A., J. Piette, and S. Legrand-Poels, *The protein Nod2: an innate receptor more complex than previously assumed.* Biochem Pharmacol, 2010. **80**(12): p. 2021-31.
47. Strober, W., et al., *Signalling pathways and molecular interactions of NOD1 and NOD2.* Nat Rev Immunol, 2006. **6**(1): p. 9-20.
48. Martinon, F., K. Burns, and J. Tschopp, *The inflammasome: a molecular platform triggering activation of inflammatory caspases and processing of proIL-beta.* Mol Cell, 2002. **10**(2): p. 417-26.
49. Martinon, F., A. Mayor, and J. Tschopp, *The inflammasomes: guardians of the body.* Annu Rev Immunol, 2009. **27**: p. 229-65.
50. Agostini, L., et al., *NALP3 forms an IL-1beta-processing inflammasome with increased activity in Muckle-Wells autoinflammatory disorder.* Immunity, 2004. **20**(3): p. 319-25.
51. Pop, C. and G.S. Salvesen, *Human caspases: activation, specificity, and regulation.* J Biol Chem, 2009. **284**(33): p. 21777-81.
52. Boatright, K.M. and G.S. Salvesen, *Mechanisms of caspase activation.* Curr Opin Cell Biol, 2003. **15**(6): p. 725-31.
53. Miao, E.A., J.V. Rajan, and A. Aderem, *Caspase-1-induced pyroptotic cell death.* Immunol Rev, 2011. **243**(1): p. 206-14.
54. Suzuki, T., et al., *Differential regulation of caspase-1 activation, pyroptosis, and autophagy via Ipaf and ASC in Shigella-infected macrophages.* PLoS Pathog, 2007. **3**(8): p. e111.
55. Broz, P., et al., *Differential requirement for Caspase-1 autoproteolysis in pathogen-induced cell death and cytokine processing.* Cell Host Microbe, 2010. **8**(6): p. 471-83.
56. Kufer, T.A. and P.J. Sansonetti, *NLR functions beyond pathogen recognition.* Nat Immunol, 2011. **12**(2): p. 121-8.
57. Ting, J.P., J.A. Duncan, and Y. Lei, *How the noninflammasome NLRs function in the innate immune system.* Science, 2010. **327**(5963): p. 286-90.
58. Cooney, R., et al., *NOD2 stimulation induces autophagy in dendritic cells influencing bacterial handling and antigen presentation.* Nat Med, 2010. **16**(1): p.

90-7.
59. Travassos, L.H., et al., *Nod1 and Nod2 direct autophagy by recruiting ATG16L1 to the plasma membrane at the site of bacterial entry.* Nat Immunol, 2010. **11**(1): p. 55-62.
60. Yoo, N.J., et al., *Nod1, a CARD protein, enhances pro-interleukin-1beta processing through the interaction with pro-caspase-1.* Biochem Biophys Res Commun, 2002. **299**(4): p. 652-8.
61. Dowds, T.A., et al., *Regulation of cryopyrin/Pypaf1 signaling by pyrin, the familial Mediterranean fever gene product.* Biochem Biophys Res Commun, 2003. **302**(3): p. 575-80.
62. Ting, J.P., D.L. Kastner, and H.M. Hoffman, *CATERPILLERs, pyrin and hereditary immunological disorders.* Nat Rev Immunol, 2006. **6**(3): p. 183-95.
63. Kadota, Y., K. Shirasu, and R. Guerois, *NLR sensors meet at the SGT1-HSP90 crossroad.* Trends Biochem Sci, 2010.
64. Hahn, J.S., *Regulation of Nod1 by Hsp90 chaperone complex.* FEBS Lett, 2005. **579**(20): p. 4513-9.
65. Mayor, A., et al., *A crucial function of SGT1 and HSP90 in inflammasome activity links mammalian and plant innate immune responses.* Nat Immunol, 2007. **8**(5): p. 497-503.
66. da Silva Correia, J., et al., *SGT1 is essential for Nod1 activation.* Proc Natl Acad Sci U S A, 2007. **104**(16): p. 6764-9.
67. Lee, K.H., et al., *Proteasomal degradation of Nod2 mediates tolerance to bacterial cell wall components.* J Biol Chem, 2012.
68. Akira, S. and K. Takeda, *Toll-like receptor signalling.* Nat Rev Immunol, 2004. **4**(7): p. 499-511.
69. Franchi, L., et al., *Nucleotide-binding oligomerization domain-like receptors: intracellular pattern recognition molecules for pathogen detection and host defense.* J Immunol, 2006. **177**(6): p. 3507-13.
70. O'Neill, L.A., *When signaling pathways collide: positive and negative regulation of toll-like receptor signal transduction.* Immunity, 2008. **29**(1): p. 12-20.
71. Eisenbarth, S.C., et al., *Crucial role for the Nalp3 inflammasome in the immunostimulatory properties of aluminium adjuvants.* Nature, 2008. **453**(7198): p. 1122-6.
72. Franchi, L. and G. Nunez, *The Nlrp3 inflammasome is critical for aluminium hydroxide-mediated IL-1beta secretion but dispensable for adjuvant activity.* Eur J Immunol, 2008. **38**(8): p. 2085-9.
73. Kool, M., et al., *Cutting edge: alum adjuvant stimulates inflammatory dendritic cells through activation of the NALP3 inflammasome.* J Immunol, 2008. **181**(6): p. 3755-9.
74. Li, H., et al., *Cutting edge: inflammasome activation by alum and alum's adjuvant effect are mediated by NLRP3.* J Immunol, 2008. **181**(1): p. 17-21.
75. Fritz, J.H., et al., *Nod1-mediated innate immune recognition of peptidoglycan contributes to the onset of adaptive immunity.* Immunity, 2007. **26**(4): p. 445-59.
76. Kobayashi, K.S., et al., *Nod2-dependent regulation of innate and adaptive immunity in the intestinal tract.* Science, 2005. **307**(5710): p. 731-4.
77. Higgins, S.C. and K.H. Mills, *TLR, NLR Agonists, and Other Immune Modulators as Infectious Disease Vaccine Adjuvants.* Curr Infect Dis Rep, 2010. **12**(1): p. 4-12.
78. Geddes, K., J.G. Magalhaes, and S.E. Girardin, *Unleashing the therapeutic potential of NOD-like receptors.* Nat Rev Drug Discov, 2009. **8**(6): p. 465-79.
79. Steinhagen, F., et al., *TLR-based immune adjuvants.* Vaccine, 2011. **29**(17): p. 3341-55.
80. McGonagle, D., S. Savic, and M.F. McDermott, *The NLR network and the immunological disease continuum of adaptive and innate immune-mediated inflammation against self.* Semin Immunopathol, 2007. **29**(3): p. 303-13.
81. Liu-Bryan, R., *Intracellular innate immunity in gouty arthritis: role of NALP3 inflammasome.* Immunol Cell Biol, 2010. **88**(1): p. 20-3.
82. Hysi, P., et al., *NOD1 variation, immunoglobulin E and asthma.* Hum Mol Genet, 2005. **14**(7): p. 935-41.
83. Tschopp, J., F. Martinon, and K. Burns, *NALPs: a novel protein family involved in inflammation.* Nat Rev Mol Cell Biol, 2003. **4**(2): p. 95-104.

84. Inohara, N. and G. Nunez, *NODs: intracellular proteins involved in inflammation and apoptosis.* Nat Rev Immunol, 2003. **3**(5): p. 371-82.
85. Meissner, T.B., et al., *The nucleotide-binding domain of NLRC5 is critical for nuclear import and transactivation activity.* Biochem Biophys Res Commun, 2012.
86. Moore, C.B., et al., *NLRX1 is a regulator of mitochondrial antiviral immunity.* Nature, 2008. **451**(7178): p. 573-7.
87. Tattoli, I., et al., *NLRX1 is a mitochondrial NOD-like receptor that amplifies NF-kappaB and JNK pathways by inducing reactive oxygen species production.* EMBO Rep, 2008. **9**(3): p. 293-300.
88. Koonin, E.V. and L. Aravind, *The NACHT family - a new group of predicted NTPases implicated in apoptosis and MHC transcription activation.* Trends Biochem Sci, 2000. **25**(5): p. 223-4.
89. Inohara, N. and G. Nunez, *The NOD: a signaling module that regulates apoptosis and host defense against pathogens.* Oncogene, 2001. **20**(44): p. 6473-81.
90. Leipe, D.D., E.V. Koonin, and L. Aravind, *STAND, a class of P-loop NTPases including animal and plant regulators of programmed cell death: multiple, complex domain architectures, unusual phyletic patterns, and evolution by horizontal gene transfer.* J Mol Biol, 2004. **343**(1): p. 1-28.
91. Danot, O., et al., *Wheel of Life, Wheel of Death: A Mechanistic Insight into Signaling by STAND Proteins.* Structure, 2009. **17**(2): p. 172-82.
92. Monie, T.P., M.C. Moncrieffe, and N.J. Gay, *Structure and regulation of cytoplasmic adapter proteins involved in innate immune signaling.* Immunol Rev, 2009. **227**(1): p. 161-75.
93. Park, H.H., et al., *The death domain superfamily in intracellular signaling of apoptosis and inflammation.* Annu Rev Immunol, 2007. **25**: p. 561-86.
94. Kohl, A. and M.G. Grutter, *Fire and death: the pyrin domain joins the death-domain superfamily.* C R Biol, 2004. **327**(12): p. 1077-86.
95. Coussens, N.P., et al., *Crystal structure of the Nod1 caspase activation and recruitment domain.* Biochem Biophys Res Commun, 2007. **353**(1): p. 1-5.
96. Manon, F., et al., *Solution structure of NOD1 CARD and mutational analysis of its interaction with the CARD of downstream kinase RICK.* J Mol Biol, 2007. **365**(1): p. 160-74.
97. Srimathi, T., et al., *Monomer/dimer transition of the caspase-recruitment domain of human Nod1.* Biochemistry, 2008. **47**(5): p. 1319-25.
98. Bae, J.Y. and H.H. Park, *Crystal structure of NALP3 protein pyrin domain (PYD) and its implications in inflammasome assembly.* J Biol Chem, 2011. **286**(45): p. 39528-36.
99. Eibl, C., et al., *Structural and functional analysis of the NLRP4 pyrin domain.* Biochemistry, 2012. **51**(37): p. 7330-41.
100. Hiller, S., et al., *NMR structure of the apoptosis- and inflammation-related NALP1 pyrin domain.* Structure, 2003. **11**(10): p. 1199-205.
101. Pinheiro, A.S., et al., *The NLRP12 pyrin domain: structure, dynamics, and functional insights.* J Mol Biol, 2011. **413**(4): p. 790-803.
102. Pinheiro, A.S., et al., *Three-dimensional structure of the NLRP7 pyrin domain: insight into pyrin-pyrin-mediated effector domain signaling in innate immunity.* J Biol Chem, 2010. **285**(35): p. 27402-10.
103. Kersse, K., et al., *The death-fold superfamily of homotypic interaction motifs.* Trends Biochem Sci, 2011. **36**(10): p. 541-52.
104. Vajjhala, P.R., R.E. Mirams, and J.M. Hill, *Multiple binding sites on the ASC pyrin domain allow self-association and interaction with NLRP3.* J Biol Chem, 2012.
105. Herman, M.D., et al., *Structures of BIR domains from human NAIP and cIAP2.* Acta Crystallogr Sect F Struct Biol Cryst Commun, 2009. **65**(Pt 11): p. 1091-6.
106. Sun, C., et al., *NMR structure and mutagenesis of the third Bir domain of the inhibitor of apoptosis protein XIAP.* J Biol Chem, 2000. **275**(43): p. 33777-81.
107. Salvesen, G.S. and C.S. Duckett, *IAP proteins: blocking the road to death's door.* Nat Rev Mol Cell Biol, 2002. **3**(6): p. 401-10.
108. Maier, J.K., et al., *The neuronal apoptosis inhibitory protein is a direct inhibitor of caspases 3 and 7.* J Neurosci, 2002. **22**(6): p. 2035-43.

109. Kobe, B. and A.V. Kajava, *The leucine-rich repeat as a protein recognition motif.* Curr Opin Struct Biol, 2001. **11**(6): p. 725-32.
110. Kobe, B. and J. Deisenhofer, *A structural basis of the interactions between leucine-rich repeats and protein ligands.* Nature, 1995. **374**(6518): p. 183-6.
111. Hong, M., S.I. Yoon, and I.A. Wilson, *Structure and Functional Characterization of the RNA-Binding Element of the NLRX1 Innate Immune Modulator.* Immunity, 2012. **36**(3): p. 337-47.
112. Hu, Y., et al., *WD-40 repeat region regulates Apaf-1 self-association and procaspase-9 activation.* J Biol Chem, 1998. **273**(50): p. 33489-94.
113. Srinivasula, S.M., et al., *Autoactivation of procaspase-9 by Apaf-1-mediated oligomerization.* Mol Cell, 1998. **1**(7): p. 949-57.
114. Yang, X., H.Y. Chang, and D. Baltimore, *Essential role of CED-4 oligomerization in CED-3 activation and apoptosis.* Science, 1998. **281**(5381): p. 1355-7.
115. Riedl, S.J., et al., *Structure of the apoptotic protease-activating factor 1 bound to ADP.* Nature, 2005. **434**(7035): p. 926-33.
116. Yan, N., et al., *Structure of the CED-4-CED-9 complex provides insights into programmed cell death in Caenorhabditis elegans.* Nature, 2005. **437**(7060): p. 831-7.
117. Proell, M., et al., *The Nod-like receptor (NLR) family: a tale of similarities and differences.* PLoS One, 2008. **3**(4): p. e2119.
118. Lupas, A.N. and J. Martin, *AAA proteins.* Curr Opin Struct Biol, 2002. **12**(6): p. 746-53.
119. Hanson, P.I. and S.W. Whiteheart, *AAA+ proteins: have engine, will work.* Nat Rev Mol Cell Biol, 2005. **6**(7): p. 519-29.
120. Reubold, T.F., S. Wohlgemuth, and S. Eschenburg, *Crystal structure of full-length Apaf-1: how the death signal is relayed in the mitochondrial pathway of apoptosis.* Structure, 2011. **19**(8): p. 1074-83.
121. Moffett, P., et al., *Interaction between domains of a plant NBS-LRR protein in disease resistance-related cell death.* EMBO J, 2002. **21**(17): p. 4511-9.
122. Tameling, W.I., et al., *Mutations in the NB-ARC domain of I-2 that impair ATP hydrolysis cause autoactivation.* Plant Physiol, 2006. **140**(4): p. 1233-45.
123. van Ooijen, G., et al., *Structure-function analysis of the NB-ARC domain of plant disease resistance proteins.* J Exp Bot, 2008. **59**(6): p. 1383-97.
124. Lukasik, E. and F.L. Takken, *STANDing strong, resistance proteins instigators of plant defence.* Curr Opin Plant Biol, 2009.
125. Riedl, S.J. and G.S. Salvesen, *The apoptosome: signalling platform of cell death.* Nat Rev Mol Cell Biol, 2007. **8**(5): p. 405-13.
126. Zou, H., et al., *Apaf-1, a human protein homologous to C. elegans CED-4, participates in cytochrome c-dependent activation of caspase-3.* Cell, 1997. **90**(3): p. 405-13.
127. Jiang, X. and X. Wang, *Cytochrome c promotes caspase-9 activation by inducing nucleotide binding to Apaf-1.* J Biol Chem, 2000. **275**(40): p. 31199-203.
128. Acehan, D., et al., *Three-dimensional structure of the apoptosome: implications for assembly, procaspase-9 binding, and activation.* Mol Cell, 2002. **9**(2): p. 423-32.
129. Yu, X., et al., *A structure of the human apoptosome at 12.8 A resolution provides insights into this cell death platform.* Structure, 2005. **13**(11): p. 1725-35.
130. Yuan, S., et al., *Structure of an apoptosome-procaspase-9 CARD complex.* Structure, 2010. **18**(5): p. 571-83.
131. Yuan, S., et al., *Structure of the Drosophila apoptosome at 6.9 a resolution.* Structure, 2011. **19**(1): p. 128-40.
132. Chamaillard, M., et al., *An essential role for NOD1 in host recognition of bacterial peptidoglycan containing diaminopimelic acid.* Nat Immunol, 2003. **4**(7): p. 702-7.
133. Poyet, J.L., et al., *Identification of Ipaf, a human caspase-1-activating protein related to Apaf-1.* J Biol Chem, 2001. **276**(30): p. 28309-13.
134. Tanabe, T., et al., *Regulatory regions and critical residues of NOD2 involved in muramyl dipeptide recognition.* Embo J, 2004. **23**(7): p. 1587-97.
135. Girardin, S.E., et al., *Identification of the critical residues involved in peptidoglycan detection by Nod1.* J Biol Chem, 2005. **280**(46): p. 38648-56.
136. Ye, Z., et al., *ATP binding by monarch-1/*

NLRP12 is critical for its inhibitory function. Mol Cell Biol, 2008. **28**(5): p. 1841-50.
137. Duncan, J.A., et al., *Cryopyrin/NALP3 binds ATP/dATP, is an ATPase, and requires ATP binding to mediate inflammatory signaling.* Proc Natl Acad Sci U S A, 2007. **104**(19): p. 8041-6.
138. Lu, C., et al., *Nucleotide binding to CARD12 and its role in CARD12-mediated caspase-1 activation.* Biochem Biophys Res Commun, 2005. **331**(4): p. 1114-9.
139. Lautz, K., et al., *NLRP10 enhances Shigella-induced pro-inflammatory responses.* Cell Microbiol, 2012.
140. Zurek, B., et al., *Mutational analysis of human NOD1 and NOD2 NACHT domains reveals different modes of activation.* Innate Immun, 2011.
141. Faustin, B., et al., *Reconstituted NALP1 inflammasome reveals two-step mechanism of caspase-1 activation.* Mol Cell, 2007. **25**(5): p. 713-24.
142. Askari, N., et al., *Expression, purification, and characterization of recombinant NOD1 (NLRC1): A NLR family member.* J Biotechnol, 2011.
143. Mo, J.Y., et al., *Pathogen sensing by nucleotide-binding oligomerization domain-containing protein 2 (NOD2) is mediated by direct binding to muramyl dipeptide and ATP.* J Biol Chem, 2012.
144. Bao, Q., S.J. Riedl, and Y. Shi, *Structure of Apaf-1 in the auto-inhibited form: a critical role for ADP.* Cell Cycle, 2005. **4**(8): p. 1001-3.
145. Reubold, T.F. and S. Eschenburg, *A molecular view on signal transduction by the apoptosome.* Cell Signal, 2012. **24**(7): p. 1420-5.
146. Qi, S., et al., *Crystal structure of the Caenorhabditis elegans apoptosome reveals an octameric assembly of CED-4.* Cell, 2010. **141**(3): p. 446-57.
147. Yuan, S., et al., *The holo-apoptosome: activation of procaspase-9 and interactions with caspase-3.* Structure, 2011. **19**(8): p. 1084-96.
148. Fridh, V. and K. Rittinger, *The Tandem CARDs of NOD2: Intramolecular Interactions and Recognition of RIP2.* PLoS One, 2012. **7**(3): p. e34375.
149. Wagner, R.N., et al., *Evaluation of Nod-like receptor (NLR) effector domain interactions.* PLoS One, 2009. **4**(4): p. e4931.
150. Damiano, J.S., et al., *CLAN, a novel human CED-4-like gene.* Genomics, 2001. **75**(1-3): p. 77-83.
151. Srinivasula, S.M., et al., *The PYRIN-CARD protein ASC is an activating adaptor for caspase-1.* J Biol Chem, 2002. **277**(24): p. 21119-22.
152. Shiozaki, E.N., J. Chai, and Y. Shi, *Oligomerization and activation of caspase-9, induced by Apaf-1 CARD.* Proc Natl Acad Sci U S A, 2002. **99**(7): p. 4197-202.
153. Park, H.H., et al., *Death domain assembly mechanism revealed by crystal structure of the oligomeric PIDDosome core complex.* Cell, 2007. **128**(3): p. 533-46.
154. Renatus, M., et al., *Dimer formation drives the activation of the cell death protease caspase 9.* Proc Natl Acad Sci U S A, 2001. **98**(25): p. 14250-5.
155. Yu, X., et al., *Three-dimensional structure of a double apoptosome formed by the Drosophila Apaf-1 related killer.* J Mol Biol, 2006. **355**(3): p. 577-89.
156. Wu, C.C. and S.B. Bratton, *DARK apoptosome secrets come to light.* Structure, 2011. **19**(1): p. 4-6.
157. Albrecht, M., et al., *Structural localization of disease-associated sequence variations in the NACHT and LRR domains of PYPAF1 and NOD2.* FEBS Lett, 2003. **554**(3): p. 520-8.
158. Inohara, et al., *NOD-LRR proteins: role in host-microbial interactions and inflammatory disease.* Annu Rev Biochem, 2005. **74**: p. 355-83.
159. Bendahmane, A., et al., *Constitutive gain-of-function mutants in a nucleotide binding site-leucine rich repeat protein encoded at the Rx locus of potato.* Plant J, 2002. **32**(2): p. 195-204.
160. Wilmanski, J.M., T. Petnicki-Ocwieja, and K.S. Kobayashi, *NLR proteins: integral members of innate immunity and mediators of inflammatory diseases.* J Leukoc Biol, 2008. **83**(1): p. 13-30.
161. Michallet, M.C., et al., *Innate receptors for adaptive immunity.* Curr Opin Microbiol, 2013.
162. Radian, A.D., et al., *NLRP7 and related*

inflammasome activating pattern recognition receptors and their function in host defense and disease. Microbes Infect, 2013.

163. Damm, A., K. Lautz, and T.A. Kufer, *NLRP10 roles in innate and adaptive immunity.* Microbes Infect, 2013.

Chapter **2**

Optimization of Recombinant Protein Production in Transiently Transfected HEK293-EBNA1 cells by Plasmid Titration: a case study for NLRs

Els F. Halff, Marian Versteeg, T. Harma C. Brondijk, Eric G. Huizinga

Crystal and Structural Chemistry, Bijvoet Center for Biomolecular Research, Department of Chemistry, Faculty of Science, Utrecht University, The Netherlands

Manuscript in preparation

Optimization of Recombinant Protein Production in Transiently Transfected HEK293-EBNA1 cells by Plasmid Titration: a case study for NLRs

Transient transfection of the human HEK293-EBNA1 cell line using polyethyleneimine (PEI) is widely adopted for recombinant protein production. We used this system to express the Nod-like receptors (NLRs) NOD1, NOD2, NLRP3, and NLRC4, and find that, although the standard transfection protocol results in high NLR expression, the NLRs aggregate and little or no soluble protein is obtained. In addition, NLR expression causes a drastic reduction of cell viability. As the standard transfection protocol has been optimized for high transcription and translation rates, we hypothesized that NLR overexpression causes an overload of the cellular folding machinery, resulting in protein aggregation and cell death. To attenuate the rate of expression in a systematic manner we applied plasmid titration, i.e. a dilution series of expression vector with dummy plasmid transfected in small scale cultures. Application to GFP shows that plasmid titration reduces expression while maintaining high transfection efficiencies even at 500-fold dilution. Plasmid titration delays the onset of NLR aggregation and improves cell viability and the buildup of biomass. Together, these factors increase the amount of soluble protein. We find the combination of dilution factor and harvest day that maximizes soluble expression to be protein specific. For NOD1, 50-fold plasmid dilution increases the amount of soluble protein 5-fold, however, the protein is associated with chaperones at all plasmid concentrations and could not be purified to homogeneity. For NLRC4, 10-fold plasmid dilution increases the yield of purified protein 2-fold. This improvement, albeit modest, is obtained with minimal effort due to the simplicity of the method. We speculate that plasmid titration will also improve soluble expression of other proteins that aggregate upon overexpression in HEK293-EBNA1 cells.

Introduction

Structural and functional characterization of proteins using biochemical and biophysical techniques often requires their purification in large quantities and high purity. Expression levels and purification efficiencies of endogenous proteins are frequently too low to obtain sufficient amounts of native protein. Recombinant protein expression provides the advantage of enhanced expression and the possibility to genetically alter proteins such as the addition of purification tags or the introduction of mutations that alter protein behavior. The Human Embryonic Kidney 293 (HEK293) cell line expressing Epstein-Barr virus nuclear antigen 1 (EBNA1) is well established for recombinant expression of secreted, membrane, and intracellular proteins[1-3]. Binding of EBNA1 to an expression vector containing OriP ensures episomal replication of the vector during mitosis. High expression in HEK293E cells is furthermore obtained by using optimized OriP-based expression vectors containing the strong CMV promoter. Efficient transient transfection of milliliter to liter volumes of HEK293E cells can be achieved using polyethyleneimine (PEI), which circumvents the tedious selection procedure required for stable transfection. Using this system protein production up to 50 mg per liter of cell culture has been reported for intracellular proteins[1, 4].

We used the HEK293E system to express

Nod-Like Receptors (NLRs), which are cytosolic receptors of the innate immune system that respond to a wide variety of pathogen and danger associated molecular patterns. NLRs have become major targets in immunological research since their discovery just over a decade ago (reviewed in ref. 5). Among the most intensively studied NLRs are NOD1, NOD2, NLRP3, and NLRC4. NOD1 and NOD2 evoke an immune response upon detection of distinct peptidoglycan fragments, resulting in the activation of NF-κB[6-8]. NLRC4, together with different members of the NAIP subfamily of NLRs, recognizes flagellin and other, structurally related, bacterial proteins, resulting in caspase-1 activation followed by processing of proIL-1β and pyroptosis[9-12]. NLRP3 likewise mediates caspase-1 activation in response to a multitude of stimuli (reviewed in ref. 13). Mutations in these NLRs have been associated with a broad range of inflammatory diseases including arthritis[14], familial cold autoinflammatory syndrome (FCAS)[15], Inflammatory Bowel Diseases (IBD) such as Crohn's disease [16-17], and asthma[18].

Recently we reported on the purification of human NLRC4 and murine NAIP5 from HEK293E cells and showed that the purified proteins form an inflammasome upon addition of flagellin (Chapter 3 of this thesis and ref. 12). In this study we describe how we optimized the expression of NLRC4 in HEK293E cells and thoroughly analyze the application of this method to the expression of NOD1, NOD2, and NLRP3. We show that the standard transfection protocol leads to high NLR expression, but nearly all of the protein is aggregated. In an attempt to shift the balance from aggregated to soluble protein we reduced total NLR expression by stepwise dilution of the expression plasmid with non-coding dummy plasmid in a procedure coined plasmid titration. Expression plasmid dilution reduces protein aggregation, improves cell viability, and increases the amount of soluble protein. At optimized expression plasmid concentrations a moderately improved yield is obtained from large scale cultures as we illustrate for NLRC4. We expect that this method may also improve soluble expression of other proteins that proved difficult to express using the standard transfection protocol.

Results

NLR proteins are highly overexpressed in HEK293 cells.

In order to develop a strategy for improved NLR protein production in transiently transfected HEK293E cells we assessed the effect of different purification tags on expression levels of NOD1, NOD2, NLRP3, and NLRC4. We first tested 11 different constructs of NOD1 and NLRC4, using standardized transfection protocols. All constructs contained an N- or C-terminal His_6-tag, either alone or in combination with a $Flag_3$, $StrepII_3$, or GFP tag (Figure 1A). Total expression was visualized on Western blot using a mixture of anti-His tag antibodies (see Experimental procedures). As reference we used bovine cGMP-dependent protein kinase I alpha (PKG), a protein that is highly expressed in HEK293 cells and has been purified in yields of up to 75 mg/liter of culture (ref. 20 and Dr. W. Hemrika (U-Protein Express BV, The Netherlands; personal communication)). Most NLR constructs expressed well. Visual comparison suggests NLR expression levels for some constructs to be as high as that of PKG. Considerable variation is observed in NLR expression depending on the type of tag and its position. The same type of tag results in different expression levels depending on whether it is located at the N or C terminus, and also the presence or absence of a TEV protease site can affect the expression level. Similar variation in expression levels was observed for a

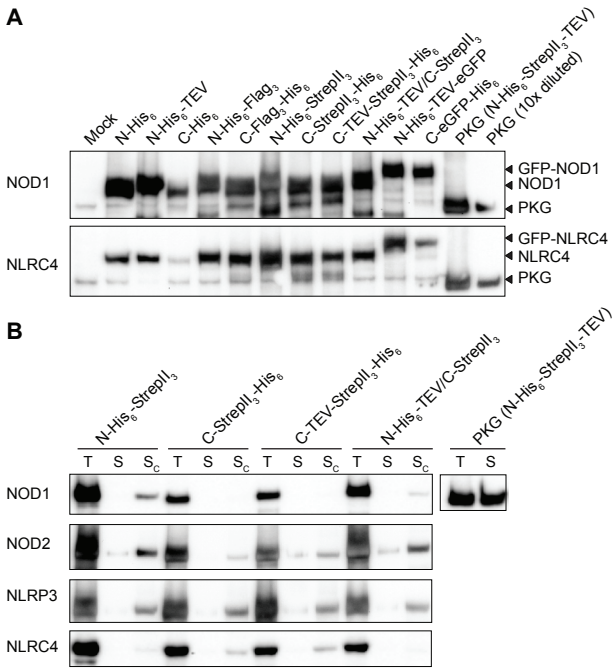

Figure 1. NLR expression in HEK293E cells. (A) Western blot analysis of total lysate of cells expressing NOD1, NLRC4, and the reference protein PKG containing the indicated tags. (B) Comparison of total and soluble expression of NLRs containing different His_6 and $StrepII_3$ tag combinations. Total lysate (T), cleared lysate (S), and cleared lysate at a 10-fold higher concentration (S_C) were analyzed. Cells were harvested 48h ptf; Western blots were probed with anti-His tag antibody.

range of constructs of NOD2 and NLRP3 (unpublished data). Notwithstanding the observed variation, the total expression levels of all four NLRs are high.

Overexpressed NLRs are mainly insoluble.

For each of the four target proteins we aimed to select the construct expressing the highest amount of soluble protein. For ease of protein purification we selected a sub-set of vectors encoding both a His_6 and $StrepII_3$ tag. The $StrepII_3$ tag is highly selective, yielding relatively pure protein in a single purification step, and is therefore convenient for rapid testing on small scale. The combination with the His_6 tag offers the possibility of attaining higher purity by tandem affinity purification. In our initial tests these dual-tag vectors all gave high total expression.

The relative amount of soluble protein in the cleared lysates was estimated by blotting side by side total cell protein and cleared lysates, each corresponding to the same culture volume (Figure 1B). Whereas a clear band is visible for total cell protein, we could not or barely detect soluble protein for any of the NLR constructs. In contrast, for PKG the bands for total and soluble protein are equally intense, indicating that most of the protein is soluble. Soluble NLRs were, however, visible for most of the constructs at a 10-fold higher concentration of the lysate (Figure 1B). As is the case for the total expression level, the amount of soluble protein varies depending on tag position. Notably, the highest soluble expression is not always obtained with the construct that gives the highest total expression. For NOD1 and NOD2 soluble expression was highest with an N-terminal TEV-cleavable His_6-$StrepII_3$ tag, whereas a C-terminal non-cleavable $StrepII_3$-His_6 tag was optimal for NLRP3 and NLRC4. All subsequent expression studies were performed using these constructs.

Overexpression of NLRs leads to protein aggregation and cell death.

To determine the optimal time point for cell harvest we monitored the time course of total and soluble protein production as well as cell viability and total cell count in 4 ml cultures (Figure 2A-C). The amount of total and soluble protein shows a steady increase over time for the reference protein PKG (Figure 2A). For NOD1, NOD2, and NLRP3 total protein expression increases up

to 72h post transfection (ptf); the amount of soluble protein, however, has reached its maximum already at 24h ptf and then decreases until, at 96h ptf, no soluble protein is detected anymore. The time course of NLRC4 expression differs from that of the other NLRs as the amount of soluble and total protein both increase until 72h ptf, and then decrease only slightly.

The viability of NLR-expressing cells decreases rapidly, in particular for NOD1 and NOD2, whereas the viability of cells overexpressing the reference protein PKG is comparable to mock-transfected cells (Figure 2B). Additionally, whereas the number of viable cells increases up to 72h ptf in PKG and mock-transfections, a continuous decrease is observed in NLR-transfections (Figure 2C).

To visualize the behavior of NLRs upon overexpression, we transfected GFP-NLR fusion proteins in adherent HEK293E cells and analyzed their distribution using fluorescence microscopy (Figure 2D). The control proteins GFP and GFP-luciferase fusion show a diffuse distribution up to 72h

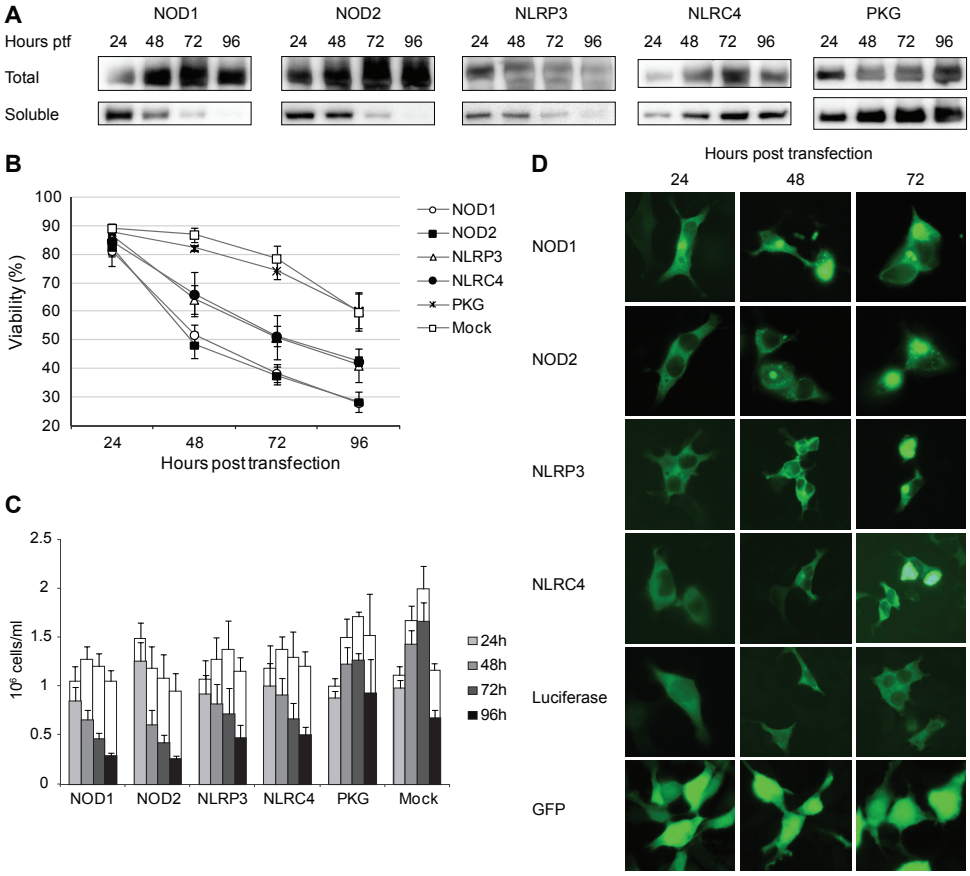

Figure 2. Overexpressed NLRs rapidly aggregate and reduce cell viability. (A) Time course analysis of total and soluble expression of NLRs and PKG. Total lysate and concentrated cleared lysate were analyzed on Western blot probed with anti-His tag antibody. (B) Time course of the viability of 4-ml HEK293E cultures after mock transfection or transfection with NLRs or PKG. Standard deviations were derived from at least three independent transfections. (C) Total cell count (white bars) and viable cell count (superimposed grey and black bars) of the cultures depicted in Figure 2B. (D) Fluorescence micrographs of adherent HEK293E cells transfected with GFP-NLR fusion proteins, GFP-luciferase fusion, or GFP alone. Cells were fixed at the indicated time points after transfection.

ptf. GFP-NLR fusions also show a mainly diffuse distribution with some punctuate structures at 24h ptf, however, at later time points, large aggregates are present. At 72h ptf many cells have detached, and only very few adherent GFP-NLR expressing cells remain.

Thus, overexpression of NLRs leads to accumulation of protein in large aggregates and rapid cell death. The formation of aggregates fits our observation that only a small fraction of the expressed protein resides in the soluble fraction of the cell lysate (Figure 1B,2A). Whether aggregation is the cause of cell death and whether non-viable cells still contribute soluble protein cannot be concluded from our data, but obviously the formation of aggregates is at the expense of the amount of soluble NLR.

Plasmid titration reduces protein aggregation

We wondered whether protein aggregation could be reduced by lowering the amount of expression plasmid used in transfections. We reasoned that protein aggregation may well be caused by overloading of the cellular protein folding machinery, in which case reducing the expression level by using less plasmid may improve folding and reduce aggregation. We therefore progressively lowered the amount of expression plasmid and, in order to maintain high transfection efficiency and transcription rates[21], replaced it with an empty pCR4 filler plasmid. This method is hereafter referred to as plasmid titration. A similar approach was used by Carpentier *et al.* to study factors limiting the transient expression of GFP and secreted alkaline phosphatase (SEAP) in HEK293E cells[22]. These authors showed that 50-fold dilution of expression plasmid reduces protein expression while retaining high transfection efficiency. We extended the dilution range and show by FACS analysis of GFP-transfected cells that even at 500-fold plasmid dilution the transfection efficiency is high (Supplemental Figure S1). The observation that even at such high dilution a large fraction of cells express GFP is consistent with the finding that as many as 10^4 plasmids are taken up by a single cell, of which 5-10% is found in the nucleus[22]. Thus, plasmid dilution is a suitable method to study the effect of expression levels on protein aggregation.

Next, we analyzed the effect of plasmid titration on NLR aggregation in GFP-NOD1 transfected cells (Figure 3A). We observe a delay in the onset of aggregate formation; aggregates are formed in a smaller fraction of the GFP-NOD1 expressing cells, and more live cells are found at 72h ptf. Plasmid titration also improves the viability of suspension HEK293E cells that express NOD1 (Figure 3B). Whereas the viability of these cells drops rapidly at lower plasmid dilutions, a clear improvement is observed at dilutions of 20-fold and higher; at these dilutions also the total number of cells increases (Figure 3C). For cells expressing the reference protein PKG, which already have a high viability at standard transfection conditions (Figure 2B), plasmid titration only slightly improves viability and total cell count (Supplemental Figure S2A,B).

Taken together, plasmid titration reduces expression per cell without significantly affecting transfection efficiency. In the case of NLR overexpression, plasmid titration leads to a reduction of protein aggregation, improved cell viability, and an increase in biomass.

The effect of plasmid titration on total and soluble expression

The primary aim of plasmid titration was not to reduce protein aggregation and cell death, but to increase the amount of soluble protein. Therefore, we set forth to analyze the effect of plasmid titration on total and soluble expression by Western blotting. We analyzed NOD1, NLRC4, and the reference protein PKG extensively, and did a more limited analysis of NOD2 and NLRP3.

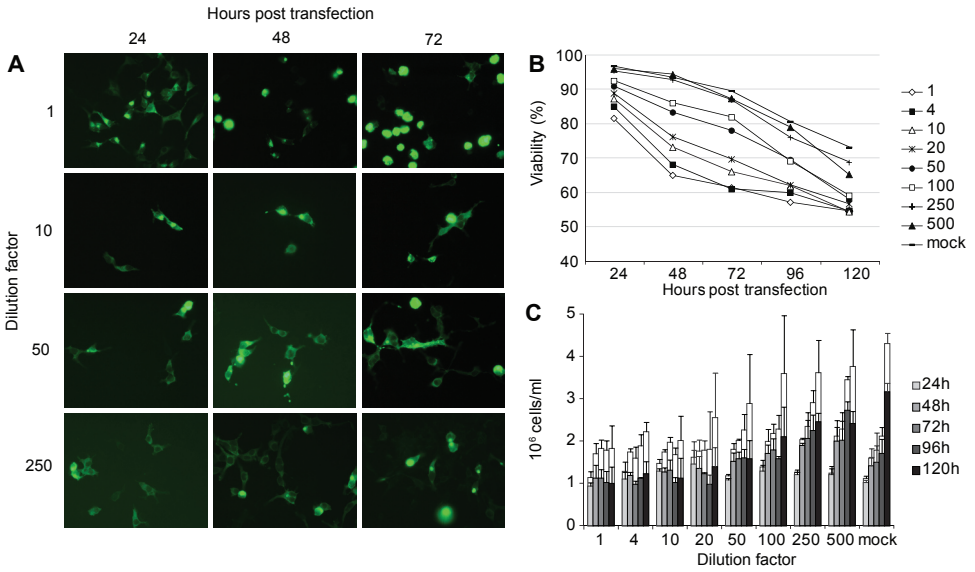

Figure 3. Plasmid titration reduces NOD1 aggregation and cell death. (A) Fluorescence micrographs of adherent HEK293E cells transfected with a range of dilutions of GFP-NOD1 expression plasmid. Cells were fixed at the indicated time points after transfection. (B) Time course of the viability of 20-ml cultures transfected with different dilutions of NOD1 expression plasmid or mock transfected. The graphs are an average of three independent transfections. Standard deviations are not shown for clarity. (C) Total cell count (white bars) and viable cell count (superimposed grey and black bars) of the cultures depicted in panel B.

For PKG, at 24h ptf, plasmid titration reduces the amount of total and soluble protein (Figure 4A,B). By 72h ptf dilutions up to 20-fold have converged to similar expression levels; for higher dilutions the final expression level becomes progressively lower. In the case of NOD1, the total amount of protein expressed follows a similar pattern showing a clear decrease at higher dilutions (Figure 4C). Soluble expression, however, shows a radically different pattern: initially, the amount of soluble protein is highest for the low dilutions, but as time progresses, more soluble protein is present at higher dilutions (Figure 4D). For all dilutions tested soluble expression reaches a maximum and then decreases (Figure 4E). With increasing dilution factors the maximum gradually shifts from 24h to 72h ptf. Importantly, the data show that for the standard protocol with undiluted expression plasmid and cell harvesting after 3-5 days, all protein is aggregated at the time of harvest and the presence of soluble protein at earlier time points will be overlooked.

For NLRC4, total expression is clearly reduced by plasmid titration (Figure 4F) as was also seen for the other proteins. In contrast to NOD1, the amount of soluble NLRC4 does not display a pronounced maximum as a function of time (Figure 4H). Although at standard transfection conditions a slight decrease in soluble protein is observed after 72h ptf, this decrease is minimal. Most other dilutions show an increase in soluble protein over time. Western blot analysis of soluble expression as function of dilution (Figure 4G) indicates that at 48h and 72h ptf a dilution factor of 10 improves soluble expression slightly. Limited analysis of total and soluble expression of NOD2 and NLRP3 at 48h and 72h ptf (Supplemental Figure S3) shows that for optimal soluble expression NOD2, like NOD1, requires a dilution factor of at least 50, whereas for NLRP3, as is the case for NLRC4, a 10-fold dilution is sufficient. The substantially higher dilution factor required for NOD1 and NOD2 may be

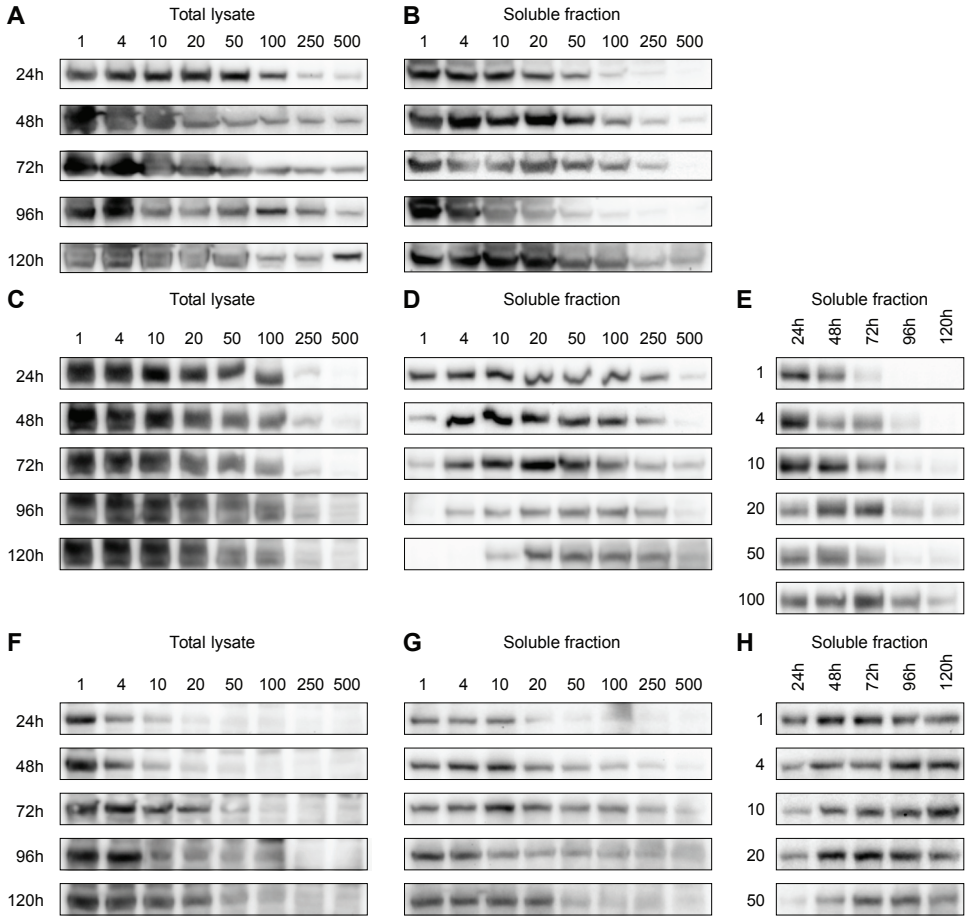

Figure 4. The effect of plasmid titration on total and soluble expression. Western blot analysis of total and soluble expression of PKG (A,B), NOD1 (C,D,E), and NLRC4 (F,G,H) in 20-ml HEK293E cultures transfected with the indicated plasmid dilutions and harvested at the indicated time points. To allow for better visual comparison of band intensities a subset of samples of soluble fractions were blotted twice; either arranged by harvest time (D,G) or by plasmid dilution (E,H). Western blots were probed with anti-His tag antibody

related to their higher total expression level and stronger negative effect on cell viability compared to NLRP3 and NLRC4 (Figure 2A,B).

In summary, whereas plasmid dilution markedly reduces total expression, a simultaneous increase in the amount of soluble NLR per culture volume is observed.

The effect of plasmid titration on protein yield.

We analyzed the effect of plasmid titration on the protein yield obtained from 20-ml cultures using single step purification on StrepTactin beads. Whereas relatively pure NLRC4 is obtained, we consistently observe co-purification of two proteins in the case of NOD1, NOD2, and NALP3 (Figure 5A). The co-purifying proteins were identified as HSP70 and HSP90 by Western blotting using specific antibodies (unpublished data). Association of these chaperones with NLRs has been reported previously[23-24]. Plasmid dilution has no effect on the presence or relative abundance of co-purified HSP70 and HSP90 (Supplemental Figure S4). Similar to what was observed for soluble protein, the yield of NOD1 rapidly decreases

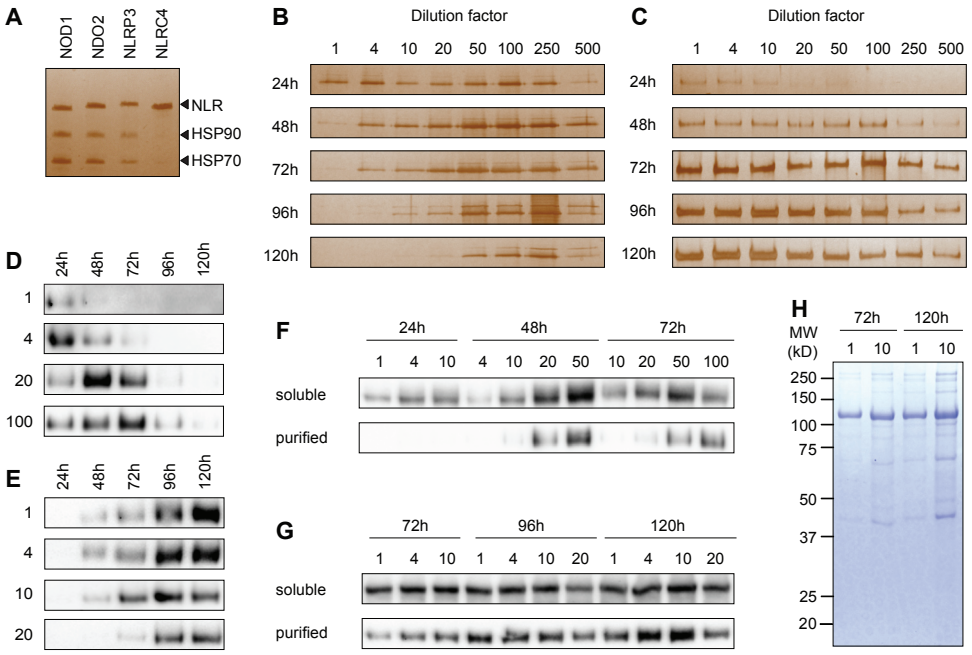

Figure 5. The effect of plasmid titration on protein yield. (A) SDS-PAGE analysis of the indicated NLRs after single-step purification on StrepTactin beads. (B and C) SDS-PAGE analysis of purified NOD1 (B) and NLRC4 (C) expressed using the indicated plasmid dilutions and harvested at the indicated time points; proteins were visualized by silver staining. (D and E) Selected samples of purified NOD1 (D) and NLRC4 (E) shown in panels B and C were analyzed on Western blot probed with anti-His tag antibody. (F and G) For quantification purposes selected samples of cleared lysates and purified protein of NOD1 (F) and NLRC4 (G) were re-analyzed on Western blot probed with anti-His tag antibody. (H) Coomassie stained SDS-PAGE gel of NLRC4 isolated by single-step purification on StrepTactin beads from four 200-ml cultures with harvest time and plasmid dilution factor as indicated. Bands were quantified to estimate protein purity and yield (Table 1).

with time, and, when plasmid dilution is applied, more protein is obtained at later time points (Figure 5B,D). To determine the optimal combination of dilution factor and harvest time, we re-analyzed selected samples on a single Western blot and quantified band intensities (Figure 5F). We find a clear optimum in both the amount of soluble protein in the cytosol and the yield after single-step purification at 50-fold dilution and cell harvesting at 48h ptf. At this optimum the amount of soluble NOD1 is increased 5-fold compared to undiluted plasmid at 24h ptf, whereas a 15-fold increase is observed after single-step purification compared to 10-fold diluted plasmid at 48h ptf. However, the association with chaperones suggests that the protein may not be properly folded. We find that the protein is prone to aggregation and we could not remove the chaperones by additional purification steps. For NLRC4 we generally see an increase in the protein yield over time (Figure

Table 1: Quantitative analysis of NLRC4 yield after single-step purification.

Harvest time (hours ptf)	72		120	
Dilution factor	**1**	**10**	**1**	**10**
Purity (%)	70	67	70	53
Yield (µg)	80	133	84	193
Volumetric yield (mg/L)	0.4	0.7	0.4	1.0

NLRC4 was isolated from four 200-ml HEK293E cultures by single-step StrepTactin purification as described. The yield was calculated based on the total protein content as measured by the absorbance at 280 nm and corrected for sample purity as quantified from the SDS-PAGE gel shown in Figure 5H.

5C,E). The effect of plasmid titration is less pronounced than observed for NOD1; quantitative analysis of band intensities indicates, however, that, compared to standard transfection conditions, 10-fold plasmid dilution and harvesting at 96h ptf improves the yield about 2-fold (Figure 5G). To assess whether the improvement in yield is reproducible also at larger scale we expressed NLRC4 in four parallel 200-ml cultures: HEK293E cells were transfected with either undiluted or 10-fold diluted expression plasmid, and harvested at 72h or 120h ptf (Table 1, Figure 5H). At 72h ptf, 10-fold plasmid dilution leads to an approximate 1.5-fold increase in yield, and at 120h ptf the yield is about 2-fold higher. The amount of protein obtained from cultures transfected at standard conditions does not increase between 72h and 120h. Although we typically observe that protein yield and cell viability differ somewhat between individual rounds of transfection, as well as between small and large-scale cultures, a modest 2-fold increase in protein yield is obtained at both scales.

Discussion

Since its first introduction, recombinant protein production in suspension growing HEK293E cells transfected using PEI[1] has gained considerable popularity. Transfection protocols for vectors containing the strong CMV promoter have been optimized for highly expressed proteins like SEAP[1,25]. Under optimized transfection conditions, transcriptional and translational processes are operating near to saturation and post-translational processes including protein folding may become limiting[22]. We expressed NLRs in the HEK293 expression system and find the standard transfection protocol to be far from optimal for this family of proteins; although it results in high NLR-expression, all or nearly all of the protein is present as insoluble aggregates and cell viability declines rapidly, limiting the build-up of biomass. Here we present plasmid titration, *i.e.* dilution of the expression vector with dummy plasmid, as a rapid and straightforward method to optimize protein production.

Standard transfections with NLR-encoding plasmids indicated that the amount of soluble protein reaches a maximum and then decreases. The effect of plasmid dilution is to reduce the rate of transcription and translation, and to shift the maximum of soluble protein expression to later time points. As it simultaneously improves cell viability, more biomass accumulates and thus more soluble protein is obtained per culture volume. A gain in yield likely arises from the combined effect of improved cell viability and an increase in the concentration of soluble protein. Since the amount of soluble protein in the culture is a function of the plasmid dilution factor and the time of harvest, the method exists of monitoring soluble expression at regular time intervals to determine the optimal combination thereof. The optimal dilution factor is highly protein specific. For NOD1, 50-fold dilution increases soluble expression in 20-ml cultures markedly, despite the fact that total protein expression is strongly reduced (Figure 4C,5F). For NLRC4, 10-fold plasmid dilution increased the protein yield obtained from 200-ml cultures 2-fold.

Whereas NOD1, like NOD2 and NLRP3, remains associated with HSP70 and HSP90, NLRC4 is relatively pure after single-step purification on StrepTactin beads (Figure 4H and Table 1). NLRC4 can be purified to near homogeneity using dual affinity tag purification followed by gelfiltration (Figure 5A in ref. 12 and Supplemental Figure S5). The purified protein is monomeric both on EM micrographs at low concentration[12] and on gelfiltration (Supplemental Figure S5B) and is functional as shown by the *in vitro* reconstitution of the NAIP5/NLRC4 inflammasome[12].

Although it was not an objective of our study to explain the mechanism underlying the effect of plasmid dilution, we speculate that it arises from attenuating the rate of transcription and translation to be more in pace with the folding capacity of the cell thereby reducing protein aggregation and cell death. The large aggregates observed by fluorescence microscopy (Figure 2D, 3A) are reminiscent of aggresomes, which are clusters of sequestered protein aggregates that form when the production of aggregation-prone proteins exceeds the capacity of the cell's folding machinery as well as that of the proteasome to clear the cytosol of improperly folded proteins[26-27]. Together with the aggregated proteins, chaperones and proteasomes are sequestered to the site of aggresome formation[27], and their formation often coincides with cellular death[28]. Possibly, protein aggregation is the direct cause of decreased cell viability during NLR expression. Consistently, the rapid decrease of cell viability seen for NOD1 and NOD2 (Figure 2B) coincides with a more severe and an earlier onset of aggregation (Figure 2D) than observed for NLRC4 and NLRP3.

We also considered downstream signaling by NLRs as a possible cause of decreased cell viability. Overexpression of NOD1 and NOD2 in HEK293T cells leads to spontaneous activation of NF-κB[29-30], whereas activation of signaling pathways downstream of NLRC4 and NRLP3 requires co-expression of additional components such as ASC and caspase-1[31-32]. NOD1 and NOD2 downstream signaling is abolished by removal of the CARD domains[30]. We expressed CARD domain deletion mutants of NOD1 and NOD2 and found these to affect cell viability far less than the full-length proteins do (unpublished data). The expression levels of the deletion mutants are, however, much lower than those of the native proteins, and thus we cannot definitively conclude whether the reduced expression level or the disruption of downstream signaling is the cause of improved cell viability.

Many proteins require transient interactions with chaperones for maturation into their native conformation. Our observation that NOD1, NOD2, and NLRP3, at all plasmid dilutions tested, remain associated with HSP70 and HSP90 in small-scale purifications (Figure 5A, Supplemental Figure 4) may indicate that these NLRs have not yet obtained their native conformation. On the other hand, association of NLRs with HSP90 and SGT1, a bona fide co-chaperone of HSP90, has been suggested to retain the protein in a signaling competent state prior to ligand detection[23-24, 33-34]. Co-expression of chaperones has been successfully used to enhance expression of soluble recombinant proteins in *E.coli* (reviewed in ref. 35). In analogy, we co-expressed HSP90 and SGT1 in HEK293E cells (unpublished data). For HSP90 we did not see any effect on cell viability or protein yield. Co-expression of SGT1 with NOD1 or NOD2 resulted in SGT1 co-purification and improved viability, but also caused a decrease in expression level of these NLRs without improving the yield of soluble protein. We were unable to separate the chaperones from these NLRs. In two recent studies NOD1 and NOD2 purified from lentivirus-transfected HEK293 cells and insect cells, respectively, were not associated with chaperones and functional protein was obtained[36-37]. At present it is not clear to us what causes the differential association with chaperones in these expression systems.

We present plasmid titration as a straightforward procedure requiring limited additional effort and therefore can be tested easily to optimize expression of recombinant proteins. Indications that a particular protein may benefit from plasmid titration are reduced cell viability and high total, but low soluble expression. Preliminary data from our lab on the application of this method to secreted

proteins suggest that some of these may benefit more from plasmid titration than NLRs do (unpublished data). We anticipate that plasmid titration may become a routine step in the optimization of recombinant protein production in HEK293E cells when the standard transfection protocol leads to severe protein aggregation.

Experimental procedures

Cell culture and transfection

Suspension growing HEK293E cells were cultured at 120 rpm in Freestyle medium (Invitrogen), containing 0.2% FCS and 50 µg/ml G418 disulfate in a humidified 5% CO_2 atmosphere at 37 °C. Adherent HEK293E cells were cultured in Dulbecco's Modified Eagle Medium with 4.5 g/L D-glucose (DMEM + Glutamax-II, Gibco), 10% FCS, 100 units/ml penicillin G sodium (Gibco), and 100 µg/ml Streptomycin sulfate (Gibco).

Small scale (4 mL, 20 mL) and large scale (1 L) transfections of suspension growing HEK293E cells were performed according to Durocher *et al*. [1], using 0.5 µg DNA/ml cell culture and 3 µg PEI/µg DNA. Series of transfections in which the amount of vector was systematically varied (referred to as plasmid titration) were performed by replacing expression vector DNA by empty pCR4-TOPO vector (Invitrogen), while keeping the total amount of DNA constant. Cell viabilities and cell counts were measured using a Casy Model TTC cell counter (Schärfe Systems, Germany).

Plasmids

cDNA of human *Nlrc4* and human *Nlrp3* was purchased from Invivogen. cDNA of human *Nod1* and human *Nod2* was a kind gift from M.G. Netea (Dept. of Medicine, Radboud University Nijmegen Medical Center, The Netherlands). The coding sequence for bovine cGMP-dependent protein kinase I alpha (PKG) was a kind gift from U-Protein Express BV (Utrecht, The Netherlands).

Coding sequences were amplified by PCR using forward primers that introduce a *BamHI* restriction site while omitting the start codon, and reverse primers that introduce a *NotI* restriction site and omit the stop-codon. At the protein level this procedure results in the introduction of a Gly-Ser sequence at the N-terminus and three Ala residues at the C-terminus. PCR products were subcloned into pCR4-TOPO vector (Invitrogen). The *BamHI*/*NotI* DNA fragments were subcloned into pUPE vectors (U-Protein Express BV, The Netherlands) that contain an expression cassette under control of the CMV promoter. Expression vectors encoded an N-terminal His_6-$StrepII_3$-TEV tag for *Nod1* and *Nod2*, and a C-terminal $StrepII_3$-His_6 tag for *Nlrp3* and *Nlrc4*, unless indicated otherwise. For fluorescence microscopy, each NLR and luciferase were expressed with an N-terminal His_6-TEV-eGFP tag. The empty pCR4-TOPO vector used as dummy DNA was created by restriction of the two *EcoRI* sites that flank the TA cloning site, followed by self-ligation.

Cell harvest and lysis

For analysis of total and soluble expression, cells were harvested by centrifugation at 600 x *g* for 2 min. Cell pellets were stored for 30 min up to 1 week at -20 °C. Prior to cell lysis, pellets were thawed at room temperature. Cytoplasmic extracts were obtained using a method described by Tsai et al. [19], with omission of the PBS washing step. This lysis method leaves the nuclear membranes intact. In short, cell pellets were resuspended in $1/10^{th}$ of the culture volume in cold small scale lysis buffer containing 10 mM HEPES pH 7.6, 5 mM $MgCl_2$, 10 mM KCl, 5 mM DTT, 1 µg/ml DNase, 0.3% NP40, and 1 tablet Complete mini, EDTA-free tablets (Roche) per 20 ml buffer. Cleared lysates were obtained by centrifugation at 10.000 x *g* for 10 min.

Protein purification and quantification

$StrepII_3$-tagged proteins were purified from the cleared lysates using StrepTactin Sepharose beads (GE Healthcare). After incubation for 1-2h at 4 °C, beads were washed in StrepTactin wash buffer (100 mM NaCl, 25 mM HEPES pH 7.5, 5 mM benzamidin, 5% glycerol, 2 mM DTT), and subsequently protein was eluted in wash buffer supplemented with 5 mM *d*-desthiobiotin (Sigma).

For the purification of NLRC4-$StrepII_3$-His_6 from 200 ml HEK293E cultures, cells were harvested by centrifugation at 600 x *g* for 15 min. Cell pellets were stored for 1 hour up to 2 days at -80 °C. Cell lysis was performed as described above. The cleared lysates was obtained by centrifugation at 22.000 x *g* for 15 min. The protein was purified as described above. The protein concentration in samples of purified NLRC4 was determined from the absorbance at 280 nm as measured on a NanoDrop Spectrophotometer ND-1000 (NanoDrop Technologies; Wilmington, Delaware) using a value for A_{280} (1 mg/ml) of 0.9.

Gel electrophoresis and protein detection
Prior to gel electrophoresis, samples of total cell lysate were diluted 10-fold with lysis buffer to obtain a volume equal to the original harvest volume. The soluble fraction was obtained from the cleared lysates or, for the gel depicted in Figure 1B, diluted 10-fold. Reduced protein samples were separated on standard Laemmli 9% SDS-PAGE gels. Gels were silver stained, Coomassie stained, or transferred to polyvinylidene difluoride (PVDF) membrane (BioRad). Proteins were detected on Western blot using a mixture of mouse anti-polyHistidine (Sigma) and mouse anti-Penta-His (Qiagen) as primary antibodies and rabbit anti-mouse-HRP (Dako) as the secondary antibody. The signal was detected using ECL (GE Healthcare). Quantification of stained SDS-PAGE gels or Western blots was done using ImageLab Software (version 3.0.1 Beta 2, Bio-Rad Laboratories).

Fluorescence microscopy and flow cytometry
Adherently growing HEK293E cells were seeded in 12-well plates on coverslips at a density of $0.2x10^6$ cells/well the day prior to transfection. For each condition, 1 µg of total DNA was transfected using PEI as described by Durocher et al. [1]. At 24-72h post transfection, medium was removed, coverslips were washed once with PBS, and then fixed with 4% paraformaldehyde (Fluka) in PBS for 15 min. Coverslips were washed three times in PBS for 5 min, stained with DAPI for 10 min, and again washed three times with PBS for 5 min. Finally, coverslips were fixed on glass slides with FluoSafe (Calbiochem). Fluorescent images were acquired using an Olympus AX70 widefield fluorescence microscope, and imaged with a Nikon digital camera DXM1200 using its associated software Nikon ACT-1 (version 2.63).
FACS analysis of suspension growing HEK293E cells expressing GFP was performed 48h post transfection. As the background from Freestyle medium is negligible, cells were analyzed directly from the medium. GFP fluorescence was measured by BD FACSCalibur (BD biosciences), and the data was analyzed using the software CellQuest Pro (version 5.1).

References

1. Durocher, Y., S. Perret, and A. Kamen, *High-level and high-throughput recombinant protein production by transient transfection of suspension-growing human 293-EBNA1 cells.* Nucleic Acids Res, 2002. **30**(2): p. E9.
2. Geisse, S. and M. Henke, *Large-scale transient transfection of mammalian cells: a newly emerging attractive option for recombinant protein production.* J Struct Funct Genomics, 2005. **6**(2-3): p. 165-70.
3. Pham, P.L., A. Kamen, and Y. Durocher, *Large-scale transfection of mammalian cells for the fast production of recombinant protein.* Mol Biotechnol, 2006. **34**(2): p. 225-37.
4. Foecking, M.K. and H. Hofstetter, *Powerful and versatile enhancer-promoter unit for mammalian expression vectors.* Gene, 1986. **45**(1): p. 101-5.
5. Chen, G., et al., *NOD-like receptors: role in innate immunity and inflammatory disease.* Annu Rev Pathol, 2009. **4**: p. 365-98.
6. Chamaillard, M., et al., *An essential role for NOD1 in host recognition of bacterial peptidoglycan containing diaminopimelic acid.* Nat Immunol, 2003. **4**(7): p. 702-7.
7. Girardin, S.E., et al., *Nod2 is a general sensor of peptidoglycan through muramyl dipeptide (MDP) detection.* J Biol Chem, 2003. **278**(11): p. 8869-72.
8. Inohara, N., et al., *Host recognition of bacterial muramyl dipeptide mediated through NOD2. Implications for Crohn's disease.* J Biol Chem, 2003. **278**(8): p. 5509-12.
9. Kofoed, E.M. and R.E. Vance, *Innate immune recognition of bacterial ligands by NAIPs determines inflammasome specificity.* Nature, 2011.
10. Zhao, Y., et al., *The NLRC4 inflammasome receptors for bacterial flagellin and type III secretion apparatus.* Nature, 2011. **477**(7366): p. 596-600.
11. Miao, E.A., et al., *Innate immune detection of the type III secretion apparatus through the NLRC4 inflammasome.* Proc Natl Acad Sci U S A, 2010. **107**(7): p. 3076-80.
12. Halff, E.F., et al., *Formation and structure of a NAIP5-NLRC4 inflammasome induced by direct interactions with conserved N- and C-terminal regions of flagellin.* J Biol Chem, 2012.
13. Franchi, L., R. Munoz-Planillo, and G. Nunez, *Sensing and reacting to microbes through*

the inflammasomes. Nat Immunol, 2012. **13**(4): p. 325-32.
14. Joosten, L.A., et al., *Differential function of the NACHT-LRR (NLR) members Nod1 and Nod2 in arthritis.* Proc Natl Acad Sci U S A, 2008. **105**(26): p. 9017-22.
15. Hoffman, H.M., et al., *Mutation of a new gene encoding a putative pyrin-like protein causes familial cold autoinflammatory syndrome and Muckle-Wells syndrome.* Nat Genet, 2001. **29**(3): p. 301-5.
16. Ogura, Y., et al., *A frameshift mutation in NOD2 associated with susceptibility to Crohn's disease.* Nature, 2001. **411**(6837): p. 603-6.
17. Hugot, J.P., et al., *Association of NOD2 leucine-rich repeat variants with susceptibility to Crohn's disease.* Nature, 2001. **411**(6837): p. 599-603.
18. Hysi, P., et al., *NOD1 variation, immunoglobulin E and asthma.* Hum Mol Genet, 2005. **14**(7): p. 935-41.
19. Tsai, A. and R.P. Carstens, *An optimized protocol for protein purification in cultured mammalian cells using a tandem affinity purification approach.* Nat Protoc, 2006. **1**(6): p. 2820-7.
20. Alverdi, V., et al., *cGMP-binding prepares PKG for substrate binding by disclosing the C-terminal domain.* J Mol Biol, 2008. **375**(5): p. 1380-93.
21. Rajendra, Y., et al., *Role of non-specific DNA in reducing coding DNA requirement for transient gene expression with CHO and HEK-293E cells.* Biotechnol Bioeng, 2012. **109**(9): p. 2271-8.
22. Carpentier, E., et al., *Limiting factors governing protein expression following polyethylenimine-mediated gene transfer in HEK293-EBNA1 cells.* J Biotechnol, 2007. **128**(2): p. 268-80.
23. Hahn, J.S., *Regulation of Nod1 by Hsp90 chaperone complex.* FEBS Lett, 2005. **579**(20): p. 4513-9.
24. Mayor, A., et al., *A crucial function of SGT1 and HSP90 in inflammasome activity links mammalian and plant innate immune responses.* Nat Immunol, 2007. **8**(5): p. 497-503.
25. Pham, P.L., et al., *Transient gene expression in HEK293 cells: peptone addition posttransfection improves recombinant protein synthesis.* Biotechnol Bioeng, 2005. **90**(3): p. 332-44.
26. Johnston, J.A., C.L. Ward, and R.R. Kopito, *Aggresomes: a cellular response to misfolded proteins.* J Cell Biol, 1998. **143**(7): p. 1883-98.
27. Kopito, R.R., *Aggresomes, inclusion bodies and protein aggregation.* Trends Cell Biol, 2000. **10**(12): p. 524-30.
28. Markossian, K.A. and B.I. Kurganov, *Protein folding, misfolding, and aggregation. Formation of inclusion bodies and aggresomes.* Biochemistry (Mosc), 2004. **69**(9): p. 971-84.
29. Inohara, N., et al., *Nod1, an Apaf-1-like activator of caspase-9 and nuclear factor-kappaB.* J Biol Chem, 1999. **274**(21): p. 14560-7.
30. Ogura, Y., et al., *Nod2, a Nod1/Apaf-1 family member that is restricted to monocytes and activates NF-kappaB.* J Biol Chem, 2001. **276**(7): p. 4812-8.
31. Poyet, J.L., et al., *Identification of Ipaf, a human caspase-1-activating protein related to Apaf-1.* J Biol Chem, 2001. **276**(30): p. 28309-13.
32. Agostini, L., et al., *NALP3 forms an IL-1beta-processing inflammasome with increased activity in Muckle-Wells autoinflammatory disorder.* Immunity, 2004. **20**(3): p. 319-25.
33. Lee, K.H., et al., *Proteasomal degradation of Nod2 mediates tolerance to bacterial cell wall components.* J Biol Chem, 2012.
34. da Silva Correia, J., et al., *SGT1 is essential for Nod1 activation.* Proc Natl Acad Sci U S A, 2007. **104**(16): p. 6764-9.
35. Francis, D.M. and R. Page, *Strategies to optimize protein expression in E. coli.* Curr Protoc Protein Sci, 2010. **Chapter 5**: p. Unit 5 24 1-29.
36. Mo, J.Y., et al., *Pathogen sensing by nucleotide-binding oligomerization domain-containing protein 2 (NOD2) is mediated by direct binding to muramyl dipeptide and ATP.* J Biol Chem, 2012.
37. Askari, N., et al., *Expression, purification, and characterization of recombinant NOD1 (NLRC1): A NLR family member.* J Biotechnol, 2011.

Supplementary figures

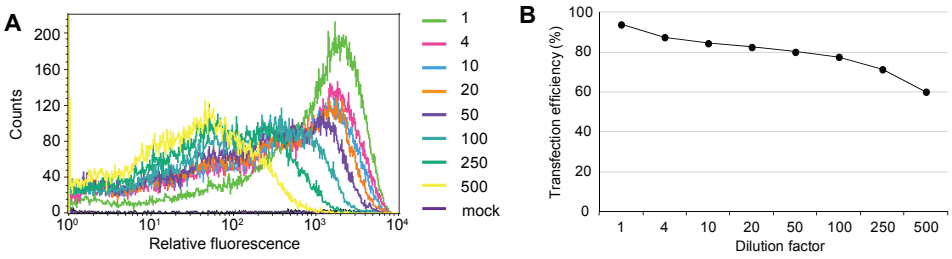

Supplementary Figure S1. The effect of plasmid titration on GFP expression and transfection efficiency. (A) Flow cytometry analysis of GFP expression in HEK293E cells at 48h ptf. HEK293E cells were transfected with the indicated dilution factors of GFP expression plasmid or mock-transfected. The gain was adjusted such that 99% of mock transfected cells have a relative GFP fluorescence intensity (FL1-H) below 10^1. For each condition a total of 50.000 live cells was counted. (B) Transfection efficiency as function of plasmid dilution. The transfection efficiency was calculated as the percentage of live cells that expressed GFP (relative fluorescence > 10^1) compared to the total number of live cells.

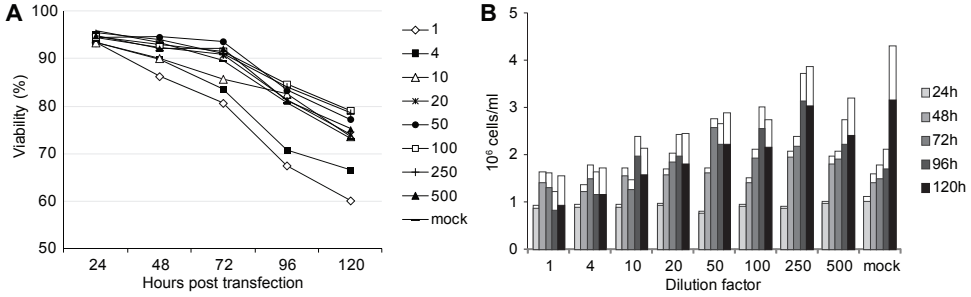

Supplementary Figure S2. The effect of PKG plasmid titration on cell viability and biomass. (A) Time course of the viability of 20-ml HEK293E cultures transfected with different dilutions of PKG expression plasmid or mock transfected. (B) Total cell count (white bars) and viable cell count (superimposed grey and black bars) of the cultures depicted in panel A.

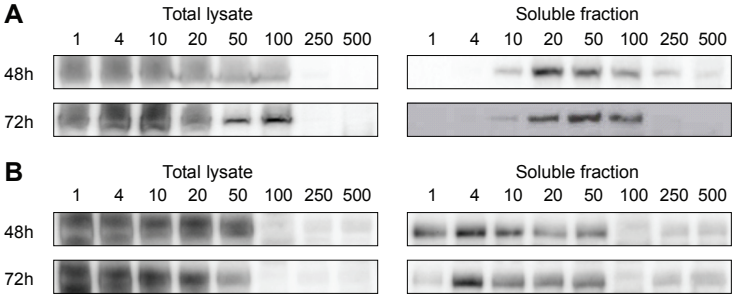

Supplementary Figure S3. Analysis of NOD2 and NLRP3 plasmid titration. Western blot analysis of total and soluble expression of NOD2 (A) or NLRP3 (B) in 4-ml HEK293E cell cultures transfected with the indicated dilution factors and harvested at 48h or 72h ptf. Blots were probed with anti-His tag antibody.

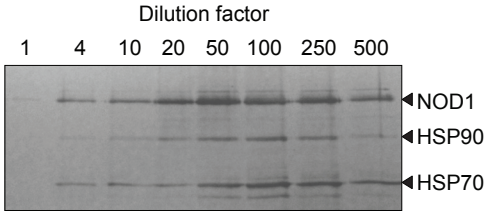

Supplementary Figure S4. NOD1 co-purifies with HSP70 and HSP90 at all plasmid dilutions. SDS-PAGE analysis of NOD1 purified by single step purification on StrepTactin beads, visualized by silver staining. NOD1 was expressed using the indicated plasmid dilutions and harvested at 72h ptf.

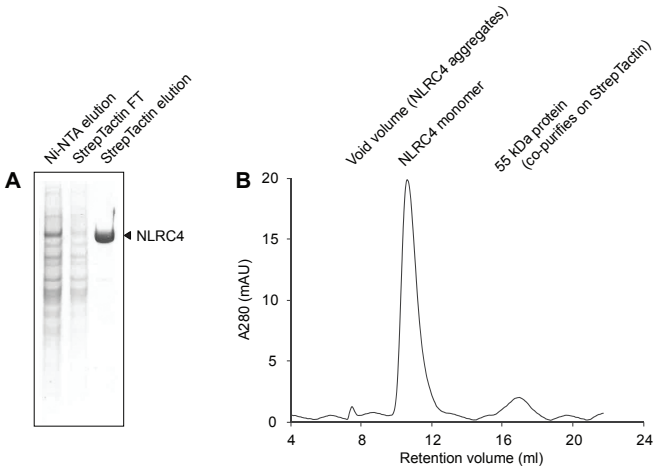

Supplementary Figure S5. Analysis of NLRC4 purification. (A) SDS-PAGE analysis of the NLRC4 from 2L cultures showing sample purity after His_6 tag and $StrepII_3$ tag affinity purification, visualized by Coomassie staining. (B) Gelfiltration chromatogram of NLRC4 applied on Superdex200 after His_6 tag and $StrepII_3$ tag tandem affinity purification.

Chapter **3**

Formation and Structure of a NAIP5-NLRC4 Inflammasome Induced by Direct Interactions with Conserved N- and C-terminal Regions of Flagellin

Els F. Halff[1], Christoph A. Diebolder[1,2], Marian Versteeg[1], Arie Schouten[1], T. Harma C. Brondijk[1], Eric G. Huizinga[1]

1. Crystal and Structural Chemistry, Bijvoet Center for Biomolecular Research, Department of Chemistry, Faculty of Science, Utrecht University, The Netherlands
2. Section Electron Microscopy, Department of Molecular Cell Biology, Leiden University Medical Center, The Netherlands

J Biol Chem; Vol. 287, Issue 46 (2012)

Formation and Structure of a NAIP5-NLRC4 Inflammasome Induced by Direct Interactions with Conserved N- and C-terminal Regions of Flagellin

TThe NOD-like receptors NAIP5 and NLRC4 play an essential role in the innate immune response to the bacterial tail protein flagellin. Upon flagellin detection NAIP5 and NLRC4 form a hetero-oligomeric inflammasome that induces caspase-1 dependent cell death. So far, both the mechanism of formation of the NAIP5-NLRC4 inflammasome and its structure are poorly understood. In this study we combine inflammasome reconstitution in HEK293 cells, purification of inflammasome components, and negative stain electron microscopy to address these issues. We find that a Salmonella typhimurium flagellin fragment comprising the D0 domain and the neighboring spoke region is able to co-precipitate NAIP5 and induce formation of the NAIP5-NLRC4 inflammasome. Comparison with smaller fragments indicates that flagellin recognition is mediated by its C-terminal residues as well as the spoke region. We reconstitute the inflammasome from purified flagellin, NAIP5, and NLRC4, thus proving that no other cellular components are required for its formation. Electron micrographs of the purified inflammasome provide unprecedented insight into its architecture revealing disk-like complexes consisting of eleven or twelve protomers in which NAIP5 and NLRC4 appear to occupy equivalent positions. On the basis of our data we propose a model for inflammasome formation wherein direct interaction of flagellin with a single NAIP5 induces the recruitment and progressive incorporation of NLRC4 resulting in the formation of a hetero-oligomeric inflammasome.

Introduction

The NOD-like receptor (NLR) family comprises cytosolic receptors of the innate immune system that respond to a wide variety of pathogen and danger associated molecular patterns. The NLR family members NLRC4 (also known as IPAF) and NAIP5 play important roles in the control of *Legionella* and *Salmonella* infections in mice by sensing the bacterial tail protein flagellin[1-6].

NLRs are characterized by a highly conserved nucleotide binding NACHT (NAIP, CIIA, HET-E, and TP1) domain. The NLRs share a C-terminal leucine-rich repeat (LRR) domain, which is thought to be involved in ligand recognition and retaining the NLR in an inactive state. At their N-terminus NLRs possess one or more copies of an effector domain, the identity of which varies between family members; NLRC4 contains an N-terminal caspase activating and recruitment domain (CARD) that interacts with the CARD domain of pro-caspase-1[7-9], whilst NAIP5 contains three N-terminal baculovirus inhibitor of apoptosis protein repeat (BIR) domains.

Upon ligand-recognition, several NLRs form high molecular weight complexes, known as inflammasomes, that activate pro-caspase-1[10-12]. Activated caspase-1 mediates the proteolytic processing of pro-interleukins pro-IL-1β and pro-IL-18[10,13], and induces an inflammatory cell death known as pyroptosis[14]. Several purified NLR NACHT domains were shown to bind nucleotides[15-19], but the exact role of ATP binding and whether hydrolysis takes place is unclear. In some studies mutation of the conserved Walker A lysine that coordinates the nucleotide gamma-phosphate reduces

spontaneous and ligand-induced self-association and downstream signaling[6,16-18,20], whereas others reported no significant effects[6].

Information on inflammasome structure so far derives from negative stain electron microscopy on NLRP1, which revealed pentameric and heptameric ring-like structures[21]. Likely, the architecture of inflammasomes resembles that of apoptosomes formed by Apaf-1, CED4, and Dark, which, like NLRs, contain a NACHT domain essential for oligomerization. For apoptosomes higher resolution data is available that shows heptameric or octameric rings that are stabilized via homotypic interactions between the NACHT domains[22-26].

Recently, it has been shown that ligand-specificity of the NLRC4 inflammasome is determined by members of the NAIP family[5-6]. In mice, NLRC4 and NAIP2 form an inflammasome in response to PrgJ, a component of the bacterial type III secretion system, whereas NLRC4 together with either NAIP5 or NAIP6 recognizes flagellin. In humans only one NAIP variant exists, which forms a complex with NLRC4 upon detection of CprI, a PrgJ homologue. NAIP5-NLRC4 dependent cell death can be induced by a 35 residue C-terminal region of flagellin, and was suggested to depend on three conserved leucine residues near the C-terminus[4-5].

In this study we show that besides the flagellin C-terminal 35-residues other elements in its N- and C-terminal regions contribute to inflammasome formation. We reconstitute the inflammasome from its purified components and find by electron microscopy that NAIP5-NLRC4 complexes contain 11 or 12 subunits and therefore are considerably larger than was expected based on homologous structures. We propose a model for the formation of the NAIP5-NLRC4 inflammasome in which flagellin binding to NAIP5 leads to the recruitment of multiple copies of NLRC4 resulting in the formation of a disk-shaped hetero-oligomeric complex in which both NLRs occupy equivalent positions.

Results

Full length flagellin, but not its F41 fragment, induces inflammasome formation

To study flagellin-induced NAIP5-NLRC4 inflammasome formation, we reconstituted the inflammasome by transient transfection of its components in HEK293E cells, which do not endogenously express *Naip5, Nlrc4,* and caspase-1. Expression of caspase-1 alone does not lead to a significant reduction in cell viability, showing that caspase-1 auto-activation is negligible (Fig. 1*A*). Likewise, in the absence of caspase-1, expression of *Naip5* or *Nlrc4* does not cause a decrease in cell viability. As described previously[6] we noted some loss of cell viability upon co-expression of *Nlrc4* with caspase-1. This effect depends on the *Nlrc4* expression level and is diminished when less *Nlrc4* DNA is transfected (data not shown). Co-expression with flagellin likewise reduces *Nlrc4* expression to a level at which no effect on cell viability is detected (Fig. 1*A* and supplemental Fig. S1) and therefore NLRC4 auto-activation does not affect the measurements of flagellin induced activation in our reconstituted system.

The reconstituted system was used to study inflammasome activation by flagellin from *Salmonella typhimurium* and *Salmonella enterica.* In addition to full-length flagellin, we tested the flagellin F41 fragment that lacks the amino- and carboxy-terminal helices that are essential for flagellin filament assembly[32-33]. All transfections were performed with and without caspase-1, and the difference in cell-viability, determined 48 hours post-transfection, was taken as a measure for caspase-1 induced cell-death (Fig. 1*A*). No significant increase in cell death is observed when flagellin is

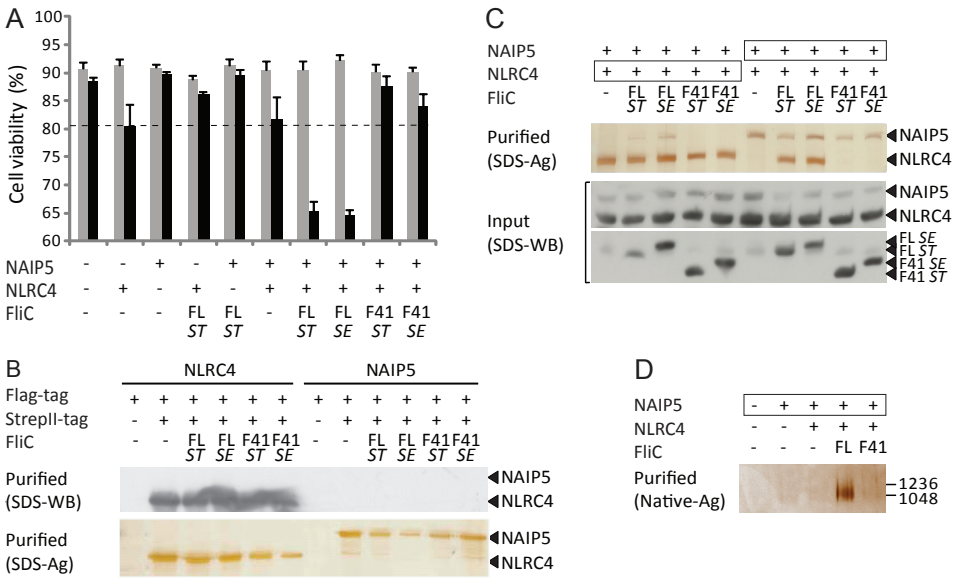

Figure 1: NLRC4 and NAIP5 form a caspase-1 activating complex in the presence of full length but not F41 *Salmonella* flagellin. *A*, Viabilities of HEK293E cells 48h after transfection with the indicated proteins. Flagellin (FL) or its F41 fragment originate from the flagellin gene (*FliC*) of *Salmonella typhimurium* (*ST*) or *Salmonella enteritidis* (*SE*). Gray and black bars represent transfections without and with caspase-1, respectively. Average values and standard deviations were derived from at least three independent transfections. Expression of all proteins was verified by Western blot (not shown). The dashed line represents non-specific cell death during NLRC4/caspase-1 co-expression in the absence of ligand as explained in the text. *B*, Analysis of NAIP5 and NLRC4 homo-oligomerization in HEK293E cells transfected with flagellin and differentially tagged mNAIP5 or mNLRC4 as indicated. Proteins isolated by StrepII-tag purification were analyzed on Western blot probed with anti-Flag-tag antibody (top panel) or analyzed by SDS-PAGE followed by silver staining (bottom panel). *C*, Analysis of inflammasome formation in HEK293E cells transfected with the proteins indicated. The boxed proteins carry the His_6-$StrepII_3$ purification handle. Other proteins were expressed with a His_6-$Flag_3$-TEV tag. Purified protein was analyzed by SDS-PAGE followed by silver staining (top panel). The cleared cell lysate was analyzed on Western blot probed with anti-His-tag antibody (middle and bottom panel). *D*, Native PAGE analysis of proteins purified as described in panel C on silver stained native PAGE (3-12%). Numbers on the right indicate the molecular weight of the marker in kDa.

co-expressed with either *Naip5* or *Nlrc4*. However, co-expression of *Salmonella* flagellin with *Naip5* plus *Nlrc4* leads to a 20-25% reduction of cell viability indicating formation of a functional inflammasome. Notably, co-expression of the flagellin F41 fragment with *Nlrc4* and *Naip5* does not induce caspase-1 dependent cell death, suggesting that the F41 fragment lacks a region that is essential for NAIP5-NLRC4 inflammasome formation.

To analyze the formation and composition of flagellin induced complexes, we purified the inflammasome from cell lysates using streptavidin-affinity purification. We selected StrepII-tag based purification, which involves a mild elution procedure, to minimize inflammasome dissociation. To this end we fused either NLRC4 or NAIP5 to a C-terminal His_6-$StrepII_3$-tag while the other NLR as well as flagellin were fused to a His_6-$Flag_3$-tag. Self-association of NLRs was analyzed by co-transfection of two variants carrying either a His_6-$StrepII_3$-tag or a His_6-$Flag_3$-tag. We find that NLRC4 self-associates in the absence of ligand (Fig. 1*B*), consistent with the mild increase in caspase-1 dependent cell death associated with *Nlrc4* expression in the viability assay (Fig. 1*A*). For NAIP5 we do not observe self-association even in the presence of flagellin (Fig. 1*B*). NAIP5 and NLRC4, when co-

expressed in the absence of ligand, do not co-purify (Fig. 1*C*). In the presence of flagellin, NAIP5 and NLRC4 do co-purify, whereas co-expression with the F41 fragment does not induce complex formation. Analysis of the purified inflammasome by silver-stained native PAGE shows that flagellin, unlike the F41 fragment, induces formation of a large complex that runs at about the same height as the 1.0 and 1.2 MDa marker proteins (*i.e.* IgM pentamer and hexamer respectively; Fig. 1*D*). NAIP5-NLRC4 complex formation is observed independent of which protein harbors the $StrepII_3$-tag (Fig. 1*C*). No other proteins were seen to co-purify in amounts detectable by silver-stained SDS-PAGE, suggesting that the inflammasome complex consists of NAIP5 and NLRC4 only. Flagellin was also not detectable on silver-stained gels, but could be detected on Western blot (not shown), which indicates that flagellin is not present in the inflammasome complex in stoichiometric amounts.

Thus we show that flagellin, but not its F41 fragment, induces binding between NAIP5 and NLRC4, resulting in the formation of a high molecular weight complex. The formation of this NAIP5-NLRC4 complex is correlated with the ability to activate caspase-1, resulting in cell death. We conclude that the part of flagellin that is missing in the F41 fragment contains one or more determinants that are essential for NAIP5-NLRC4 inflammasome formation.

Elements within flagellin contributing to inflammasome formation

Flagellin essentially consists of four distinct domains: D0, D1, D2 and D3 (Fig. 2*A*)[33-34]. The D0 and D1 domains, which form the flagellar inner and outer tube respectively, are connected by the so-called spokes. The F41 fragment lacks the complete D0 domain, the spokes, and a small part of the D1 domain. Since this region is clearly indispensible for NAIP5-NLRC4 inflammasome formation, we wondered which element(s) within this region are involved. We designed two constructs comprising the D0 domain of *S. typhimurium* flagellin. The longer construct, $D0_L$, is exactly complementary to the F41 fragment. The design of the shorter construct, $D0_S$, was based on the EM structure of flagellin[33] and comprises the D0 domain plus a small part of the spokes (Fig. 2*A,B*). In both $D0_L$ and $D0_S$ a Gly-Ser-repeat-loop connects N- and C-terminal halves of the construct. In addition, we made deletion constructs of *S. typhimurium* flagellin lacking either the N-terminal half of $D0_L$ (FliC-ΔN) or its C-terminal half (FliC-ΔC), as well as constructs comprising the isolated N-terminal half of $D0_L$ (FliC-N) or its C-terminal half (FliC-C) (Fig. 2*A*). For these constructs domain boundaries are complementary to the F41 fragment.

When co-expressed with *Nlrc4* and *Naip5,* the $D0_L$ construct as well as the shorter $D0_S$ construct induce caspase-1 dependent cell-death (Fig. 2*C*). The same is true for the N-terminal deletion mutant FliC-ΔN. The deletion of the C-terminal region in FliC-ΔC, however, abrogates caspase-1 induced cell-death. Whereas this finding suggests that the main determinant for caspase-1 activation is located in the C-terminus, co-expressions with the isolated N- and C-terminal flagellin fragments show that these induce caspase-1 dependent cell-death equally effective. The effect of the N- and C-terminal regions therefore appears to be context dependent. All flagellin fragments that induced caspase-1 dependent cell death also induce NAIP5-NLRC4 complex formation as evidenced by co-purification of NLRC4 with StrepII-tagged NAIP5 (Fig. 2*D*, top panel). The flagellin fragments do not co-purify with the complex in stoichiometric amounts, as we also observed for full-length flagellin, suggesting their interaction with the complex is relatively weak. As expected, the FliC-ΔC fragment that failed to induce cell death also failed to induce complex formation.

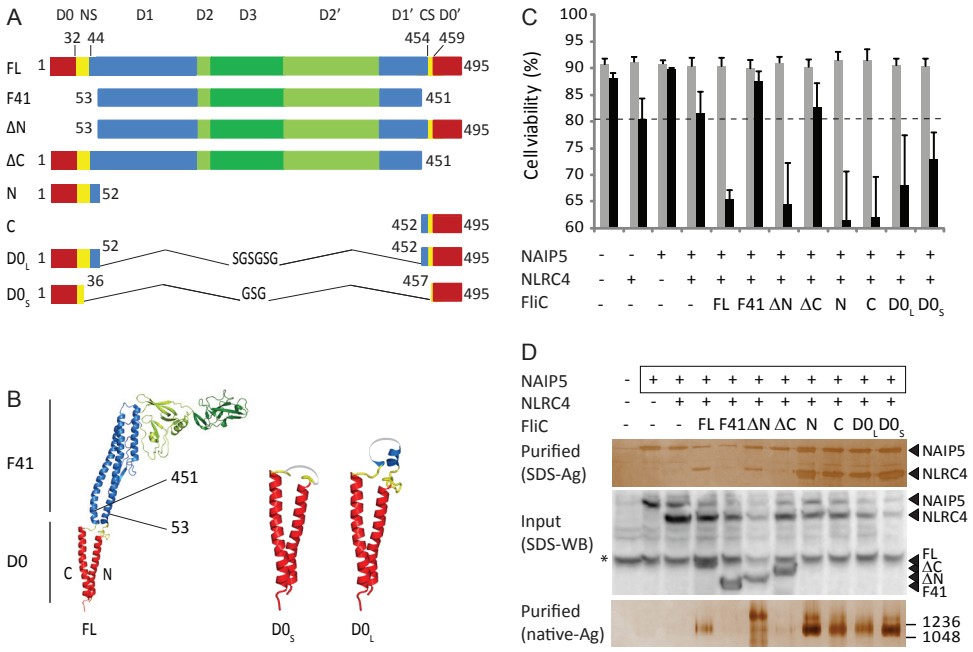

Figure 2: Flagellin fragments contribute differently to caspase-1 dependent cell death and inflammasome formation. *A*, Schematic representation of the flagellin constructs used in this study. Numbers indicate the inclusive amino acid boundaries of the various constructs or of the N-terminal spoke (NS) and C-terminal spoke (CS). For the F41 fragment domain boundaries were taken from Samatey *et al.*[34]; boundaries for D0 and the spokes were taken from Yonekura *et al.*[33]. *B*, Cartoon representation of the flagellin EM structure (PDB ID: 1UCU). Numbers indicate the boundaries of the F41 fragment. Domains are colored as in panel A. The Gly-Ser-repeat-loops that connect the N- and C-terminal halves of $D0_L$ and $D0_S$ are depicted in gray. *C*, Viabilities of HEK293E cells 48h after transfection with the indicated proteins. For further explanation see Fig. 1*A*. *D*, Analysis of inflammasome formation in HEK293E cells transfected with the proteins indicated. The boxed proteins carry the His_6-$StrepII_3$ purification handle. Other proteins were expressed with a His_6-$Flag_3$-TEV tag. Purified protein was analyzed by SDS-PAGE (top panel) or native PAGE (3-12%; bottom panel) followed by silver staining. For the native gel, numbers on the right indicate the molecular weight of the marker in kDa. The cleared cell lysate was analyzed on Western blot probed with anti-His-tag antibody (middle panel). The asterisk denotes a protein that interacts non-specifically with the antibody.

When analyzed by native PAGE, the purified complexes give rise to at least two bands of high molecular weight indicating heterogeneity in the complexes formed. The relative abundance of these bands varies between individual purifications and appears to be independent of the flagellin fragment employed (not shown).

Taken together, we show that all elements required for NAIP5-NLRC4 inflammasome formation are located within the flagellin $D0_L$ fragment, and that, although their effect appears to be context dependent, both the N-terminal and the C-terminal half of $D0_L$ are capable of inducing inflammasome formation and the associated caspase-1 induced cell death.

Contribution of flagellin C-terminal leucines to inflammasome formation

Previously, it was shown that mutation of three conserved leucines near the C-terminus of flagellin severely reduces its capacity to induce NAIP5-NLRC4 inflammasome formation[4-5]. Our observation that FliC-N also induces inflammasome formation indicates, however, that other segments besides the C-terminus are involved. To investigate the relative importance of the conserved leucine residues, we mutated

them to alanine (-3LA) in the various flagellin constructs.

Flagellin-3LA and $D0_L$-3LA still induce a caspase-1 dependent decrease in cell viability as well as formation of a NAIP5-NLRC4 complex, although the amount of complex detected was less than observed for wild type flagellin (Figure 3*A,B*). In contrast, the capacity of the shorter constructs $D0_S$-3LA and especially FliC-C-3LA to decrease cell viability appears reduced and these constructs are no longer able to induce formation of detectable amounts of the NAIP5-NLRC4 complex. Thus, whereas our data confirm the importance of the three leucine residues near the flagellin C-terminus, their role appears less prominent for larger fragments. The different responses to $D0_L$-3LA versus $D0_S$-3LA suggests that the spoke region, that is mostly missing in $D0_S$, also contributes to NAIP5-NLRC4 complex formation.

Association of flagellin fragments with the NAIP5-NLRC4 inflammasome and its components

Flagellin induces formation of a high molecular weight NAIP5-NLRC4 complex. However, our inability to detect flagellin in purified samples of the complex on silver-stained SDS-PAGE gels may indicate that the flagellin-inflammasome interaction is rather weak. Since interactions between full-length flagellin and the inflammasome components have been observed[5-6], we decided to use an alternative approach in which flagellin and its fragments were fused to a 15-residue biotin acceptor peptide (BAP) that is biotinylated *in vivo* by co-expression of the *E. coli* biotin ligase BirA[35]. The BAP-tagged flagellin constructs were co-expressed with His_6-$Flag_3$-tagged *Naip5* and/or *Nlrc4* and precipitated using StrepTactin-sepharose beads. In this set-up, biotinylated flagellin precipitated a NAIP5-NLRC4 complex that was clearly visible on silver-stained SDS-PAGE gels (Fig. 4), showing that direct binding of flagellin to the NAIP5-NLRC4 complex does occur.

Biotinylated versions of the flagellin fragments that induced inflammasome formation and caspase-1 dependent cell death also co-precipitate the NAIP5-NLRC4 complex, except for biotinylated FliC-N. Possibly the interaction between the N-terminus and the complex, even in this set-up, is too weak to withstand the isolation procedure.

Binding of biotinylated flagellin to the individual NLRs was not detected (Fig. 4). Remarkably however, the $D0_L$ fragment interacted with NAIP5 even in the absence of NLRC4 as evidenced by the co-precipitation of significant quantities of NAIP5. None of the other flagellin fragments was able to precipitate NAIP5 in detectable amounts.

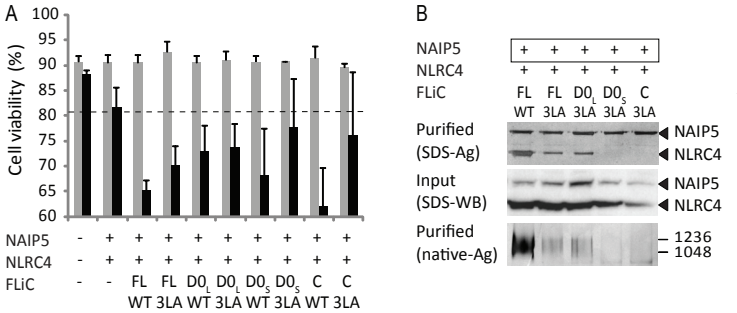

Figure 3: Contribution of flagellin C-terminal leucines to inflammasome formation. *A*, Viabilities of HEK293E cells 48h after transfection with the indicated proteins. For further explanation see Fig. 1*A*. *B*, Analysis of inflammasome formation in HEK293E cells transfected with the proteins indicated. The boxed proteins carry the His_6-StrepII$_3$ purification handle. Other proteins were expressed with a His_6-$Flag_3$-TEV tag. Purified protein was analyzed by SDS-PAGE (top panel) or native PAGE (3-12%; bottom panel) followed by silver staining. For the native gel, numbers on the right indicate the molecular weight of the marker in kDa. Cleared cell lysate was analyzed on Western blot probed with anti-His-tag antibody (middle panel).

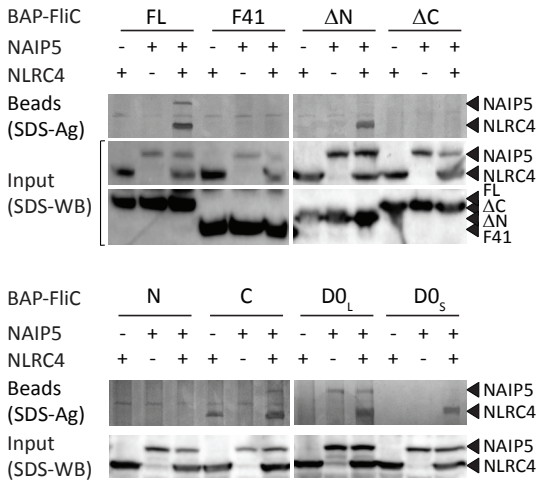

Figure 4: Association of NLRC4 and NAIP5 with biotinylated flagellin fragments. HEK293E cells were transfected with His_6-$Flag_3$-TEV tagged NAIP5 and NLRC4 and BAP-tagged flagellin fragments as indicated. The BAP-tagged flagellin fragments were biotinylated *in vivo* by co-expressing biotin ligase from *E. coli.* StrepTactin beads were used for pull down. Proteins bound to the beads were visualized by SDS-PAGE followed by silver staining (top panel). Cleared cell lysate was analyzed on Western blot probed with anti-His-tag antibody (middle and bottom panel).

The C-terminal fragment FliC-C was unique in its ability to precipitate NLRC4 albeit in relatively small amounts and not consistently so in all experiments.

Thus, $D0_L$ shows relatively strong binding to NAIP5, whereas the C-terminus of flagellin shows a weaker interaction with NLRC4. Most other inflammasome inducing fragments did not precipitate the individual NLRs; they were, however, able to precipitate the NAIP5-NLRC4 complex. Higher affinity for the complex possibly results from a conformational change in one or both of the NLRs upon inflammasome formation. Alternatively, flagellin could be stabilized in the complex by binding at the interface of NAIP5 and NLRC4.

In vitro reconstitution of the inflammasome

In order to show unequivocally that apart from NAIP5 and NLRC4 no other cellular factors are required for flagellin-induced inflammasome formation, we set out to reconstitute the inflammasome *in vitro* from its purified components. Flagellin was purified from *Salmonella enteritidis* according to established protocols[28] (Fig. 5*A*). NLR-purification proved challenging as insoluble aggregates tend to form upon overexpression. Production of soluble NAIP5 and NLRC4 was tested in several expression hosts using different combinations of N- and C-terminal purification tags. We succeeded in purifying small quantities of murine NAIP5 (mNAIP5) from transiently transfected HEK293E cells using tandem-affinity purification on Ni-NTA and StrepTactin-sepharose columns. One liter of HEK293E culture yielded 5-10 µg pure mNAIP5 (Fig. 5*A*). Unfortunately, we did not succeed in purifying murine NLRC4 (mNLRC4); we did, however, obtain relatively large quantities (up to 150 µg/L culture) of human NLRC4 (hNLRC4) using the same expression and purification strategy as used for mNAIP5. Purified hNLRC4 is monomeric at low concentrations, but when concentrated above ca 1 mg/ml the protein forms oligomers as indicated by the formation of a ladder-pattern on native gel (Fig. 5*B*).

Our ability to purify hNLRC4 but not mNLRC4 posed a problem for reconstitution of a flagellin responsive inflammasome. hNLRC4 and the sole human NAIP (hNAIP) do not form a complex in the presence of flagellin, nor do they cause a flagellin induced caspase-1 dependent decrease in cell-viability (Fig. 5*C,D*). Instead, a hNAIP-hNLRC4 inflammasome is formed in response to the Type III secretion system needle protein CprI[5]. Thus, a flagellin responsive inflammasome cannot be reconstituted from hNAIP and hNLRC4. We therefore assessed whether hNLRC4, which shares 75% sequence identity with mNLRC4, can substitute its murine orthologue in

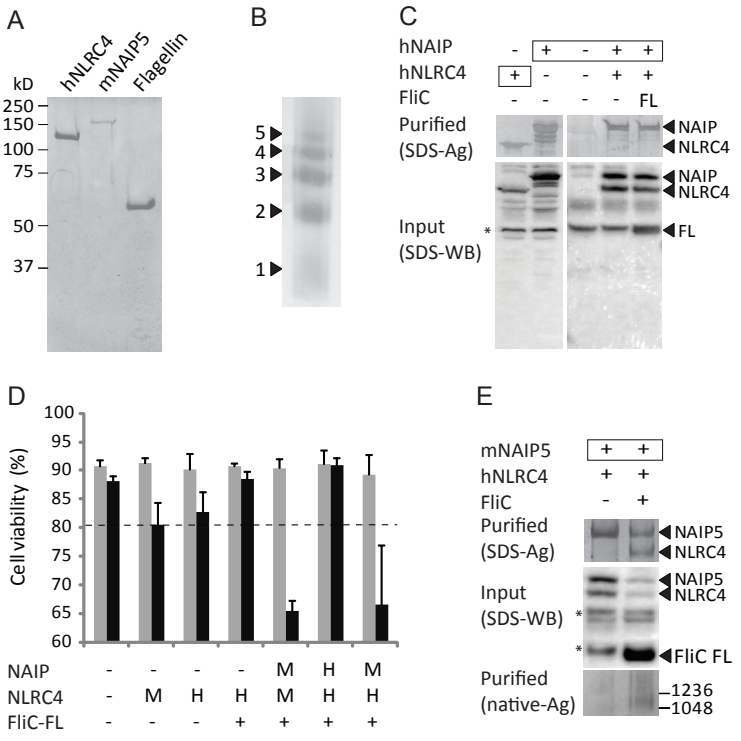

Figure 5: Murine NAIP5 and human NLRC4 form an inflammasome in response to flagellin. *A*, SDS-PAGE analysis of purified proteins visualized by Coomassie staining. *B*, Analysis of the spontaneous multimerization of concentrated (> 1mg/ml) solutions of purified hNLRC4 on native PAGE (4-15%). The protein was visualized by silver staining. Numbers indicate the probable number of monomers present in each multimer. *C*, Inability of hNAIP and hNLRC4 to form a flagellin-induced inflammasome in HEK293E cells. Boxed proteins carry the His_6-$StrepII_3$ purification handle; other proteins were expressed with a His_6-$Flag_3$-TEV tag. Purified fractions were analyzed by SDS-PAGE followed by silver staining (top panel). The cleared cell lysate was analyzed on Western blot probed with His-tag antibody (bottom panel). The asterisk denotes a protein that interacts non-specifically with the antibody. *D*, Viabilities of HEK293E cells 48h after transfection with the indicated proteins. The letters H and M indicate whether the human or mouse protein was expressed. For further explanation see Fig. 1*A*. *E*, Analysis of inflammasome formation in HEK293E cells transfected with *mNaip5* and *hNlrc4* in the presence and absence of flagellin. mNAIP5 carried the His_6-$StrepII_3$ purification handle. Other proteins were expressed with a His_6-$Flag_3$-TEV tag. Purified protein was analyzed by SDS-PAGE (top panel) or native PAGE (3-12%; bottom panel) followed by silver staining. For the native gel, numbers on the right indicate the molecular weight of the marker in kDa. The cleared cell lysate was analyzed on Western blot probed with anti-His-tag antibody (middle panel). The asterisks denote proteins that interact non-specifically with the antibody.

flagellin-induced inflammasome formation. Overexpression of *hNlrc4*, like *mNlrc4*, causes a mild caspase-1 dependent decrease of cell viability, which is reduced when flagellin is co-expressed (Fig. 5*D*). Upon co-expression of *hNlrc4* and *mNaip5* with flagellin, we observed a clear decrease in cell viability similar to what was observed for mNLRC4 plus mNAIP5 and flagellin. Furthermore, hNLRC4 co-purifies with mNAIP5 in the presence of flagellin and this mNAIP5/hNLRC4 complex runs in native PAGE at a molecular weight comparable to the mNAIP5/mNLRC4 complex (Fig. 5*E*). Thus, hNLRC4 and mNAIP5 are capable of forming a fully active inflammasome in response to flagellin.

For *in vitro* reconstitution the purified proteins were mixed in the presence of either Mg^{2+}-ATP or EDTA; complex formation was analyzed by native PAGE (Fig. 6). Incubation of flagellin with either mNAIP5 or hNLRC4 causes no band shift, confirming our previous finding that flagellin does not form a stable complex with NLRC4 or mNAIP5 *in vivo* (Fig. 4). When all three proteins are present, a high molecular weight complex is formed that runs at a similar apparent molecular weight as the NAIP5-NLRC4 complexes purified from HEK293E cell lysates. Complex formation occurs in the presence of Mg^{2+}-ATP as well

as EDTA. In both cases *in vitro* formation of the NAIP5-NLRC4 complex appears rather inefficient as only a small fraction of the proteins is incorporated. Nevertheless, our observations prove that the flagellin-induced inflammasome can be formed by direct interaction of flagellin, NAIP5, and NLRC4 only, and that no additional cellular factors are required.

The role of ATP-binding in inflammasome formation

It has been suggested that ATP-binding by NLRs is essential for their oligomerization[16-18] as well as for responsiveness to their specific ligand[20]. The reconstitution of a NAIP5-NLRC4 inflammasome in the presence of EDTA (Fig. 6, right panel) suggests, however, that ATP-binding might not be required for these NLRs. To explore the role of ATP-binding further, we mutated the conserved lysine residue in the Walker A motif of both mNAIP5 (K475) and mNLRC4 (K175) to arginine. This mutation has been shown to strongly reduce ATP binding and downstream signaling in NLRs[36-37] and homologous proteins containing NACHT domains[38-42]. The mutants will be referred to as NAIP5-KR and NLRC4-KR, respectively. The ability of the NAIP5 and NLRC4 mutants to assemble into the inflammasome and to induce caspase-1 dependent cell death was analyzed (Fig. 7*A-C*). The NAIP5-KR mutant causes a slight, but not significant, reduction in caspase-1 dependent cell death and the amount of complex formed, albeit reduced, is still substantial (Fig. 7*A,B*). In addition, NAIP5-KR, like NAIP5, co-precipitates with biotinylated FliC-D0$_L$ (Fig. 7*C*). Therefore, NAIP5-KR appears fully functional in inflammasome formation and induction of cell-death. Analysis of the NLRC4-KR mutant was complicated by the fact that the amount of soluble NLRC4-KR in cell lysates is markedly reduced compared to the wild type protein (Fig. 7*B,* middle panel), indicating that NLRC4 stability is compromised by the mutation. NLRC4-KR does not induce significant caspase-1 dependent cell-death, neither in ligand-independent auto-activation when expressed alone nor when co-expressed with *Naip5* and flagellin (Fig. 7*A*). Whereas these observations suggest that ATP-binding contributes to inflammasome activity, lack of activity could also be caused by the strongly reduced expression level of the NLRC4-KR mutant. Complex formation is not abolished completely: small amounts of NLRC4-KR do co-purify with wild type and mutant NAIP5 in the presence of FliC-D0$_L$ (Fig. 7*B* top panel) and a high molecular weight complex is just visible on native PAGE (Fig. 7*C*, bottom panel). In addition, biotinylated FliC-D0$_L$ precipitates a NLRC4-KR/NAIP5 complex and even a NLRC4-KR/

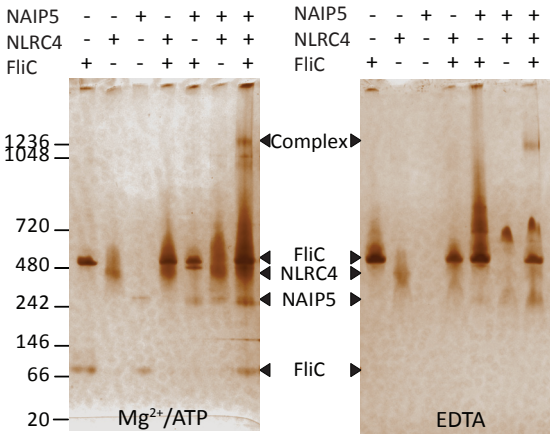

Figure 6: *In vitro* reconstitution of a flagellin-induced NAIP5-NLRC4 inflammasome. Inflammasome components were mixed and incubated in the presence of Mg^{2+}/ATP (left panel) or EDTA (right panel). Samples were analyzed after 3h and 24h incubation by native PAGE (3-12%) followed by silver staining. Since the results at both time points are indistinguishable, only the 24h samples are shown. Numbers on the left indicate the molecular weight of the marker in kDa.

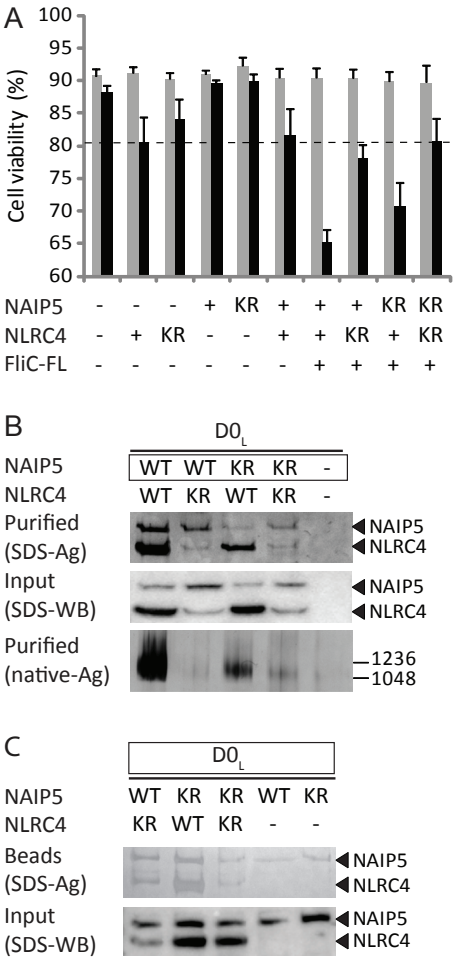

Figure 7: Effect of WalkerA mutations on inflammasome formation. *A*, Viabilities of HEK293E cells 48h after transfection with the indicated wild type (+) or mutant (KR) proteins. For further explanation see Fig. 1*A*. *B*, Analysis of inflammasome formation in HEK293E cells transfected with $D0_L$ and wild type (WT) or mutant (KR) NLRs as indicated. For further explanation see Fig. 2*D*. *C*, Analysis of the binding of wild type (WT) or mutant (KR) inflammasome components to biotinylated $D0_L$ in HEK293E cells. For further explanation see Fig. 4.

NAIP5-KR double mutant complex (Fig. 7*C*). The observed complex formation suggests that nucleotide binding by NLRC4 may not be essential for inflammasome assembly. However, as a consequence of NLRC4-KR instability, only small amounts of complexes are formed and we cannot determine whether these are signaling competent.

In conclusion, our data strongly indicate that ATP-binding by NAIP5 is not essential for inflammasome formation. For NLRC4 our data are not conclusive.

Analysis of the NAIP5-NLRC4 inflammasome by electron microscopy

To gain insight in the macromolecular organization of the NAIP5-NLRC4 inflammasome, we visualized the complex as well as the individual NLRs by negative stain electron microscopy (EM). Electron micrographs of the mNAIP5 and hNLRC4 preparations that were used for the *in vitro* reconstitution experiments show particles with a globular shape and a diameter of about 8 nm, which presumably represent monomers or at most dimers (Fig. 8*A,B*). Micrographs of a hNLRC4 sample that had been concentrated to ~8 mg/ml before it was diluted for EM analysis show large rod-shaped particles that are about 25 $\pm$ 2 nm in width and vary in length from about 30 nm to over 200 nm (Fig. 8*C*). Studied in closer detail by electron tomography (Fig. 8*D*) these rods appear to have a layered structure composed of stacked rings or, alternatively, a helical arrangement. The limited quality of the data did not allow us to discriminate between both arrangements, as Fourier analysis and subvolume averaging were unsuccessful. Since these rod-shaped particles are only observed at very high protein concentrations, their physiological relevance is debatable. Nevertheless, their formation may be related to the previously observed induction of caspase-1 dependent cell death upon overexpression of *Nlrc4* as well as its ligand independent self-association (Fig. 1*A*,*B*).

As the *in vitro* reconstitution of the NAIP5-NLRC4 complex was rather inefficient, we purified the inflammasome directly from cells co-transfected with murine *Naip5, Nlrc4,* and FliC-$D0_L$. Electron micrographs reveal top and side views of disk-shaped particles with a radius of 28 $\pm$ 2 nm (Fig.

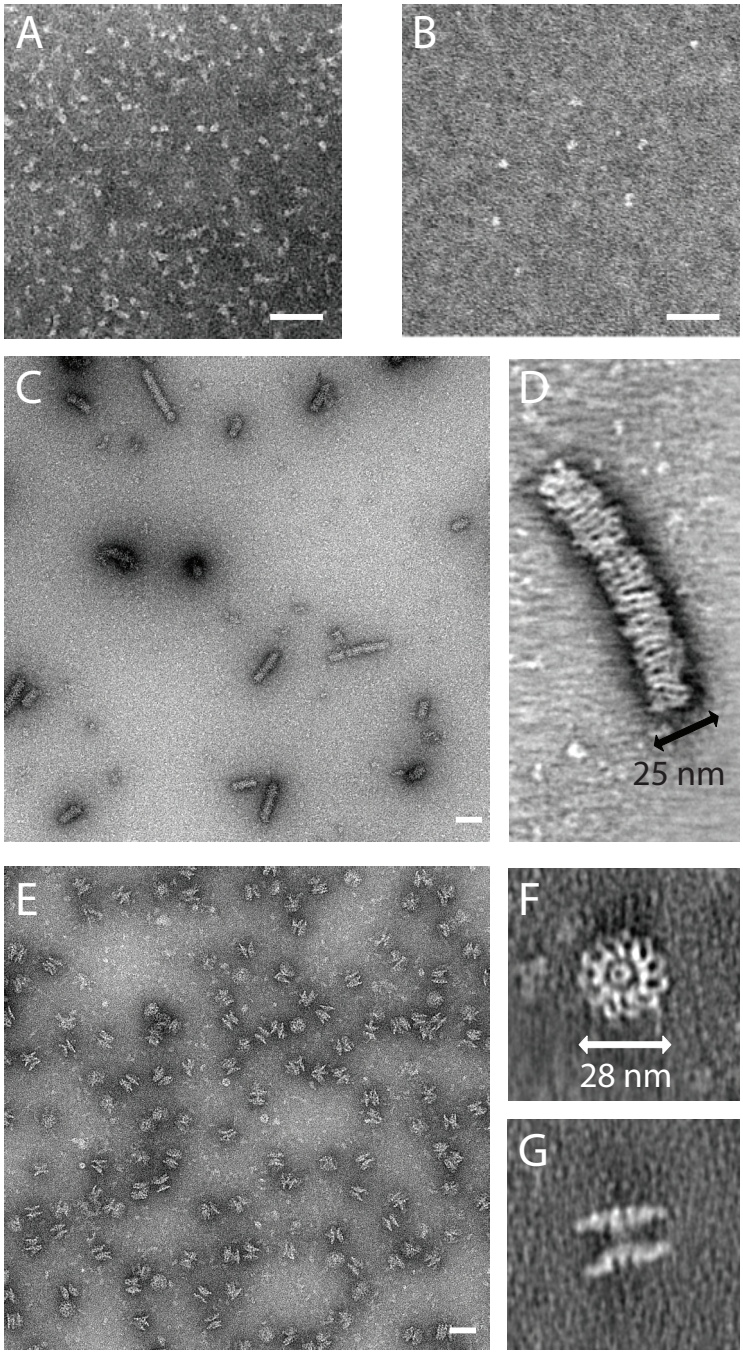

Figure 8: Electron micrographs of the NAIP5-NLRC4 inflammasome. *A-C and E*, EM projection images of negatively stained samples of purified hNLRC4 (*A*), mNAIP5 (*B*), hNLRC4 stored at high concentration (*C*) and $D0_L$-induced mNAIP5/mNLRC4 inflammasome freshly purified from HEK293E cells (*E*). *D and F-G*, Virtual sections through electron tomograms of the concentrated hNLRC4 sample (*D*) and the freshly purified inflammasome sample in top view (*F*) and side view (*G*). Scale bars represent 50 nm. Quantitative analysis of inflammasome symmetry (Supplemental Fig. S3) shows that the particle depicted in panel *F* has 11-fold symmetry.

8*E-G*). A top view tomogram of a particularly well-stained NAIP5-NLRC4 inflammasome (Fig. 8*F*) reveals considerable detail. The flagellin $D0_L$ fragment would be too small to be resolved, but the curved LRR domains of the individual NLR monomers can clearly be distinguished at the perimeter of the disk. From the number of LRR domains it is evident that this particular particle consists of 11 protomers. Rotational autocorrelation analysis of 15 putative top view inflammasomes reveals that among six particles that could be classified unambiguously, four display 11-fold symmetry, whereas two particles display 12-fold symmetry (Supplemental Fig. S3). Due to the limited number of particles analyzed we cannot exclude that other symmetries occur as well. The number of protomers is remarkable because EM structures of the NALP1 inflammasome as well as the Apaf-1, CED4, and Dark apoptosomes, revealed similarly shaped, but considerably smaller disks consisting of 5-8 protomers only[21,23,25,26]. Although at this resolution no distinction can be made between NAIP5 and NLRC4, the absence of non-symmetric density-features that are sufficiently large to represent an NLR monomer, strongly suggest that the two proteins are incorporated into the disks at equivalent positions. In analogy with the EM structures of homologous inflammasomes and apoptosomes, the central region, where the individual monomers interact, is expected to be formed by the NACHT-domains of NAIP5 and NLRC4. The N-terminal effector-binding domains likely are centrally located on one side of the disk, forming a platform for procaspase-1 to bind. In the side view tomogram of the NAIP5-NLRC4 complex (Fig. 8*G*) disks are seen to stack in pairs. Similar pairwise stacking was observed in EM studies of the Dark and Apaf-1 apoptosomes and was attributed to non-physiological CARD-CARD domain interactions occurring at high protein concentrations[24,26,43]. Assuming that a similar mechanism is responsible for the formation of the stacked NAIP5-NLRC4 disks, the density connecting two disks most likely represents the NLR effector binding domains. In this case the physiologically active unit of the NAIP5-NLRC4 inflammasome is the single disk.

In summary, we show that flagellin induces formation of disk-shaped inflammasomes, consisting of eleven or twelve protomers, in which NAIP5 and NLRC4, to a first approximation, occupy equivalent positions. Inflammasomes of this size have not been previously observed and may represent a unique feature of NAIP/NLRC4 complexes.

Discussion

The flagellin D0 domain and the neighboring spoke-region are essential for formation and stabilization of the flagellar filament and therefore indispensible for bacterial motility[32-33]. The structural importance of this region is reflected by high sequence conservation between bacterial species (supplemental Fig. S2). From evolutionary viewpoint this makes the extended D0 domain an appropriate target for recognition by the innate immune system. Previously, inflammasome activation was attributed to the C-terminal 35 amino acids of flagellin[4]. We now show that the N-terminal 52 amino acids of flagellin likewise contain an element that induces the association of NAIP5 with NLRC4 and concomitant caspase-1 dependent cell-death. The difference in response to $D0_L$ and $D0_S$ suggests that this element resides in the spoke region; $D0_L$ precipitates NAIP5, whereas $D0_S$, which lacks this region (Supplemental Fig. S2), does not (Fig. 4). Moreover, the role of the three conserved leucine residues located near the C-terminus of flagellin is more prominent in fragments that lack the spoke region (Fig. 3). This shows that, in addition to the C-terminus, the spoke region

contributes significantly to inflammasome activation.

It has been observed that polymerized flagellin is less potent in activating NAIP5[44], which is consistent with the role of $D0_L$ in inflammasome induction, as D0 is not exposed in the flagellar filament[33]. Polymerization of over-expressed flagellin in our reconstituted system in HEK293E cells could explain why we observe no co-precipitation of NAIP5 with biotinylated flagellin, whereas biotinylated $D0_L$, which we presume does not polymerize, does precipitate NAIP5 (Fig. 4). Likewise, polymerization of purified flagellin may have contributed to the low efficiency of complex formation in the *in vitro* reconstitution of the NAIP5-NLRC4 inflammasome (Fig. 6*A*).

Electron microscopy reveals that the NAIP5-NLRC4 inflammasome is far larger than previously observed for complexes of other NACHT-domain containing proteins, and contains 11 or 12 protomers arranged in a disk-shaped complex. Due to the limited number of particles analyzed we cannot exclude that other sizes occur as well. Although the resolution of the EM micrographs is insufficient to distinguish NAIP5 from NLRC4, the highly symmetrical structure and the absence of obvious protrusions or deviations (Fig. 8*F*) indicates that both NLRs occupy equivalent positions within the inflammasome, and thus likely exhibit equivalent NACHT-NACHT interactions. As explained in the results section, the observed dimerization of the inflammasome disks (Fig. 8*G*) is presumably non-physiological. The functional unit is expected to be a single disk that exposes the effector binding domains on one side, thereby forming a platform for procaspase-1 recruitment and activation. Low level caspase-1 activation also occurs independent of flagellin as a consequence of overexpression-induced homo-oligomerization of NLRC4 (Fig. 1*A,B*). Similar overexpression-induced homo- and hetero-oligomerization of NLR NACHT domains has been reported more frequently[8,45-47]. Although NLRC4 homo-oligomers are unlikely to play a role at physiological expression levels, electron micrographs (Fig. 8*C,D*) show that NLRC4 assembles into a rod-like structure with a diameter that is very similar to that of the NAIP5-NLRC4 disk. We are unable to determine whether these rods consist of stacked NLRC4 disks or an NLRC4 helix, nevertheless the similarity in diameters suggests that the arrangement of monomers in the NLRC4 rod and the NAIP5-NLRC4 disk is similar.

Our data leads us to propose a model for NAIP5-NLRC4 inflammasome formation by the following sequence of events (Fig. 9): The initiation step involves recognition of flagellin by NAIP5. This is supported by our co-precipitation experiments that show association of $D0_L$ with NAIP5, and is consistent with a role for NAIP proteins in providing specificity to NLRC4 containing inflammasomes[5-6]. Since NAIP5 does not oligomerize in the presence of flagellin (Fig. 1*B*), the next step in inflammasome formation must involve binding of NLRC4 to the NAIP5-flagellin complex. Finally, as NLRC4 is able to self-associate, we speculate that a conformational change in complex-incorporated NLRC4 can be recognized by the free protein, and induces the progressive incorporation of NLRC4 monomers into the complex through homotypic interactions until a disk-shaped inflammasome is formed.

The sequence of events described above would produce disks that contain a single NAIP5 molecule. Although at this point we can only speculate about the exact ratio between NAIP5 and NLRC4 in the complex, our data strongly indicates that the major part of the inflammasome is formed by NLRC4. In inflammasome preparations we generally observe a clear excess of NLRC4, even though the isolation procedure results in co-purification of any residual monomeric

NAIP5. Likewise, an excess of NLRC4 is also observed in co-precipitation of the inflammasome with biotinylated flagellin (Fig. 4), which does not co-precipitate the monomeric NLRs. Thus, we can exclude a 1:1 composition and therefore models with disks composed of alternating NAIP5 and NLRC4 monomers, as well as a structure consisting of two stacked disks each consisting of only one of the NLRs. Our data, however, does not exclude the presence of more than one NAIP5 molecule per disk.

The question arises whether flagellin also interacts with NLRC4. We find no solid evidence for a direct interaction other than the precipitation of NLRC4 by the flagellin C-terminal fragment in some, but not all experiments (Fig. 4). Also, NLRC4 self-association and related caspase-1 activation are not enhanced in the presence of flagellin (Fig 1*A,B*). NLRC4 does, however, appear to increase flagellin binding-affinity as many flagellin fragments are not capable of precipitating NAIP5, but do precipitate the complex (Fig. 4). Although this observed stabilization may arise from NLRC4-induced conformational changes in NAIP5, it could also result from flagellin binding at the NAIP5-NLRC4 interface. Flagellin-binding at the NAIP5-NLRC4 interface, or to NAIP5 only, would both be consistent with our finding that relatively small amounts of flagellin co-purify with the inflammasome, but we cannot exclude that this finding results from flagellin dissociation after inflammasome formation. The C-terminal

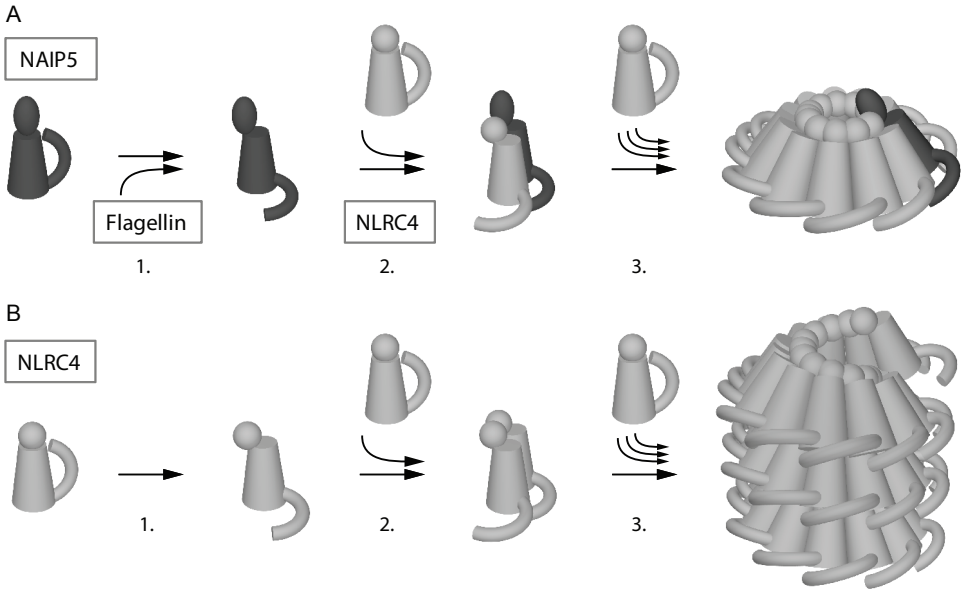

Figure 9: Model of NAIP5-NLRC4 inflammasome formation versus NLRC4-multimerization. *A*, Steps involved in inflammasome formation; Resting NAIP5 undergoes a conformational change upon interaction with flagellin (1). Activated NAIP5 subsequently recruits resting NLRC4, which in turn undergoes a conformational change (2). This activated form of NLRC4 is recognized by resting NLRC4, which results in the progressive incorporation of NLRC4 (3) into a disk-like complex that exposes the NLRC4 CARD domains at one face creating a platform suitable for procaspase-1 recruitment and activation. *B*, Steps involved in the non-physiological formation of NLRC4 multimers; NLRC4 is spontaneously activated at low frequency (1). As with the formation of the hetero-oligomeric complex, activated NLRC4 is recognized by resting NLRC4 (2), which, in over-expression conditions, results in the progressive incorporation of additional NLRC4 monomers and the formation of rod-like structures (3). In these rods, consisting either of stacked disks or, as depicted here, a helical arrangement, the CARD domains are possibly only partially exposed, resulting in limited procaspase-1 activation. LRR domains are depicted as arches; NACHT domains as tubes; CARD domains as spheres, and BIR domains as ellipsoid.

residues of flagellin show a striking similarity to the C-terminal residues of the ligands of other NLRC4-containing inflammasomes[5-6,48]. This region includes the three leucines that proved essential for induction of inflammasome formation by FliC-C and $D0_s$ (Fig 3). If NLRC4 has a direct interaction with the different NAIP-inflammasome ligands, the conserved C-terminal region may well constitute a common NLRC4-binding motif.

The role of ATP-binding and/or hydrolysis in inflammasome formation remains unclear. Our mutagenesis data suggest that at least for NAIP5 an intact ATP-binding site is not a prerequisite for inflammasome formation or signaling. For NLRC4 data analysis is complicated by the instability of the NLRC4-KR mutant. The observation of *in vitro* inflammasome formation in the presence of EDTA (Fig. 6) does, by itself, not rule out a possible role for ATP binding; for instance, nucleotide dependent apoptosome formation by Apaf-1 and Dark is enhanced by EDTA[24, 26]. Thus far, various studies on the effect of ATP-binding by NAIP5 and NLRC4, including mutations and deletions of the ATP-binding site, yielded inconsistent outcomes on NLR-association and inflammasome signaling[6, 17, 46]. Further biochemical studies using purified NAIP5, NLRC4, and their ATP-binding mutants may resolve this issue.

In conclusion, using a number of experimental approaches, we show that (i) a flagellin-responsive NAIP5-NLRC4 inflammasome can be reconstituted from the purified components and thus no additional cellular factors are required for its formation, (ii) flagellin recognition is determined by its conserved N- and C-terminal regions, (iii) NLRC4 is the main inflammasome constituent, and (iv) the inflammasome is a disk-like complex consisting of eleven or twelve NLR molecules. We propose a model of the inflammasome in which NAIP5 functions as a flagellin-sensor and NLRC4 provides a platform for caspase-1 recruitment. Although the exact ratio of NAIP5 and NLRC4 in the inflammasome remains to be determined, we speculate that it contains a single NAIP5 molecule.

Our data provide a solid basis for further investigations into the formation of NAIP-NLRC4 inflammasomes and we anticipate that the ability to purify the individual NLRs as well as the complete inflammasome will boost studies aimed at the elucidation of their three-dimensional structures.

Experimental procedures

Cell culture and transfection

HEK293E cells were cultured in Freestyle medium (Invitrogen), containing 0.2% FCS, 50 µg/ml G418 disulfate at 37 °C in a 5% CO_2 humidified atmosphere. The cells were grown in suspension at 120 rpm. Small scale (4 mL) and large scale (1L) transfections were performed according to Durocher *et al*. [27]. When appropriate, cell viabilities were measured 48h post-transfection using a Casy Model TTC cell counter (Schärfe Systems, Germany).

Plasmids

cDNA was purchased from Invivogen (human *Nlrc4*), Imagenes (murine *Naip5* and murine *Casp1*) and OriGene (human *Naip*). Murine spleen cDNA, used for the isolation of *Nlrc4*, was a kind gift from G. Folkerts (Department of Pharmacology and Pathophysiology, Utrecht University, The Netherlands). DNA encoding *Salmonella typhimurium* and *Salmonella enteritidis* flagellin *(FliC)* were a kind gift from J.P.M. van Putten (Faculty of Veterinary Medicine, Department of Infection and Immunity, Utrecht University, The Netherlands).

Coding sequences were amplified by PCR using forward primers that introduce a BamHI restriction site while omitting the start codon, and reverse primers that introduce a NotI restriction site and omit the stop-codon, unless indicated otherwise. At the protein level this procedure results in the introduction of a Gly-Ser sequence at the N-terminus and three Ala residues at the C-terminus. Domain boundaries of *S. typhimurium* flagellin constructs are indicated in Fig. 2*A*. The F41 fragment of *S. enteritidis* comprises amino acids R53-R461. For the FliC-C construct a reverse primer was used that preserves the stop-codon and therefore no triple Ala sequence is present at its C-terminus.

For the FliC-D0$_L$ and FliC-D0$_S$ fragments synthetic DNA (DNA2.0) was used that also included a stop codon preceding the NotI site. PCR products were subcloned into pCR-TOPO vector (Invitrogen).
Point-mutations were created using the QuickChange method (Stratagene). The *FliC* 3LA mutants (L491A, L493A, L494A) contain a stop codon preceding the NotI site.
The BamHI/NotI DNA fragments were subcloned into pUPE vectors (U-Protein Express BV, The Netherlands) that contain an expression cassette under control of a CMV promoter. Expression vectors encoded a C-terminal TEV-StrepII$_3$-His$_6$, Flag$_3$-His$_6$, or StrepII$_3$-His$_6$ tag, or an N-terminal His$_6$-Flag$_3$ or His$_6$-BAP-TEV tag. The BAP (biotin acceptor peptide)[a] tag comprises amino acids GLNDIFEAQKIEWHE. A vector encoding the *E. coli* BirA enzyme was a kind gift from H.T.M. Timmers (Faculty of Medicine, Utrecht University, The Netherlands). Murine *Casp1* was expressed without tags.

Protein purification
Native flagellin of *S. enteritidis* was purified as described previously [28]. For NLR purification from small scale (4 ml) HEK293E cultures, cells were harvested 48 hours post-transfection by centrifugation at 600 g for 5 min. Cell pellets were stored for 1 hour up to 1 week at -20 °C. For purification, pellets were thawed at room temperature. Cytoplasmic extracts were obtained using a method described by Tsai et al. [29], with omission of the PBS washing step. Cell pellets were resuspended in 320 µl cold small scale lysis buffer containing 10 mM HEPES pH 7.6, 5 mM $MgCl_2$, 10 mM KCl , 5 mM DTT, 1 µg/ml DNase and 1 tablet Complete mini, EDTA-free tablets (Roche) per 20 ml buffer. StrepII-tagged proteins were purified from the cleared cytoplasmic extracts using StrepTactin Sepharose beads (GE Healthcare). After incubation for 1-2 hr at 4 °C, beads were washed in StrepTactin wash buffer (100 mM NaCl, 25 mM HEPES pH 7.5, 5 mM benzamidin, 5% glycerol, 2 mM DTT), and subsequently protein was eluted in wash buffer supplemented with 5 mM *d*-desthiobiotin (Sigma). In the case of biotinylated proteins washed beads were boiled for 10 min in SDS sample buffer supplemented with 3 mM *d*-desthiobiotin.
For large scale purification of NAIP5-TEV-StrepII$_3$-His$_6$ and NLRC4-StrepII$_3$-His$_6$, cells were harvested 72-96h post-transfection by centrifugation for 20 min at 500g. Cell pellets were resuspended in 1/10 culture volume of cold large scale lysis buffer (100 mM NaCl, 50 mM HEPES pH7.5, 5 mM benzamidin, 5% glycerol, 1 tablet Complete mini, EDTA-free tablets (Roche) per 20 ml lysis buffer, 5 mM DTT, 5 mM $MgCl_2$, 1 µg/ml DNase, 0.3% NP40) and subjected to two freeze/thaw cycles in liquid nitrogen before storage at -80 °C until further purification. Frozen lysates were thawed at room temperature and cell debris was removed by centrifugation at 60,000 g for 20 min. Concentrated NaCl and imidazole solutions were added to the cleared supernatant to final concentrations of 300 mM and 10 mM, respectively. Ni-Sepharose 6 Fast Flow beads (GE Healthcare) were added to the cleared lysate, incubated for 1 hour at 4 °C, and poured into a Tricorn column (GE Healthcare). The column was washed with IMAC[a] wash buffer (300 mM NaCl, 50 mM HEPES pH7.5, 5 mM benzamidin, 5% glycerol, 5 mM DTT) containing 20 mM imidazole. Protein was eluted in wash buffer containing 250 mM Imidazole. Pooled fractions, mixed with an equal volume of 50 mM HEPES pH 7.6, 5% glycerol, 5 mM benzamidin, and 2 mM DTT, were incubated with StrepTactin Sepharose beads (GE Healthcare) for 1 hour. After extensive washing of the beads with StrepTactin wash buffer as described for small scale purifications, protein was eluted in StrepTactin wash buffer supplemented with 5 mM *d*-desthiobiotin) and stored in 25-50 µl portions at -80 °C.

Gel electrophoresis and protein detection
Reduced protein samples were separated on standard Laemmli 10% SDS-PAGE gels. Samples for native gel electrophoresis were run on 3-12% NativePAGE Novex Bis-Tris gels (Invitrogen) according to the manufacturers protocol, using NativeMark Unstained Protein Standard (Invitrogen) as marker. Purified hNLRC4 was separated on 4-15% PhastGel with native buffer strips (GE Healthcare) according to the manufacturers protocol. Gels were silver stained or transferred to polyvinylidene difluoride (PVDF) membrane (BioRad). Proteins were detected on Western blot using either a mixture of mouse anti- polyHistidine (Sigma) with mouse anti-Penta-His (Qiagen), or mouse anti-Flag tag (Sigma) as primary antibodies and Rabbit-anti-mouse-HRP (Dako) as the secondary antibody. The signal was detected using ECL (GE Healthcare).

In vitro inflammasome reconstitution
Microtubes were precoated with 1 mg/ml BSA for 30 min at room temperature, washed with incubation buffer (150 mM NaCl, 50 mM HEPES pH 7.6, 5% glycerol, 5 mM benzamidin, 2 mM DTT) and dried. Next, 100 ng mNAIP5, 100 ng

hNLRC4 and 400 ng *S. Typhimurium* FliC were mixed in a total volume of 4 µl incubation buffer supplemented with either 0.5 mM ATP and 4 mM $MgCl_2$, or 4 mM EDTA. Mixtures were incubated overnight at 4 °C and then separated on 3-12% native gel (Invitrogen) according to the manufacturers protocol.

Protein purification and sample preparation for electron microscopy

For purification of the inflammasome, HEK293E cells were transfected with *Naip5*-TEV-$StrepII_3$-His_6, *Nlrc4*-$Flag_3$-His_6 and tagless *FliC*-$D0_L$. Cells were harvested 72-96h post transfection by spinning at 700g for 10 min. Pellets were stored at -80 °C until further purification. Purification was performed as described for small scale purifications, scaled up according to the culture volume.

For EM grid preparation NLRC4, NAIP5, and freshly purified inflammasome diluted to concentrations of 5-25 µg/ml were applied on 400 mesh copper grids with continuous carbon support film (Aurion, The Netherlands) and stained with freshly prepared 0.75% uranyl formate solution. For the polymerized NLRC4 sample 100 mesh copper grids with home-made formvar/carbon support film and 2% uranyl acetate stain were used.

EM data collection and processing

Human NLRC4, murine NAIP5 and polymerized NLRC4 were imaged using a Tecnai BioTWIN12 TEM with a LaB_6 electron source operated at 120 kV and a 4k x 4k Eagle CCD camera (FEI Company, The Netherlands). Imaging of the freshly purified inflammasome was performed at 200 kV on a Tecnai F20 TEM, equipped with a field emission gun and a 4k x 4k USC4000 CCD camera (Gatan, Germany). Binned 2D images were acquired at -1.5 µm defocus and 50.000 x magnification resulting in a pixel size of 0.32 nm at specimen level.

Tomograms of polymerized human NLRC4 and freshly purified inflammasome were taken in low-dose mode at -4 µm or -2 µm defocus and magnifications of 30.000 x (binned by 2) or 50000 x (unbinned), resulting in pixel sizes of 0.77 nm and 0.22 nm at specimen level. For both specimens tilt schemes with a constant increment of 2° in ranges of +-60° and +-50°, respectively, were used.

Tomograms were reconstructed in IMOD version 4.2.15 [30] using patch tracking for image alignment and the SIRT reconstruction algorithm. In the case of polymerized NLRC4, the CTF was corrected by phase flipping after defocus estimation using TOMOCTF [31].

Symmetry analysis was performed on tomographic subvolumes that showed inflammasomes close to top-view. To this end, ~10 nm thick virtual sections of the volumes were reprojected along the putative symmetry axis and rotational autocorrelation was performed after circular masking. Subsequent iterative refinement of particle center and symmetry axis orientation was guided by the maximization of peaks in the autocorrelation function. Finally, averaged reprojections of individual particles were calculated according to symmetry classification.

References

1. Franchi, L., et al., *Cytosolic flagellin requires Ipaf for activation of caspase-1 and interleukin 1beta in salmonella-infected macrophages.* Nat Immunol, 2006. **7**(6): p. 576-82.
2. Miao, E.A., et al., *Cytoplasmic flagellin activates caspase-1 and secretion of interleukin 1beta via Ipaf.* Nat Immunol, 2006. **7**(6): p. 569-75.
3. Ren, T., et al., *Flagellin-deficient Legionella mutants evade caspase-1- and Naip5-mediated macrophage immunity.* PLoS Pathog, 2006. **2**(3): p. e18.
4. Lightfield, K.L., et al., *Critical function for Naip5 in inflammasome activation by a conserved carboxy-terminal domain of flagellin.* Nat Immunol, 2008. **9**(10): p. 1171-8.
5. Zhao, Y., et al., *The NLRC4 inflammasome receptors for bacterial flagellin and type III secretion apparatus.* Nature, 2011. **477**(7366): p. 596-600.
6. Kofoed, E.M. and R.E. Vance, *Innate immune recognition of bacterial ligands by NAIPs determines inflammasome specificity.* Nature, 2011.
7. Damiano, J.S., et al., *CLAN, a novel human CED-4-like gene.* Genomics, 2001. **75**(1-3): p. 77-83.
8. Poyet, J.L., et al., *Identification of Ipaf, a*

human caspase-1-activating protein related to Apaf-1. J Biol Chem, 2001. **276**(30): p. 28309-13.
9. Geddes, B.J., et al., *Human CARD12 is a novel CED4/Apaf-1 family member that induces apoptosis.* Biochem Biophys Res Commun, 2001. **284**(1): p. 77-82.
10. Martinon, F., K. Burns, and J. Tschopp, *The inflammasome: a molecular platform triggering activation of inflammatory caspases and processing of proIL-beta.* Mol Cell, 2002. **10**(2): p. 417-26.
11. Schroder, K. and J. Tschopp, *The inflammasomes.* Cell, 2010. **140**(6): p. 821-32.
12. Martinon, F. and J. Tschopp, *Inflammatory caspases and inflammasomes: master switches of inflammation.* Cell Death Differ, 2007. **14**(1): p. 10-22.
13. Dinarello, C.A., *IL-18: A TH1-inducing, proinflammatory cytokine and new member of the IL-1 family.* J Allergy Clin Immunol, 1999. **103**(1 Pt 1): p. 11-24.
14. Fink, S.L. and B.T. Cookson, *Apoptosis, pyroptosis, and necrosis: mechanistic description of dead and dying eukaryotic cells.* Infect Immun, 2005. **73**(4): p. 1907-16.
15. Mo, J.Y., et al., *Pathogen sensing by nucleotide-binding oligomerization domain-containing protein 2 (NOD2) is mediated by direct binding to muramyl dipeptide and ATP.* J Biol Chem, 2012.
16. Duncan, J.A., et al., *Cryopyrin/NALP3 binds ATP/dATP, is an ATPase, and requires ATP binding to mediate inflammatory signaling.* Proc Natl Acad Sci U S A, 2007. **104**(19): p. 8041-6.
17. Lu, C., et al., *Nucleotide binding to CARD12 and its role in CARD12-mediated caspase-1 activation.* Biochem Biophys Res Commun, 2005. **331**(4): p. 1114-9.
18. Ye, Z., et al., *ATP binding by monarch-1/ NLRP12 is critical for its inhibitory function.* Mol Cell Biol, 2008. **28**(5): p. 1841-50.
19. Askari, N., et al., *Expression, purification, and characterization of recombinant NOD1 (NLRC1): A NLR family member.* J Biotechnol, 2011.
20. Zurek, B., et al., *Mutational analysis of human NOD1 and NOD2 NACHT domains reveals different modes of activation.* Innate Immun, 2011.
21. Faustin, B., et al., *Reconstituted NALP1 inflammasome reveals two-step mechanism of caspase-1 activation.* Mol Cell, 2007. **25**(5): p. 713-24.
22. Yu, X., et al., *A structure of the human apoptosome at 12.8 A resolution provides insights into this cell death platform.* Structure, 2005. **13**(11): p. 1725-35.
23. Acehan, D., et al., *Three-dimensional structure of the apoptosome: implications for assembly, procaspase-9 binding, and activation.* Mol Cell, 2002. **9**(2): p. 423-32.
24. Yuan, S., et al., *Structure of the Drosophila apoptosome at 6.9 a resolution.* Structure, 2011. **19**(1): p. 128-40.
25. Qi, S., et al., *Crystal structure of the Caenorhabditis elegans apoptosome reveals an octameric assembly of CED-4.* Cell, 2010. **141**(3): p. 446-57.
26. Yu, X., et al., *Three-dimensional structure of a double apoptosome formed by the Drosophila Apaf-1 related killer.* J Mol Biol, 2006. **355**(3): p. 577-89.
27. Durocher, Y., S. Perret, and A. Kamen, *High-level and high-throughput recombinant protein production by transient transfection of suspension-growing human 293-EBNA1 cells.* Nucleic Acids Res, 2002. **30**(2): p. E9.
28. Ibrahim, G.F., et al., *Method for the isolation of highly purified Salmonella flagellins.* J Clin Microbiol, 1985. **22**(6): p. 1040-4.
29. Tsai, A. and R.P. Carstens, *An optimized protocol for protein purification in cultured mammalian cells using a tandem affinity purification approach.* Nat Protoc, 2006. **1**(6): p. 2820-7.
30. Kremer, J.R., D.N. Mastronarde, and J.R. McIntosh, *Computer visualization of three-dimensional image data using IMOD.* J Struct Biol, 1996. **116**(1): p. 71-6.
31. Fernandez, J.J., S. Li, and R.A. Crowther, *CTF determination and correction in electron cryotomography.* Ultramicroscopy, 2006. **106**(7): p. 587-96.
32. Vonderviszt, F., S. Aizawa, and K. Namba, *Role of the disordered terminal regions of flagellin in filament formation and stability.* J Mol Biol, 1991. **221**(4): p. 1461-74.
33. Yonekura, K., S. Maki-Yonekura, and K. Namba, *Complete atomic model of the bacterial flagellar filament by electron*

cryomicroscopy. Nature, 2003. **424**(6949): p. 643-50.
34. Samatey, F.A., et al., *Structure of the bacterial flagellar protofilament and implications for a switch for supercoiling.* Nature, 2001. **410**(6826): p. 331-7.
35. de Boer, E., et al., *Efficient biotinylation and single-step purification of tagged transcription factors in mammalian cells and transgenic mice.* Proc Natl Acad Sci U S A, 2003. **100**(13): p. 7480-5.
36. Inohara, N., et al., *Nod1, an Apaf-1-like activator of caspase-9 and nuclear factor-kappaB.* J Biol Chem, 1999. **274**(21): p. 14560-7.
37. Ogura, Y., et al., *Nod2, a Nod1/Apaf-1 family member that is restricted to monocytes and activates NF-kappaB.* J Biol Chem, 2001. **276**(7): p. 4812-8.
38. Tameling, W.I., et al., *The tomato R gene products I-2 and MI-1 are functional ATP binding proteins with ATPase activity.* Plant Cell, 2002. **14**(11): p. 2929-39.
39. Tameling, W.I., et al., *Mutations in the NB-ARC domain of I-2 that impair ATP hydrolysis cause autoactivation.* Plant Physiol, 2006. **140**(4): p. 1233-45.
40. Chaudhary, D., et al., *The death inhibitory molecules CED-9 and CED-4L use a common mechanism to inhibit the CED-3 death protease.* J Biol Chem, 1998. **273**(28): p. 17708-12.
41. Chinnaiyan, A.M., et al., *Role of CED-4 in the activation of CED-3.* Nature, 1997. **388**(6644): p. 728-9.
42. Hu, Y., et al., *WD-40 repeat region regulates Apaf-1 self-association and procaspase-9 activation.* J Biol Chem, 1998. **273**(50): p. 33489-94.
43. Yuan, S., et al., *The holo-apoptosome: activation of procaspase-9 and interactions with caspase-3.* Structure, 2011. **19**(8): p. 1084-96.
44. Molofsky, A.B., et al., *Cytosolic recognition of flagellin by mouse macrophages restricts Legionella pneumophila infection.* J Exp Med, 2006. **203**(4): p. 1093-104.
45. Damiano, J.S., et al., *Heterotypic interactions among NACHT domains: implications for regulation of innate immune responses.* Biochem J, 2004. **381**(Pt 1): p. 213-9.
46. Zamboni, D.S., et al., *The Birc1e cytosolic pattern-recognition receptor contributes to the detection and control of Legionella pneumophila infection.* Nat Immunol, 2006. **7**(3): p. 318-25.
47. Hsu, L.C., et al., *A NOD2-NALP1 complex mediates caspase-1-dependent IL-1beta secretion in response to Bacillus anthracis infection and muramyl dipeptide.* Proc Natl Acad Sci U S A, 2008. **105**(22): p. 7803-8.
48. Miao, E.A., et al., *Innate immune detection of the type III secretion apparatus through the NLRC4 inflammasome.* Proc Natl Acad Sci U S A, 2010. **107**(7): p. 3076-80.
49. Larkin, M.A., et al., *Clustal W and Clustal X version 2.0.* Bioinformatics, 2007. **23**(21): p. 2947-8.

Supplementary figures

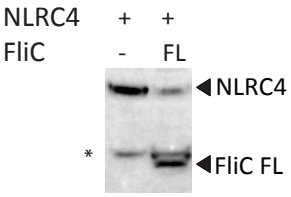

Supplementary figure S1: The expression level of NLRC4 is reduced by co-expression with flagellin. Western blot analysis of the cleared lysate of HEK293E cells transfected with *Nlrc4* and flagellin. Cells were harvested 48h post transfection. The blot was probed with anti-His-tag antibody. The asterisk denotes a protein that interacts non-specifically with the antibody.

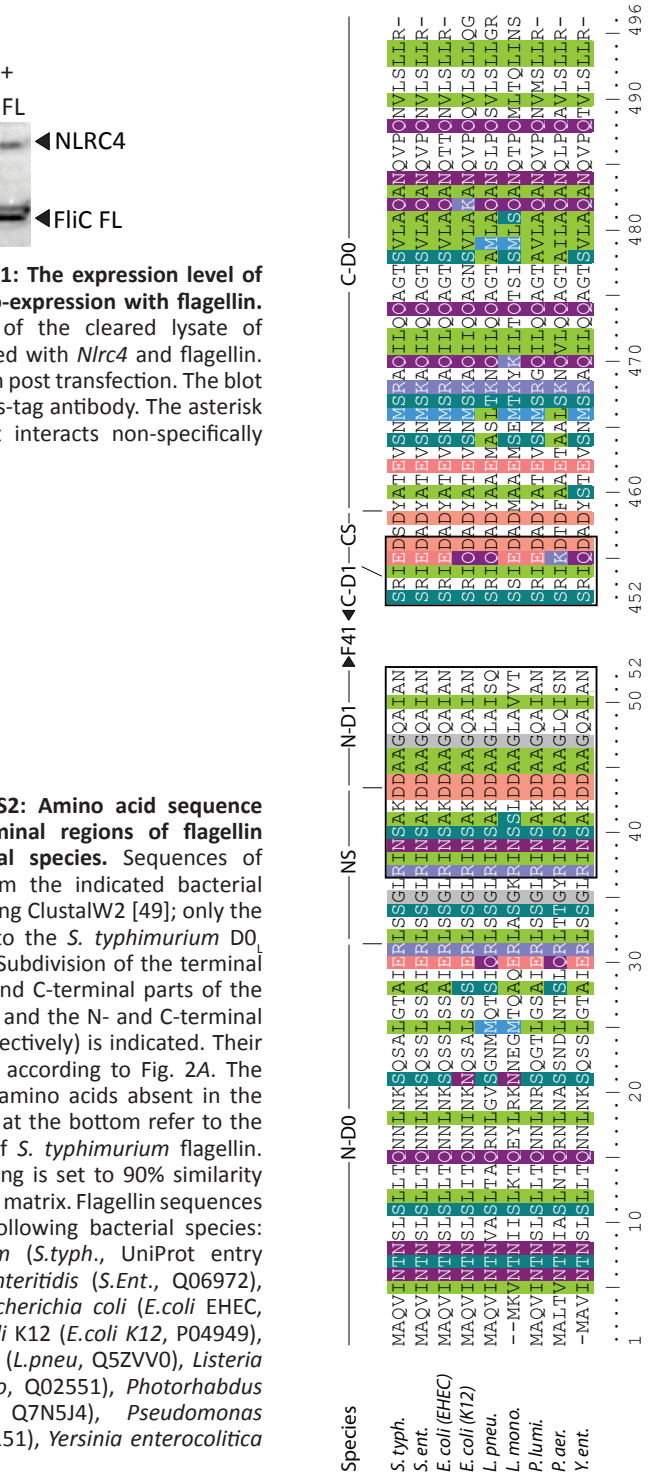

Supplementary figure S2: Amino acid sequence alignment of the terminal regions of flagellin from different bacterial species. Sequences of full length flagellin from the indicated bacterial species were aligned using ClustalW2 [49]; only the regions corresponding to the *S. typhimurium* $D0_L$ fragment are depicted. Subdivision of the terminal fragments into the N- and C-terminal parts of the D0 domain, D1 domain, and the N- and C-terminal spokes (NS and CS, respectively) is indicated. Their domain boundaries are according to Fig. 2*A*. The boxed regions indicate amino acids absent in the $D0_S$ fragment. Numbers at the bottom refer to the amino acid sequence of *S. typhimurium* flagellin. The threshold for coloring is set to 90% similarity based on the BLOSUM62 matrix. Flagellin sequences were taken from the following bacterial species: *Salmonella typhimurium* (*S.typh.*, UniProt entry P06179), *Salmonella enteritidis* (*S.Ent.*, Q06972), enterohaemorrhagic *Escherichia coli* (*E.coli* EHEC, C8TTK4), *Escherichia coli* K12 (*E.coli K12*, P04949), *Legionella pneumophila* (*L.pneu*, Q5ZVV0), *Listeria monocytogenes* (*L.mono*, Q02551), *Photorhabdus luminescens* (*P.lumi.*, Q7N5J4), *Pseudomonas aeruginosa* (*P.aer.*, P72151), *Yersinia enterocolitica* (*Y.ent.*, D3JZT5).

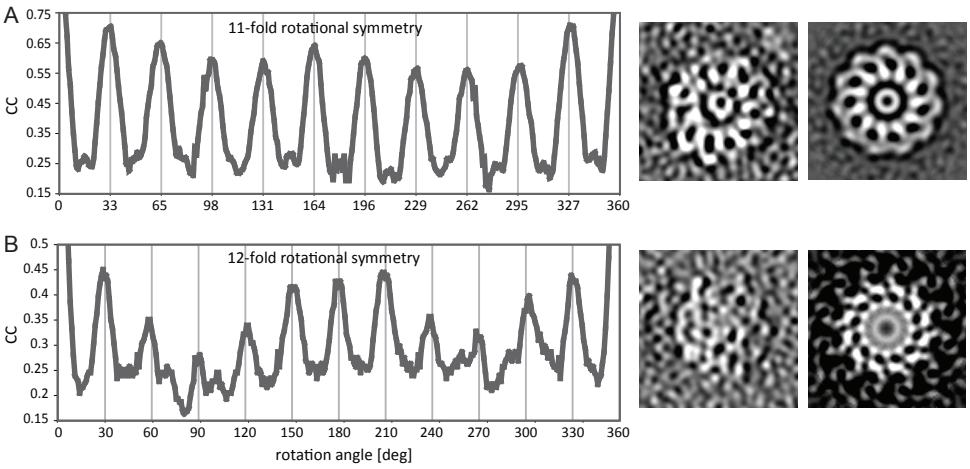

Supplementary figure S3: Symmetry analysis of NAIP5-NLRC4 inflammasomes. The rotational autocorrelation function (left) calculated for sub-tomograms that were reprojected along the symmetry axis (middle) identifies inflammasome symmetry. An example of particles with 11-fold (A; also depicted in Fig. 8F) and 12-fold symmetry (B) are shown, together with the symmetry averaged projection (right). Vertical lines in the auto-correlation graphs indicate the expected location of correlation maxima for 11- and 12-fold symmetry, respectively.

Chapter **4**

Structural Modeling of NAIP5/NLRC4 Helical Complexes Based on Cryo-Electron Tomography

Els F. Halff[1], Christoph A. Diebolder[1,2], Roman I. Koning[2], Eric G. Huizinga[1]

1. Crystal and Structural Chemistry, Bijvoet Center for Biomolecular Research, Utrecht University, The Netherlands
2. Section Electron Microscopy, Department of Molecular Cell Biology, Leiden University Medical Center, The Netherlands

Structural Modeling of NAIP5/NLRC4 Helical Complexes Based on Cryo-Electron Tomography

Inflammasomes are high molecular weight, caspase-1 activating complexes formed by NOD-like receptors (NLRs) upon ligand recognition that play a crucial role in innate immunity. In the absence of structural data on NLRs and their oligomeric complexes, inflammasome models have long been based on apoptosome structures. Here we describe an electron tomography study on the hetero-oligomeric NAIP5/NLRC4 inflammasome that is formed in response to the bacterial protein flagellin. Fusion of protein kinase G (PKG) to NAIP5 to distinguish NAIP5 from NLRC4 in the complex resulted in an increased number of long rod-like complexes, that were only occasionally observed without fusion to PKG. By subtomogram averaging of these particles we calculated an averaged density map of a right-handed helix at 36 Å resolution. In this map we modeled NLRC4 by fitting fragments of the recently determined crystal structure of CARD-deleted NLRC4 in its dormant state. In our model, ligand-binding domains are arranged at the perimeter of a concave hub formed by the NACHT domains. The effector-binding domains responsible for downstream signaling cluster in the center of the helix and appear to be exposed at one end of the helix only. Our analysis indicates that the conformational changes involved in inflammasome formation include a movement of the LRR to expose the interface for multimerization, and a conformational change within the NACHT domain that is different from the changes observed during apoptosome formation.

Introduction

The NOD-like receptor (NLR) family comprises cytosolic receptors of the innate immune system that ensure a rapid response to a wide variety of pathogen and danger associated molecular patterns[1]. Upon ligand-recognition, a subset of the NLRs oligomerize to form a high molecular weight, caspase-1 activating complex known as inflammasome[2-4]. Activated caspase-1 mediates the proteolytic processing of the cytokines pro-IL-1β and pro-IL-18[2,5] and induces an inflammatory cell death called pyroptosis[6].

NLRC4, together with members of the NAIP subfamily of NLRs, forms an inflammasome in response to the structurally related bacterial proteins flagellin and components of the bacterial type III secretion system. The NAIP family member determines ligand specificity[7-9]. Murine NAIP5 specifically recognizes the highly conserved D0 domain of flagellin[10].

Inflammasomes are thought to structurally resemble apoptosomes[11]. The crystal structure of the CED-4 apoptosome as well as the electron microscopy (EM) structures of the Apaf-1 and Dark apoptosomes revealed ring-shaped heptameric and octameric complexes stabilized by extensive interactions between neighboring NACHT domains[12-14]. Likewise, in NLRs the centrally located and conserved NACHT domain plays an essential role in their multimerization[15]. In addition to the NACHT domain, NLRs possess a C-terminal leucine-rich repeat (LRR) domain thought to be involved in ligand recognition, and an N-terminal effector binding domain, the identity of which varies between family members; NAIP5 contains three N-terminal baculovirus inhibitor of apoptosis protein repeat (BIR) domains, the function of

which has not been elucidated yet[16], whilst NLRC4 contains an N-terminal caspase activating and recruitment domain (CARD) that interacts directly with the CARD of the procaspase-1 zymogens[17-19]. Inflammasomes, like apoptosomes, supposedly expose a platform of CARD domains to obtain a high local concentration of procaspase-1, thereby enforcing its dimerization and auto-cleavage, which are required for its activation[2, 20-21].

Comparison of the crystal structure of monomeric Apaf-1 with its conformation in the apoptosome showed that ligand binding induces a series of conformational changes, including a rearrangement of NACHT subdomains[22-23], that enable apoptosome formation. Inflammasome formation is likewise thought to involve a series of conformational changes. The recently published crystal structure of monomeric CARD-deleted NLRC4 represents its inactive conformation and reveals how the dormant state is maintained by interactions between the LRR and NACHT domain as well as within the NACHT domain[24]. No high-resolution structural data is available of the active conformation of an inflammasome-incorporated NLR. We recently provided the first structural insight into the NAIP5/NLRC4 inflammasome and showed by negative stain EM a disk-shaped particle that comprises 11 or 12 protomers in a ring-like arrangement[10]. We proposed a mechanism for its formation in which a single NAIP5, upon direct recognition of flagellin, recruits multiple copies of NLRC4 to form a hetero-oligomeric inflammasome that contains an excess of NLRC4.

Here, we describe the structural analysis of the NAIP5/NLRC4 inflammasome by cryo electron tomography (ET). We find the purified particles to be heterogeneous in size and shape. In an effort to identify the position of NAIP5 in the complex, we fused NAIP5 to cGMP-dependent protein kinase I alpha (PKG). The resulting rod-like particles reveal a helical buildup. We exploited the helical symmetry to obtain initial insight into the arrangement of NLRs within the inflammasome by averaging subtomograms. Our analysis suggests that the conformational changes within an NLR, as well as the interaction between neighboring NACHT domains in the inflammasomes, are different from the rearrangements and interactions involved in apoptosome formation.

Results and discussion

NAIP5/NLRC4 complexes are heterogeneous

In order to study the NAIP5/NLRC4 inflammasome in closer detail we purified complexes from HEK293E cells co-transfected with murine NAIP5, murine NLRC4, and the *S.typhimurium* flagellin fragment FliC-D0$_L$ as published[10] and performed cryo-electron tomography. The complexes observed are heterogeneous in size and shape and, like the previously described double disks[10], occur as dimeric particles in which two complexes are connected by a small interface (Figure 1A). Besides the double disks we observe particles that contain one or multiple additional layers. These layers may represent stacked disks, or alternatively may have a helical arrangement. As noted in our previous study we presume the dimers to be stabilized by CARD-CARD interactions. In accordance, fusion of GFP to the N-terminus of NLRC4, but not to the N-terminus of NAIP5, reduces the size of the complex on native gel (Supplementary Figure S1), suggesting that GFP at this position may sterically hinder formation of dimers. Similar to what was reported for Dark apoptosomes[14], we expect that inflammasomes do not dimerize in their physiological environment.

Isosurfaces of selected particles from a single tomogram underscore the heterogeneity of the sample (Figure 1B), which make it a poor starting point for improvement of the

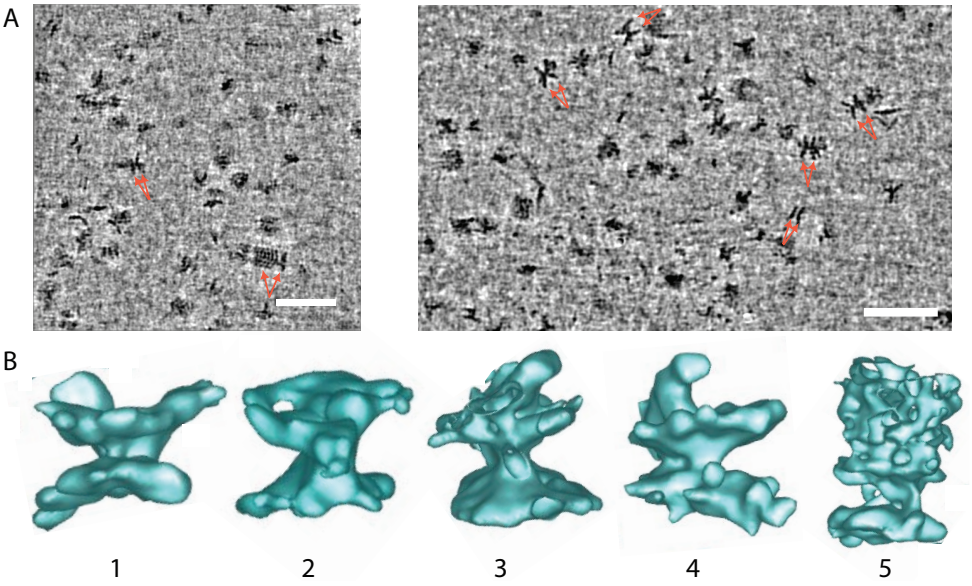

Figure 1. Dual axis cryo-electron tomography of NAIP5/NLRC4 complexes reveals considerable heterogeneity. *A.* The NAIP5/NLRC4 inflammasome imaged over a hole in the carbon support film. Dimeric complexes, of which a selected set is indicated by double arrows, are clearly discernible, but appear to vary considerably in size and conformation. The white scale bars represent 100 nm. *B.* Isosurface representation of dimeric particles selected from the tomogram depicted in panel A. These particles appear to comprise a double disk (1,2), contain additional density on at least one side (3,4) or form a longer rod-like structure (5).

resolution by subtomogram averaging.

Strategies to identify NAIP5 within the complex

One of our aims was to establish the number and position of NAIP5 molecules in the complex. NAIP5 is 43 kDa larger than NLRC4, a difference that mainly resides in the N-terminal effector binding domains. We expect this difference to be too small to discriminate between NAIP5 and NLRC4 directly. To locate the individual components in the hetero-oligomeric inflammasome we incubated the purified complexes with a combination of a primary antibody raised against either NAIP5 or the StrepII$_3$ tag, and a secondary gold-labeled antibody. Unfortunately, we could not locate NAIP5 either by negative stain or cryo-EM using this method; the labeling efficiency was too low, and, due to the size of the antibodies, the distance between the gold label and the particles is too long to identify NAIP5 with sufficient certainty. We also attempted to detect NAIP5 with nanogold-labeled Ni-NTA. To this end, we purified inflammasomes composed of untagged NLRC4 and NAIP5-TEV-StrepII$_3$-His$_6$ or, as a control, NAIP5-TEV-StrepII$_3$. The labeling efficiency of both samples, however, was equally high, indicating that labeling was mainly non-specific.

In an attempt to increase the size difference between NAIP5 and NLRC4 we expressed NAIP5 as a fusion protein with the 76 kDa intracellular protein cGMP-dependent protein kinase I alpha (PKG) at its C-terminus, adjacent to the LRR domain. As the LRR domain protrudes outward from the inflammasome, we anticipated that PKG at this position would be visible in negative stain EM as additional density and thus enable us to locate NAIP5 in the hetero-oligomeric complex.

C-terminal fusion of PKG to NAIP5 does not affect the detection of FliC-D0$_L$

We verified that PKG does not induce auto-activation of NAIP5 or abrogate ligand-

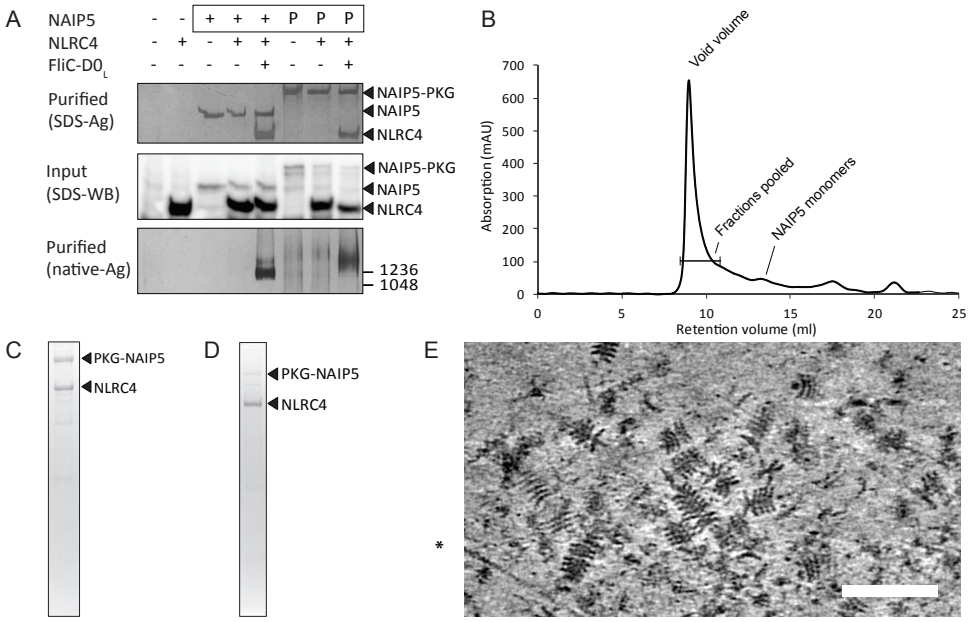

Figure 2. Formation and purification of NAIP5-PKG/NLRC4 complexes. *A.* Analysis of inflammasome formation in HEK293E cells transfected with the proteins indicated. The boxed proteins carry the $StrepII_3$-His_6 purification handle; "P" indicates fusion to PKG at the C-terminus. Purified protein was analyzed by SDS-PAGE (top panel) or native PAGE (3-12%; bottom panel) followed by silver staining. The cleared cell lysate was analyzed on Western blot probed with anti-His-tag antibody (middle panel). For the native gel, numbers on the right indicate the molecular weight of the marker in kDa. *B.* Elution profile of NAIP5-PKG/NLRC4 complexes separated by gelfiltration on a Superose-6 column, after affinity purification on StrepTactin beads. *C,D.* SDS-PAGE analysis of the purified NAIP5-PKG/NLRC4 complexes after affinity purification on StrepTactin beads (C) and after gelfiltration (D). Proteins were visualized by Coomassie staining. Fractions pooled for further analysis by cryo ET are indicated. *E.* NAIP5-PKG/NLRC4 complexes imaged over a hole in the carbon support film. The white scale bar represents 100 nm. The asterisk denotes an actin filament that apparently co-purified.

induced formation of the NAIP5/NLRC4 complex. HEK293E cells were co-transfected with *Nlrc4*-$Flag_3$-His_6, FliC-$D0_L$, and *Naip5-PKG*-TEV-$StrepII_3$-His_6 or, as a control, *Naip5*-TEV-$StrepII_3$-His_6. Complex formation was assessed by single-step purification with StrepTactin beads (Figure 2A). In the absence of FliC-$D0_L$, neither NAIP5 nor NAIP5-PKG forms a complex with NLRC4. In the presence of FliC-$D0_L$, however, NLRC4 co-purifies with both NAIP5 and NAIP5-PKG.

On native gel the NAIP5-PKG/NLRC4 complex runs higher than the NAIP5/NLRC4 complex and displays a more diffuse band than the complex without PKG-fusion, suggesting that the PKG-containing complex does differ in size and/or shape.

NAIP5-PKG/NLRC4 complexes have a helical arrangement.

We purified the NAIP5-PKG/NLRC4 inflammasome by single-step affinity purification on StrepTactin beads (Figure 2C). This procedure results in the co-purification of monomeric NAIP5-PKG. To remove NAIP5-PKG monomers we additionally performed gelfiltration (Figure 2B,D). The final yield of the NAIP5-PKG/NLRC4 complexes was about 100 µg per liter HEK293E cell culture.

We were unable to identify by negative stain EM additional density that could represent the NAIP5-PKG fusion protein (data not shown). In comparison to the NAIP5/NLRC4 inflammasome, more NAIP5-PKG/NLRC4 particles consist of multiple layers and the

number of layers is higher, giving some of the particles a rod-like appearance (Figure 2E). Like the NAIP5/NLRC4 inflammasome, these rods occur as dimers. We considered the possibility that fusion of PKG to NAIP5 causes artifacts. In the physiological context of the cell PKG occurs as a dimer, mediated by a leucine zipper motif it its N-terminal 45 amino acids[27]. In NAIP5-PKG the PKG N-terminus is fused to the LRR domain of NAIP5, which may limit its accessibility. Nevertheless, we cannot exclude that NAIP5-PKG dimerizes via PKG. Dimerization of the NAIP5-PKG/NLRC4 complexes as seen in EM is not caused by dimerization of PKG as the NAIP5/NLRC4 complexes also exist as dimers. Also, the formation of long rods is not a consequence of the PKG fusion, since a similar particle is clearly visible in the tomogram of the NAIP5/NLRC4 complex (Fig 1A). Therefore, apart from increasing the number of rod-like particles, fusion to PKG does not appear to affect inflammasome formation.

To analyze the arrangement of the NAIP5-PKG/NLRC4 complex, we created an averaged density map on the basis of boxed volumes selected from the most regular regions of the subtomograms of 15 particles. This clearly revealed a right-handed helical arrangement. Helical averaging of 50 boxed volumes, with omission of the termini of the particles, resulted in a final model at a resolution of 36 Å (Figure 3B). This helical region has a diameter of 28 nm and contains $11^{2}/_{3}$ monomers per turn, with a pitch of 6.5 nm per turn. From this unsymmetrized average, we created a helically symmetrized map (Figure 3C) using 5.57 Å rise and 30.9° rotation per protomer.

In both maps the density at the outer rim of the helix is oriented perpendicular to the helix axis. This outer rim is well defined and reveals the position and direction of the curved LRR domains. Closer to the center of the helix the density curves upward, a

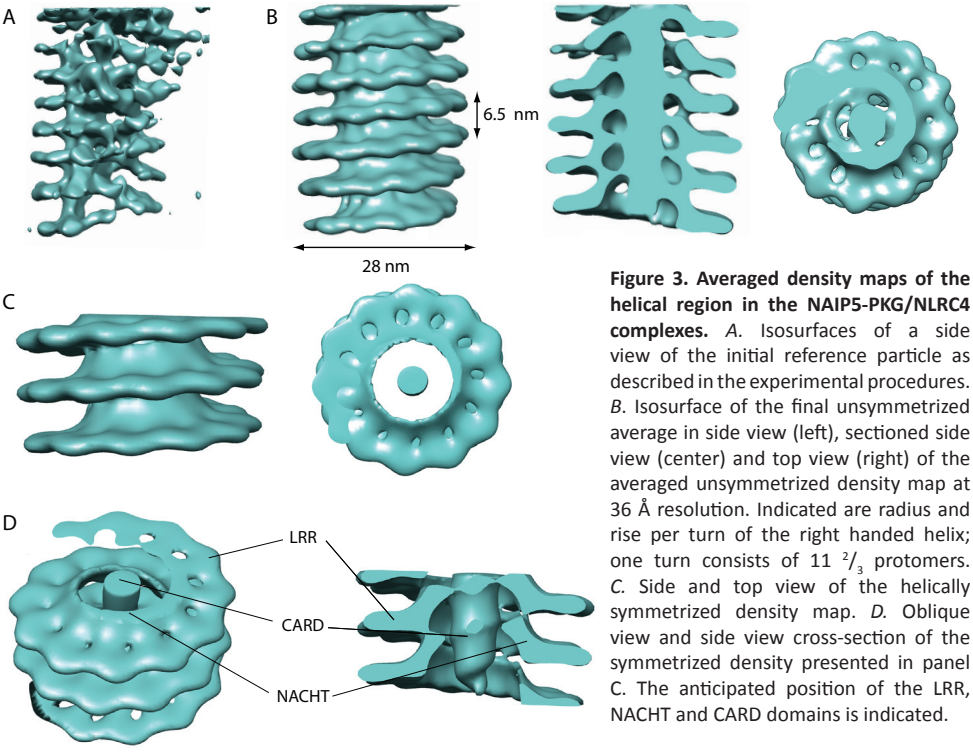

Figure 3. Averaged density maps of the helical region in the NAIP5-PKG/NLRC4 complexes. *A.* Isosurfaces of a side view of the initial reference particle as described in the experimental procedures. *B.* Isosurface of the final unsymmetrized average in side view (left), sectioned side view (center) and top view (right) of the averaged unsymmetrized density map at 36 Å resolution. Indicated are radius and rise per turn of the right handed helix; one turn consists of $11\ ^{2}/_{3}$ protomers. *C.* Side and top view of the helically symmetrized density map. *D.* Oblique view and side view cross-section of the symmetrized density presented in panel C. The anticipated position of the LRR, NACHT and CARD domains is indicated.

shape that is reminiscent of the so-called concave hub observed in apoptosomes, where it contains the NACHT domains. In apoptosomes, the concave hub forms a closed ring, whereas in our structure it forms a continuous helix. In the center of the helix we find a rod-like density; this central rod likely corresponds to the effector binding domains.

Fitting of NLRC4 domains to the EM density

In an attempt to obtain a structural interpretation of the helical inflammasome we fitted a model mainly derived from the crystal structure of NLRC4 (PDB ID 4KXF) to the averaged and symmetrized EM map. The crystal structure of NLRC4 comprises the central NACHT and C-terminal LRR domains; both domains are also present in NAIP5. The amino acid sequences of the NAIP NACHT domains are more closely related to NLRC4 than to other NLRs[11]. Sequence alignment shows that the NACHT domains of NLRC4 and NAIP5 align well (29% sequence identity) with only few small insertions and deletions in subdomains nucleotide binding domain (NBD), helical domain 1 (HD1), and winged helix domain (WHD) (Supplementary figure S2). Both NAIP5 and NLRC4 contain a larger insert, 10 and 16 amino acids, respectively, at different positions of their second helical domain (HD2), which is the least conserved region within NACHT domains. The NLRC4-LRR domain contains 16 repeats; in the NAIP5-LRR domain individual repeats are predicted to have the same length and α-helical convex face, but the total length of the NAIP5-LRR sequence suggests that it contains two additional repeats. Considering the overall similarity of their NACHT and LRR domains and given the relatively low resolution of our EM map we expect that a NACHT-LRR model based on the structure of NLRC4 will also be adequate for the corresponding region of NAIP5. The N-terminal NLRC4-CARD domain, which is replaced by 3 BIR domains in NAIP5, is absent from the crystal structure. For the modeling we therefore used the crystal structures of the Apaf-1 CARD domain (PDB ID 1Z6T) and the second BIR domain of human NAIP (PDB ID 2VM5). Although the FliC-D0$_L$ ligand may also be present in the complex, we previously observed that it co-purifies in substoichiometric amounts[10]. Considering the resolution of our map, the small size of the FliC-D0$_L$ fragment (10 kDa), and the expectation that only few protomers might be associated with the ligand, we did not include this fragment in the fitting procedure.

The crystal structure of CARD-deleted NLRC4 represents the inactive conformation in which the LRR domain covers the surface of the NACHT domain that putatively interacts with neighboring NACHT domains in the inflammasome[24]. Hu et al. proposed a mechanism for NLRC4-activation in which the WHD, HD2, and LRR domains move as a rigid body. We tried to fit this fragment manually into the density, guided by the position and direction of the LRR domain in the outer rim of the helix, however, the WHD and HD2 domains protruded significantly in this position. It appears therefore unlikely that the WHD-HD2-LRR fragment moves as one rigid body during activation. In subsequent fitting attempts we considered the LRR domain as a separate rigid body.

Since the resolution of our EM map is not sufficient to locate individual NACHT subdomains, we next assessed whether the active conformation of the NACHT domain could be similar to that of the apoptosome NACHT domains. The structural rearrangement observed in the NACHT domain of Apaf-1 upon binding of the ligand cytochrome *c* involves a 180° rigid body rotation of the WHD-HD2 fragment with respect to the NBD-HD1 fragment[13,22-23]. The overall fold of the NBD, HD1, and WHD in NLRC4 resembles that of Apaf-1 (Supplementary figure S3A,B). HD2, however, displays a different

fold. To generate an Apaf-1-like active conformation of the NLRC4 NACHT domain, we superimposed the NBD-HD1 and WHD-HD2 fragments of NLRC4 on the NBD and WHD, respectively, of apoptosome-incorporated Apaf-1. However, this model could also not be fitted well into the density, indicating that the relative position of the NACHT subdomains in apoptosomes and inflammasomes must be different.

A reasonable initial fit to the density was obtained by placing the NACHT domain in its inactive conformation in the density using the following procedure. To guide the fitting, we first created three neighboring NLRC4-NACHT domains by superposing their NBDs on three consecutive molecules of the Apaf-1 apoptosome. The three protomers were placed in the density of the central hub with the NBDs facing inward, as is the case in the apoptosome, and HD2 positioned near the LRR, with their termini in close proximity. Finally, helical symmetry was applied to a single protomer and minor adjustments in its orientation were applied to reduce clashes with its symmetry related neighbors.

During manual fitting of the CARD domain in the density of the central rod it became evident that this domain cannot follow the same helical symmetry as the NACHT-LRR region. Because the central rod is close to the helix axis, the 30.9 degrees rotation between adjacent protomers results in a displacement that is smaller than the diameter of the CARD, causing severe steric clashes with neighboring CARDs in all positions and orientations tested, while leaving a large part of the density unoccupied. When no symmetry constraints were applied, however, the CARDs could fill up the density of the central rod satisfactory (Supplementary figure S4A). In NAIP5, the CARD is replaced by three BIR domains, which together are 34 kDa larger in size. To test whether BIR domains could account for the density of the central rod, we replaced each of the CARDs by three copies of the crystal structure of the second BIR domain of human NAIP and find that their total volume by far exceeds that of the volume inside the NACHT-helix (Supplementary figure S4B). From this observation we conclude that the helical complexes cannot be composed of NAIP5 solely. Instead, since the volume of the density observed in the central rod is well accounted for by the necessary number of CARD domains, we hypothesize that the helical region of the NAIP5-PKG/NLRC4 complexes primarily contains NLRC4. The absence of NAIP5 in the helical regions is consistent with our previous finding that NAIP5 does not self-oligomerize in the presence of flagellin[10] and the fact that purified complexes contain an excess of NLRC4 (Figure 2D), as was also observed for the NAIP5/NLRC4 inflammasome. Nevertheless, since on the basis of the volume available inside the NACHT-ring replacement of a limited number of CARD domains by three BIR domains would be possible, we currently cannot exclude that NAIP5 is incorporated in the central region of the helix.

Description of the optimized model

Because the effector binding domains do not obey the same symmetry as the NACHT-LRR region, we excluded them during optimization of the model. The fit of the NACHT-LRR model optimized by density correlation refinement is shown in Figure 4A. Although some parts of the model protrude from the density, overall it appears to account well for the density of the outer rim and the central hub. In the model, the LRR domains are arranged head-to-tail and the interaction between neighboring LRR domains appears to stabilize their conformation in the complex. The NACHT domains are closely packed (Figure 4B); each of the NACHT subdomains interacts with neighboring protomers, but the main interaction involves the NBD-HD1-WHD

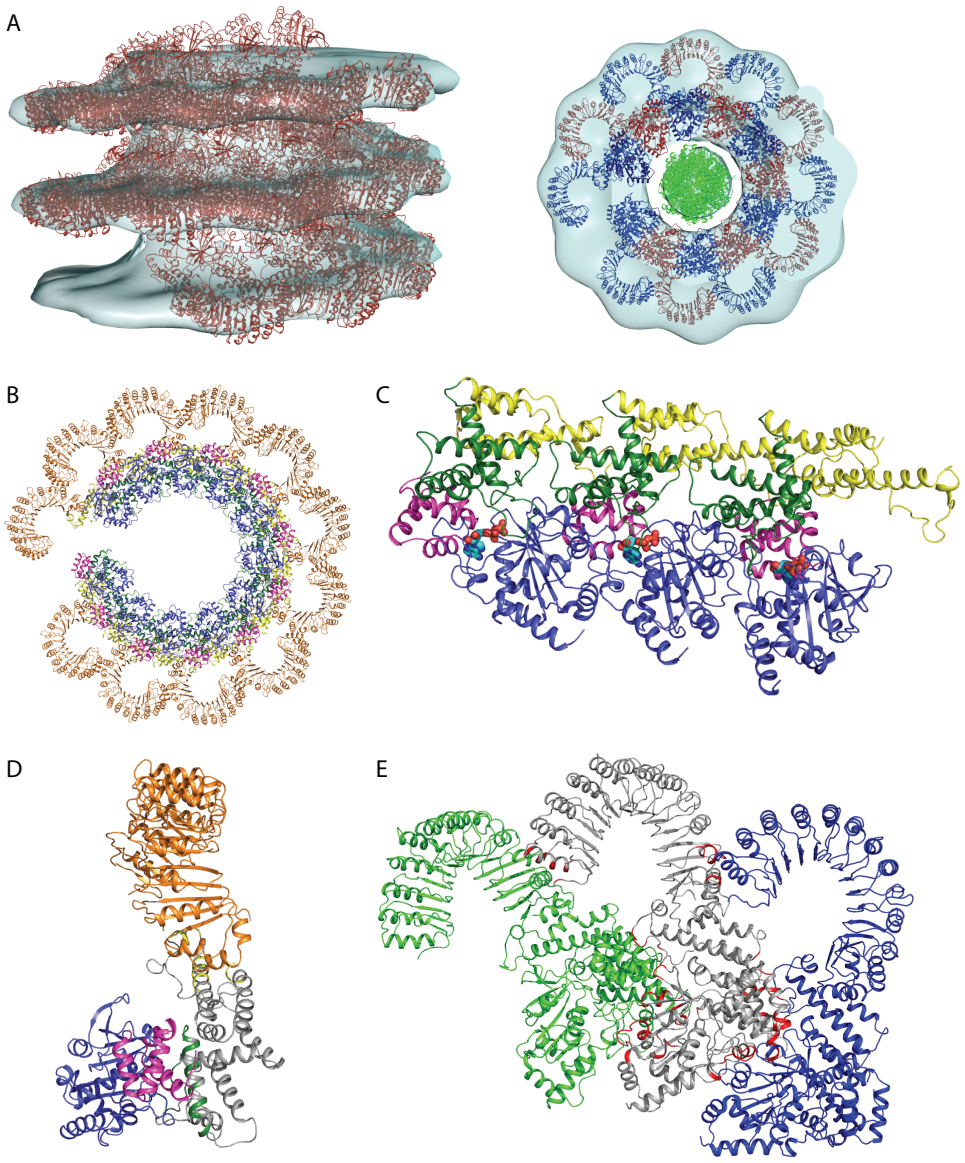

Figure 4. Analysis of the optimized model. *A.* Side view and top view of the optimized NACHT-LRR model in the symmetrized average density; protomers are shown in red (side view) or alternately in red and blue (top view). To give an impression of the volume occupied by the CARD domains, the positioning of the CARD domains obtained by fitting without imposing symmetry constraints is shown in the top view (green). *B.* Cartoon representation of a top view of the LRR and NACHT subdomains in an almost full helical turn (11 protomers). The NBD is shown in blue, HD1 in magenta, WHD in green, HD2 in yellow, and the LRR in orange. *C.* Detailed view of three neighboring NACHT domains with an ADP molecule shown in stick representation. Color coding is identical to panel B. *D.* Sterical clashes within one protomer shown in cartoon representation. Clashes are shown in green and yellow for residues of the WHD-HD1 fragment (gray) that clash with the NBD-HD1 fragment (blue-magenta) or the LRR (orange), respectively. *E.* Sterical clashes between protomers. Residues clashing between adjacent protomers are colored red in the central protomer.

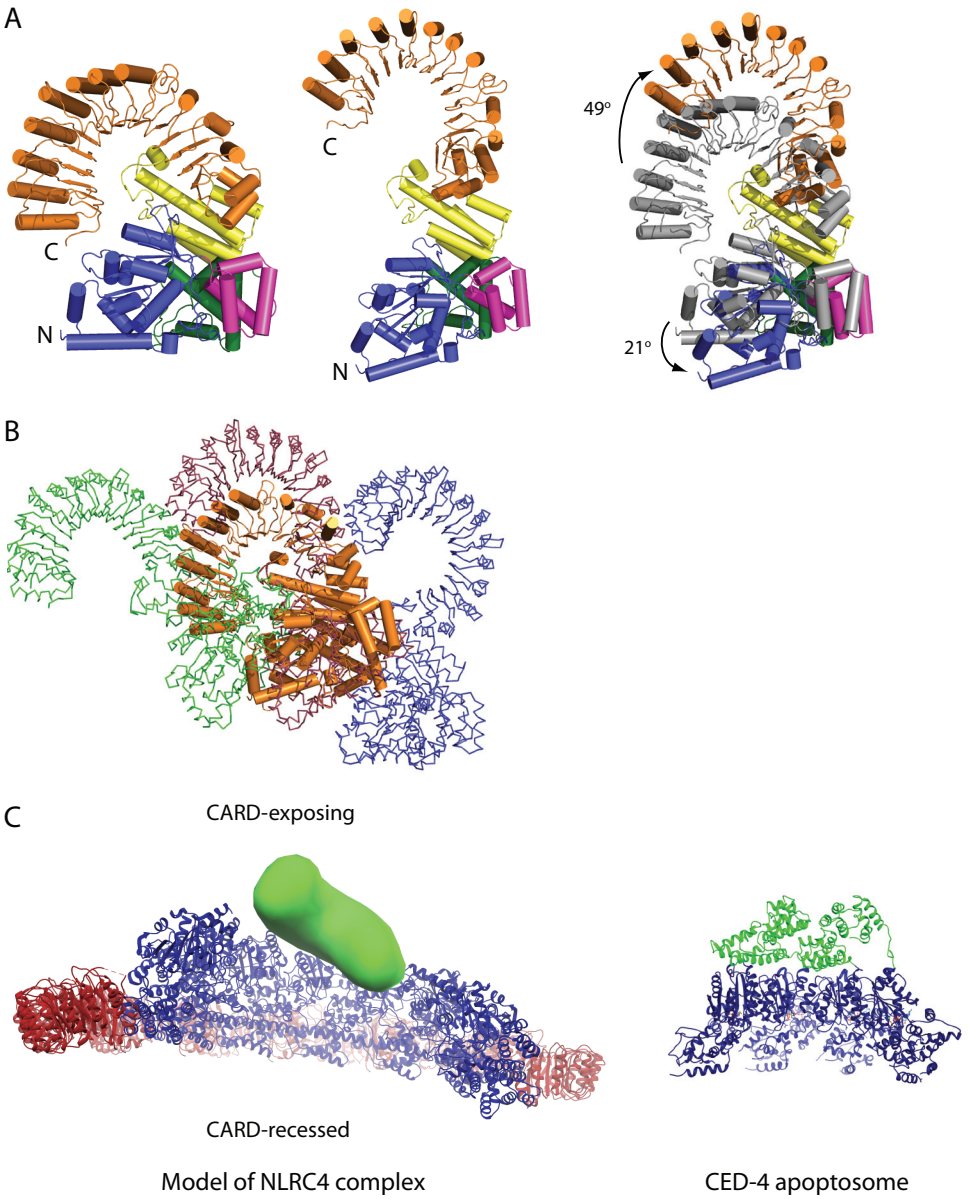

Figure 5. Interpretation of the model. *A.* Cartoon representation of the crystal structure of inactive NLRC4 (left, PDB ID 4KXF), our optimized EM-based model (center), and an overlay of both models superposed on the WHD-HD2 fragment (with the inactive structure in gray). Color coding is identical to Figure 4, panel B and C. Cylinders represent α-helices. *B.* Superposition of the crystal structure of inactive NLRC4 on three consecutive protomers of the optimized model, illustrating how LRR displacement exposes the NACHT-NACHT interaction surface. *C.* Cartoon representation of half a turn of our optimized model (left, 7 protomers) or the CED-4 apoptosome (right, 4 protomers). LRRs are colored red, NACHT domains blue, and the CED-4 CARDs green. The approximate location of the CARDs with respect to our model of the NACHT and LRR domains is indicated by a green surface, which was created by positioning the Apaf-1 CARD domain (PDB ID 1Z6T) near the N-terminus of the NACHT domain of one protomer, generating the symmetry related CARDs for the other protomers and finally calculating a density map at 20 Å resolution using UCSF Chimera.

of one protomer that contacts the NBD of the neighboring protomer in anti-clockwise direction according to the orientation depicted in Figure 4C. This arrangement differs from that observed in apoptosomes, in which NBD-NBD interactions dominate in a top ring comprising the NBDs, and WHD-HD1 interactions in a lower ring composed of alternating WHD and HD1 (see Figure 7D of chapter 1 and ref. 12). As apoptosomes contain seven or eight protomers in a flat ring, and inflammasomes contain $11^2/_3$ protomers per turn in a helical arrangement, it is to be expected that the interface between neighboring molecules are different. Compared to the structure of inactive NLRC4 the NBD-HD1 fragment in our model rotated by 21° with respect to the WHD-HD2 fragment (Figure 5A). The most prominent change is a rotation of the LRR by 49° with respect to WHD-HD2, away from its interaction surface on the NBD, enabling the latter to engage in NACHT-NACHT interactions (Figure 5B).

Although our model provides an adequate fit of the density at the current resolution, the presence of a number of steric clashes within and between protomers (Figure 4D,E) indicate that it should be interpreted with caution. While many of the clashes concern short contacts between side chains of surface exposed residues, which can easily be resolved, others may be the consequence of inaccurate positioning of the domains. Possibly, our assumption that conformational changes in the NACHT domain involve a hinge between HD1 and WHD only, is not correct. However, increasing the number of degrees of freedom in the model at the current resolution seems not justified.

As described, the CARDs were excluded during optimization of the model as they appeared not to obey the same helical symmetry as the NACHT-LRR region. Reduced symmetry for CARD domains is observed in the octameric CED-4 apoptosome in which the NACHT domains have 8-fold rotational symmetry, but the CARD domains display 4-fold symmetry by forming two stacked tetrameric rings. This is caused by an alternating CARD position in consecutive protomers: whereas one of the rings comprises CARDs that are packed against the NBD, in the remaining protomers the first α-helix of the NBD unfolds to enable positioning of the second CARD-ring at a longer distance[12]. Flexible linkage of CARD and NACHT is also evident in the structure of the Apaf-1 apoptosome in which the CARDs could not be resolved (Figure 7D of Chapter 1 and refs. 13, 28). Likewise, the CARD domains in our complexes may be positioned in an alternating or flexible way in consecutive protomers and, possibly, like in CED-4, this involves unfolding of the first helix of the NLRC4-NBD (residue 93-110). Unfolding of this helix would enable positioning of the CARDs at some distance from the NACHT domain, an arrangement that is suggested by the gap in the density between the NACHT-ring and CARD-rod. It should be noted, however, that density connecting the central rod to the concave hub may have been averaged out due to the application of helical symmetry.

Despite the uncertainty in positioning of the CARD domain in our model, its location N-terminal of the NACHT will cause the CARDs to be exposed at one end of the helix, and recessed inside the helix on its opposite end (Figure 5C). This is in agreement with our assumption that the pointed end observed at the terminus of both the NAIP5/NLRC4 and NAIP5-PKG/NLRC4 complexes (Figure 1, 2E, and ref. 10) represents the dimer interface stabilized by CARD-CARD interaction. In its physiological environment, the NAIP5/NLRC4 inflammasome presumably does not dimerize but, like apoptosomes, exposes its CARD domains as a platform for interaction with procaspase-1. Due to the close packing of protomers in our model procaspase-1

cannot reach CARD domains in the central part of the helix. As the latter region of the helical complex would therefore not be able to participate in pro-caspase activation and thus be non-functional, we envision that the smaller particles, as observed for the NAIP5/NLRC4 complexes formed with NAIP5 not fused to PKG, are closer to the biologically relevant structure.

Concluding remarks and future perspectives

We set out to analyze the structure of the NAIP5/NLRC4 inflammasome in closer detail and in particular to locate the position of NAIP5 in the complex. The apparent heterogeneity in the size and conformation of the complexes purified from HEK293E cells prohibited their crystallization for X-ray diffraction studies, therefore we have taken an EM-based approach. One of our strategies to locate NAIP5, namely its fusion to PKG, unexpectedly led to the formation of much larger complexes with a rod-like appearance that turned out to have a helical buildup. We exploited the helical symmetry for density averaging and constructed a model of NLRC4 in its complex-incorporated conformation. Our data indicate that the conformational changes involved in inflammasome formation are different from those in apoptosomes.

On the basis of the small volume available inside the NACHT-ring, we argued that NAIP5 is either absent or only present in small amounts in the helical region of our complexes. Since NAIP5 induces formation of the NAIP5/NLRC4 inflammasome, but is far less abundant in the complex than NLRC4, it is tempting to speculate that NAIP5 is present only at one or both of the termini whilst NLRC4 forms the central region of the helical rod. Analysis of the termini of the NAIP5-PKG/NLRC4 complexes by subtomogram averaging showed considerable heterogeneity in this region. Due to this heterogeneity, and since helical averaging cannot be applied, more data will be required to obtain an EM map at sufficient resolution for structural interpretation of the helix termini. Further investigation will focus in particular on determining the position of NAIP5 in the complex.

The helical rods observed in the NAIP5-PKG/NLRC4 inflammasome are reminiscent of the rods formed by spontaneous multimerization of NLRC4 at high concentration[10]. We initiated work to analyze these NLRC4-rods by single particle reconstruction (Supplementary Figure 5), which we expect to result in a higher resolution map than the electron tomography derived map obtained in this study, without the ambiguities arising from the presence of both NAIP5 and NLRC4. A higher resolution reconstruction of these particles and an improved model of activated NLRC4 obtained from these data will enable us to compare the central parts and the termini of both particles and may reveal whether NAIP5 is indeed located at the termini.

We envision that the information obtained from EM analysis of the large NLRC4-rods and NAIP5-PKG/NLRC4 complexes will aid in the interpretation of the EM data on the smaller and probably more functionally relevant NAIP5/NLRC4 inflammasomes. Until this is achieved, the model presented here provides a first insight into the hetero-oligomeric NAIP5/NLRC4 inflammasome and the conformational changes occurring in NLRs during activation.

Experimental procedures

Cell culture and transfection

HEK293E cells were cultured in Freestyle medium (Invitrogen), containing 0.2% FCS, 50 µg/ml G418 disulfate at 37 °C in a 5% CO_2 humidified atmosphere. The cells were grown in suspension at 120 rpm. Small scale (4 mL) and large scale (400 ml) transfections were performed according

to Durocher *et al*. [25].

Plasmids

Expression plasmids for murine *Naip5*, murine *Nlrc4* and the *Salmonella Typhimurium* flagellin $D0_L$ fragment were created as described [10]. To create the vector expressing bovine cGMP-dependent protein kinase I alpha (PKG) as a C-terminal fusion protein, the coding sequence of PKG was amplified by PCR using a forward primer that introduces a NotI restriction site while omitting the start codon, and a reverse primer that omits the stop-codon and introduces a C-terminal PspOMI restriction site followed by a BsmBI restriction site that creates a PspOMI overhang. At the protein level this procedure results in the introduction of three Ala residues at the N-terminus and a Gly-Ala sequence at the C-terminus of PKG. The PCR product was cloned into a pUPE vector (U-Protein Express BV, The Netherlands) to create a plasmid that encodes a C-terminal TEV-PKG-$StrepII_3$-His_6 tag. Expression vectors for mNLRC4 encoded a C-terminal $Flag_3$-His_6 tag, an N-terminal His_6-GFP-tag, or no tag as specified in the text and figure legends. Expression vectors for mNAIP5 encoded a C-terminal TEV-$StrepII_3$-His_6, TEV-$StrepII_3$ or TEV-PKG-$StrepII_3$-His_6 tag or a combination of an N-terminal His_6-GFP plus a C-terminal TEV-$StrepII_3$ tag. The FliC-$D0_L$ fragment was expressed without tags.

Protein purification and gel filtration

For small scale purification from 4 ml HEK293E cultures, cells were harvested 48 hours post-transfection by centrifugation at 600 x *g* for 5 min. Cell pellets were stored for 1 hour up to 1 week at -20 °C. For purification, pellets were thawed at room temperature. Cytoplasmic extracts were obtained using a method described by Tsai et al. [26], with omission of the PBS washing step. Cell pellets were resuspended in 320 µl cold small scale lysis buffer containing 10 mM HEPES pH 7.6, 5 mM $MgCl_2$, 10 mM KCl , 5 mM DTT, 1 µg/ml DNase and 1 tablet Complete mini, EDTA-free tablets (Roche) per 20 ml buffer. StrepII-tagged proteins were purified from the cleared cytoplasmic extracts using StrepTactin Sepharose beads (GE Healthcare). After incubation for 1-2 hr at 4 °C, beads were washed in StrepTactin wash buffer (100 mM NaCl, 25 mM HEPES pH 7.5, 5 mM benzamidin, 5% glycerol, 2 mM DTT), and subsequently protein was eluted in wash buffer supplemented with 5 mM *d*-desthiobiotin (Sigma).

For structural analysis by electron microscopy (EM), complexes were purified from 400 ml HEK293E cell cultures co-transfected with murine *Nlrc4*-$Flag_3$-His_6, tagless *FliC*-$D0_L$, and either *Naip5*-TEV-$StrepII_3$-His_6 or *Naip5*-TEV-PKG-$StrepII_3$-His_6. Cells were harvested 72-96h post transfection by spinning at 600 x *g* for 10 min. Pellets were stored at -80 °C until further purification. Affinity purification was performed as described for small scale purifications [10], scaled up according to the culture volume.

Complexes containing NAIP5-PKG were further purified by gel filtration. Affinity-purified protein was first concentrated on a 50 kDa cutoff filter spin tube (Millipore). The concentrated sample was then injected on a Superose-6 10/300 column (GE Healthcare) equilibrated in gelfiltration buffer (100 mM NaCl, 20 mM HEPES pH 7.5, 2 mM Benzamidin, 2 mM DTT). Fractions were pooled as indicated in Figure 2 and protein was concentrated to ~1.2 mg/ml.

Gel electrophoresis and protein detection

Reduced protein samples were separated on standard Laemmli 9% SDS-PAGE gels. Samples for native gel electrophoresis were run on 3-12% NativePAGE Novex Bis-Tris gels (Invitrogen) according to the manufacturer's protocol, using NativeMark Unstained Protein Standard (Invitrogen) as marker. Gels were silver stained, Coomassie stained, or transferred to polyvinylidene difluoride (PVDF) membrane (BioRad). Proteins were detected on Western blot using a mixture of mouse anti-polyHistidine (Sigma) and mouse anti-Penta-His (Qiagen) as primary antibodies and Rabbit-anti-mouse-HRP (Dako) as the secondary antibody. The signal was detected using ECL (GE Healthcare).

Sample preparation for electron microscopy

For cryo-EM, PKG-NAIP5/NLRC4 inflammasomes (1.2 mg/ml) were incubated with protein conjugated 10 nm gold beads as fiducial markers (donkey anti goat IgG, AURION). 4 µl sample was applied on EM grids, R1.2 1.3, Cu 200 mesh (Quantifoil), that had been glow discharged for 1 min at 30 mA and negative polarity using a K950X carbon coater (Emitech). After 3 s blotting with filter paper (Whatman 541) the sample was plunge-frozen in a liquid propane/ethane (2:1 v/v) mixture using an EM-GP (Leica) at room temperature and 95 % humidity. In a similar way, concentrated poly-NLRC4 (5 mg/ml) was plunge frozen after short incubation with protein A conjugated 5 nm gold beads (UMC).

The NAIP5/NLRC4 inflammasomes, at a concentration of 0.3 mg/ml, were incubated with 20 µg/ml mouse anti-Flag as primary antibody and protein A labeled with 5 nm gold beads for

20 minutes at 4 °C and then applied on glow discharged EM grids, CF-2/1-2C (C-flat), blotted for 3 s and plunge frozen in liquid ethane using a Mark IV Vitrobot (FEI) at room temperature and 100% humidity.

Cryo-EM data collection
Data was collected using a NeCEN Titan Krios (FEI) TEM at 200 kV acceleration voltage and parallel illumination.
Three dual axis tilt series of NAIP5/NLRC4 inflammasomes were acquired at -7 µm defocus and an initial magnification of 18,000 x on a unbinned Falcon (FEI) direct electron detector, resulting in images with 4.82 Å pixel size at specimen level. A total electron dose of 50 $e^-/Å^2$ was distributed over 57 images per series applying a Saxton tilt scheme with initial increment of 3°.
16 low dose single axis tilt series of NAIP5-PKG/NLRC4 inflammasomes were acquired with a GATAN Quantum imaging filter at -7 µm defocus using dose distribution and linear continuous tilt scheme with 2° increment between +/-66 °, resulting in tilt series comprising 67 images at a final pixel size of 5.46 Å and a total electron dose of ~100 $e^-/Å^2$.
For single particle data collection of NLRC4-rods 3,641 images were acquired automatically with a FEI Falcon direct electron detector on two different grid squares of the same grid, 5 images per hole, at alternating defocus of -3 and -5 µm using an electron dose of 10 $e^-/Å^2$. A nominal magnification of 37,000 x resulted in a pixel size of 2.34 Å at specimen level.

EM data processing
Reconstruction of single axis NAIP5-PKG/NLRC4 tomograms and sub tomogram averaging - NAIP5-PKG/NLRC4 single axis tomograms were reconstructed in IMOD (Kremer, Mastronarde et al. 1996). Images were aligned by patch tracking and low pass filtered to the first zero of the contrast transfer function (CTF) before applying simultaneous iterative reconstruction algorithm (SIRT) in five iterations. Of 16 tomograms the 7 best were selected for subtomogram averaging.
The averages of central parts of the particles were calculated using the IMOD PEET software (Nicastro, Schwartz et al. 2006). 15 longer (seemingly helical) particles were extracted from the tomograms and rotated in order to prealign the putative symmetry axis of the particles using a script based on IMOD *slicer* and *rotatevol*. For each of the 15 subtomograms an initial motive list with 100 reference coordinates for PEET, equally spaced along the symmetry axis, was produced with the PEET program *stalkInit*. In order to reduce missing wedge bias during particle alignment, subtomograms were extracted with random rotation around the putative symmetry axis. Averaging was performed in 10 iterations with decreasing translational and rotational step sizes (down to 1°) using a randomly chosen initial reference particle (Figure 3A) and a disc shaped binary mask with 22 pixel height and 40 pixel radius, which was created in SPIDER (Frank, Radermacher et al. 1996). For each new iteration, particles were aligned against an average comprising 5-10% of the best correlating particles. After three iterations without imposing symmetry, the symmetry axis was realigned and helical symmetry was imposed for all further iterations by creating a symmetrically averaged reference using a Imod based script. The initial symmetry parameters were obtained from image features visible in the best tomogram. The final average represented 50 best correlating particles.
The resolution of the unsymmetrized average was estimated by Fourier shell correlation of two averages obtained by even-odd splitting of particles. Again, the Imod based script that has been used to create the intermediate symmetric references was run to create a helically symmetrized map from the unsymmetrized average.
Reconstruction of dual axis NAIP5/NLRC4 tomograms - Dual axis cryo electron-tomograms of NAIP5/NLRC4 were reconstructed and merged in IMOD (Mastronarde 1997). Tilt series were locally aligned using fiducial tracking. Before tomogram reconstruction using 5 SIRT iterations, gold beads were removed from aligned tilt series and CTF was corrected by phase flipping after defocus estimation in TOMOCTF (Fernandez, Li et al. 2006). The tomogram was low pass filtered and isosurfaces of representative particles were extracted and visualized using UCSF Chimera (Pettersen, Goddard et al. 2004).

Modeling of the helical NAIP5-PKG/NLRC4 inflammasome
An averaged density map of NAIP5-PKG/NLRC4 was created on the basis of 50 boxed volumes selected from the most regular regions of the subtomograms of 15 particles (in total ~1500 protomers), with omission of the termini of the particles. As this clearly revealed a right-handed helical arrangement, we applied helical averaging to these 50 boxed volumes, resulting in a final model at a resolution of 36 Å (Figure 3B). From this unsymmetrized average, we created a helically symmetrized map (Figure 3C) using

5.57 Å rise and +30.9° rotation per protomer. A model of a complex-incorporated NLRC4 monomer, obtained from fitting fragments of the NLRC4 crystal structure (PDB ID 4KXF) as described in the results, was manually fitted in UCSF Chimera. As input for the refinement, we created 26 symmetry related protomers using the Chimera *sym* command and superposed this model with the ET average map. From this manually fitted model, an optimized model for a helical NLRC4 polymer was created by iterative, symmetry imposed, simultaneous multi fragment docking using Situs (Wriggers 2010). The NBD-HD1, WHD-HD2, and LRR fragments of each of the 26 symmetry-related molecules were locally refined as separate rigid bodies in one round of off-lattice Powell optimization using Situs *collage* (Birmanns, Rusu et al. 2011). After that, repeatedly the best fitting protomer was selected, a new set of symmetry related NLRC4s created and refined in *collage*. This cycle was repeated five times.
All figures of the model were created in UCSF Chimera or PyMOL.

References

1. Chen, G., et al., *NOD-like receptors: role in innate immunity and inflammatory disease.* Annu Rev Pathol, 2009. **4**: p. 365-98.
2. Martinon, F., K. Burns, and J. Tschopp, *The inflammasome: a molecular platform triggering activation of inflammatory caspases and processing of proIL-beta.* Mol Cell, 2002. **10**(2): p. 417-26.
3. Schroder, K. and J. Tschopp, *The inflammasomes.* Cell, 2010. **140**(6): p. 821-32.
4. Martinon, F. and J. Tschopp, *Inflammatory caspases and inflammasomes: master switches of inflammation.* Cell Death Differ, 2007. **14**(1): p. 10-22.
5. Dinarello, C.A., *Interleukin-1 beta, interleukin-18, and the interleukin-1 beta converting enzyme.* Ann N Y Acad Sci, 1998. **856**: p. 1-11.
6. Fink, S.L. and B.T. Cookson, *Apoptosis, pyroptosis, and necrosis: mechanistic description of dead and dying eukaryotic cells.* Infect Immun, 2005. **73**(4): p. 1907-16.
7. Kofoed, E.M. and R.E. Vance, *Innate immune recognition of bacterial ligands by NAIPs determines inflammasome specificity.* Nature, 2011.
8. Zhao, Y., et al., *The NLRC4 inflammasome receptors for bacterial flagellin and type III secretion apparatus.* Nature, 2011. **477**(7366): p. 596-600.
9. Miao, E.A., et al., *Innate immune detection of the type III secretion apparatus through the NLRC4 inflammasome.* Proc Natl Acad Sci U S A, 2010. **107**(7): p. 3076-80.
10. Halff, E.F., et al., *Formation and structure of a NAIP5-NLRC4 inflammasome induced by direct interactions with conserved N- and C-terminal regions of flagellin.* J Biol Chem, 2012.
11. Proell, M., et al., *The Nod-like receptor (NLR) family: a tale of similarities and differences.* PLoS One, 2008. **3**(4): p. e2119.
12. Qi, S., et al., *Crystal structure of the Caenorhabditis elegans apoptosome reveals an octameric assembly of CED-4.* Cell, 2010. **141**(3): p. 446-57.
13. Yuan, S., et al., *Structure of an apoptosome-procaspase-9 CARD complex.* Structure, 2010. **18**(5): p. 571-83.
14. Yuan, S., et al., *Structure of the Drosophila apoptosome at 6.9 a resolution.* Structure, 2011. **19**(1): p. 128-40.
15. Inohara, N. and G. Nunez, *The NOD: a signaling module that regulates apoptosis and host defense against pathogens.* Oncogene, 2001. **20**(44): p. 6473-81.
16. Kofoed, E.M. and R.E. Vance, *NAIPs: Building an innate immune barrier against bacterial pathogens: NAIPs function as sensors that initiate innate immunity by detection of bacterial proteins in the host cell cytosol.* Bioessays, 2012.
17. Damiano, J.S., et al., *CLAN, a novel human CED-4-like gene.* Genomics, 2001. **75**(1-3): p. 77-83.
18. Poyet, J.L., et al., *Identification of Ipaf, a human caspase-1-activating protein related to Apaf-1.* J Biol Chem, 2001. **276**(30): p. 28309-13.
19. Geddes, B.J., et al., *Human CARD12 is a novel CED4/Apaf-1 family member that induces apoptosis.* Biochem Biophys Res Commun, 2001. **284**(1): p. 77-82.
20. Acehan, D., et al., *Three-dimensional*

structure of the apoptosome: implications for assembly, procaspase-9 binding, and activation. Mol Cell, 2002. **9**(2): p. 423-32.
21. Bao, Q. and Y. Shi, *Apoptosome: a platform for the activation of initiator caspases.* Cell Death Differ, 2007. **14**(1): p. 56-65.
22. Reubold, T.F., S. Wohlgemuth, and S. Eschenburg, *Crystal structure of full-length Apaf-1: how the death signal is relayed in the mitochondrial pathway of apoptosis.* Structure, 2011. **19**(8): p. 1074-83.
23. Reubold, T.F. and S. Eschenburg, *A molecular view on signal transduction by the apoptosome.* Cell Signal, 2012. **24**(7): p. 1420-5.
24. Hu, Z., et al., *Crystal Structure of NLRC4 Reveals Its Autoinhibition Mechanism.* Science, 2013.
25. Durocher, Y., S. Perret, and A. Kamen, *High-level and high-throughput recombinant protein production by transient transfection of suspension-growing human 293-EBNA1 cells.* Nucleic Acids Res, 2002. **30**(2): p. E9.
26. Tsai, A. and R.P. Carstens, *An optimized protocol for protein purification in cultured mammalian cells using a tandem affinity purification approach.* Nat Protoc, 2006. **1**(6): p. 2820-7.
27. Takio, K., et al., *Guanosine cyclic 3',5'-phosphate dependent protein kinase, a chimeric protein homologous with two separate protein families.* Biochemistry, 1984. **23**(18): p. 4207-18.
28. Yuan, S., et al., *The holo-apoptosome: activation of procaspase-9 and interactions with caspase-3.* Structure, 2011. **19**(8): p. 1084-96.
29. Larkin, M.A., et al., *Clustal W and Clustal X version 2.0.* Bioinformatics, 2007. **23**(21): p. 2947-8.

4

Supplementary figures

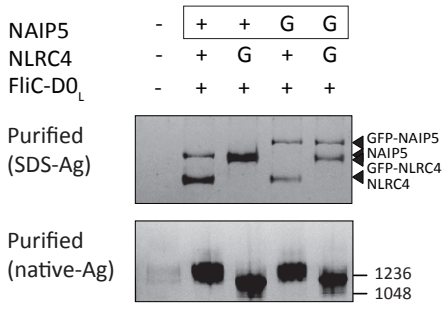

Supplementary Figure S1. Fusion of GFP at the NLRC4 N-terminus likely interferes with inflammasome dimerization. Analysis of inflammasome formation in HEK293E cells transfected with the proteins indicated. The boxed proteins carry the $StrepII_3$-His_6 purification handle; "G" indicates that the protein is fused to GFP at its N-terminus. Purified protein was analyzed by SDS-PAGE (top panel) or native PAGE (3-12%; bottom panel) followed by silver staining. For the native PAGE, numbers on the right indicate the molecular weight of the marker in kDa.

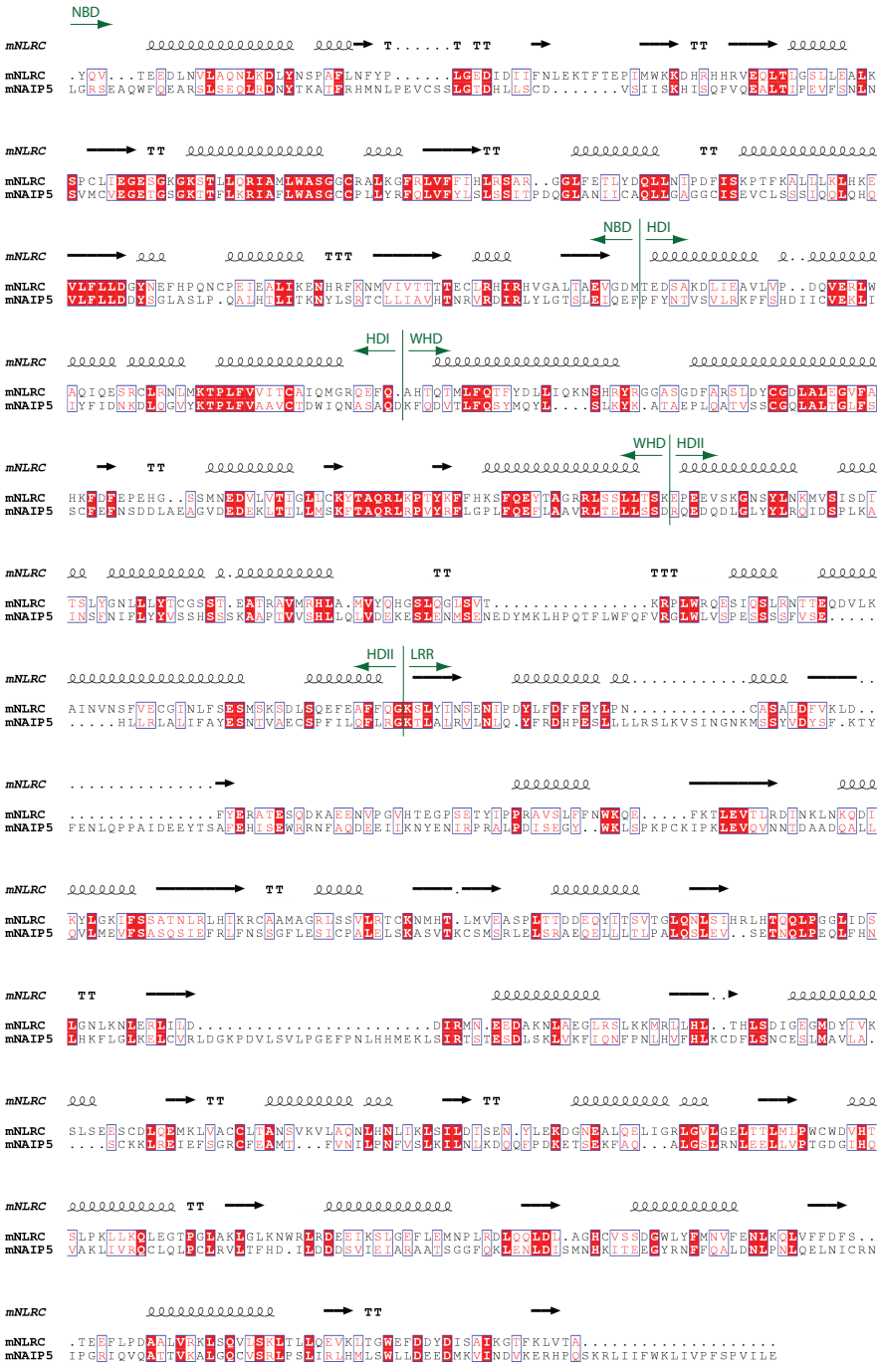

Supplementary Figure S2. Protein sequence alignment of murine NAIP5 and NLRC4. Sequences of the NACHT and LRR domains of murine NAIP5 (UniProt entry Q9R016) and murine NLRC4 (Q3UP24) were aligned using ClustalW2 (ref. 29). The secondary structure of NLRC4 is indicated at the top (PDB ID 4KXF). (Sub)domain boundaries on the basis of the NLRC4 crystal structure are indicated in green. The threshold for coloring is set to a similarity score of 0.7 based on the Risler matrix.

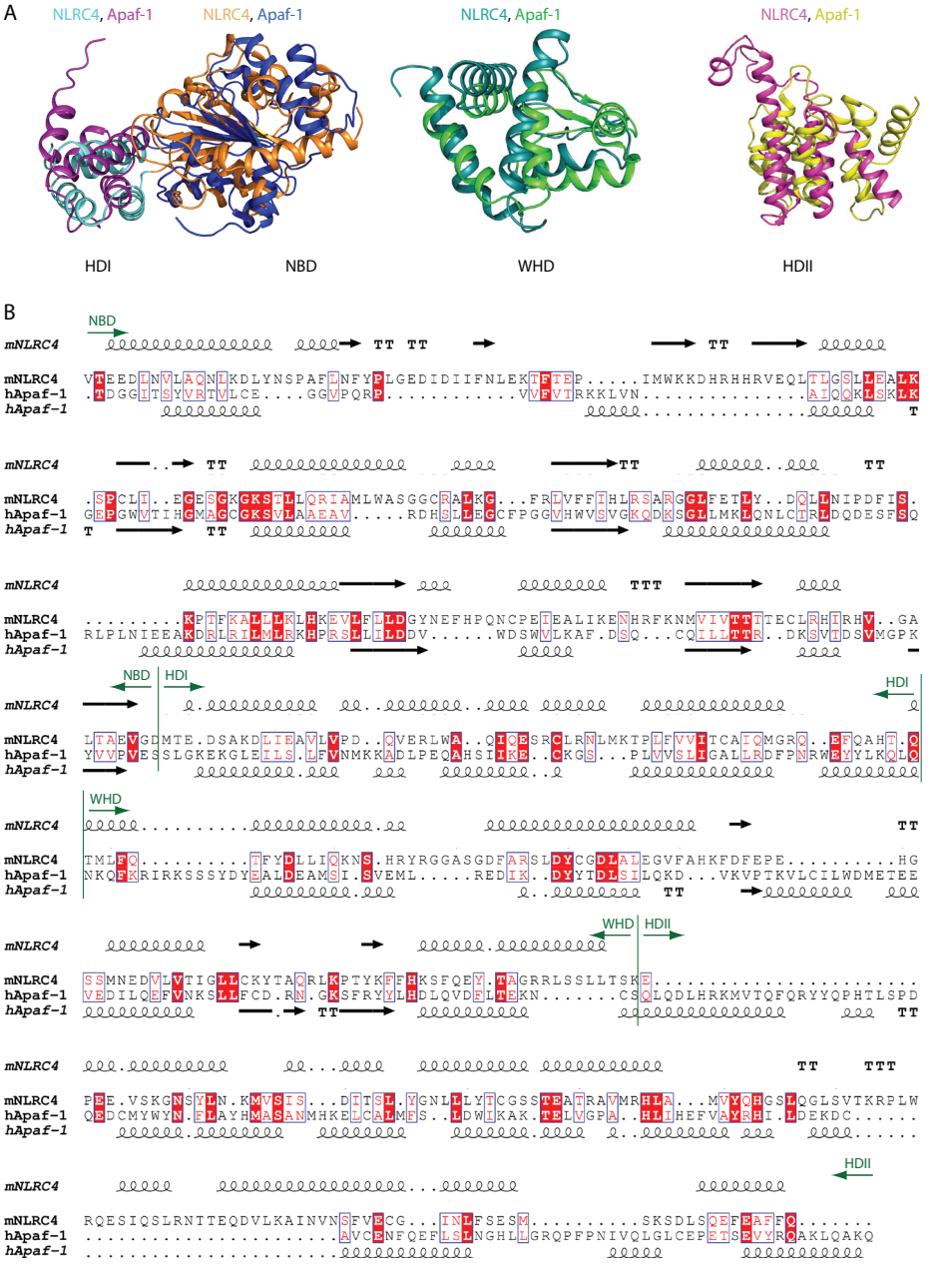

Supplementary Figure S3. Structural and sequential comparison of NLRC4 and Apaf-1 NACHT subdomains. *A.* Cartoon representation of superposed fragments of murine NLRC4 and human Apaf-1 NACHT domains (PDB ID 4KXF and 1Z6T, respectively). Color coding is indicated at the top. *B.* Structure based protein sequence alignment of the NACHT domains of murine NLRC4 (Q3UP24) and human Apaf-1 (O14727). The structures of the hApaf-1 and mNLRC4 NACHT domains were aligned per domain in USCF Chimera and the resulting sequence alignment was manually edited. The secondary structure of mNLRC4 and hApaf-1 are indicated at the top and bottom, respectively. Subdomain boundaries as derived from the superposed crystal structures are indicated in green. The threshold for coloring is set to a similarity score of 0.7 based on the Risler matrix.

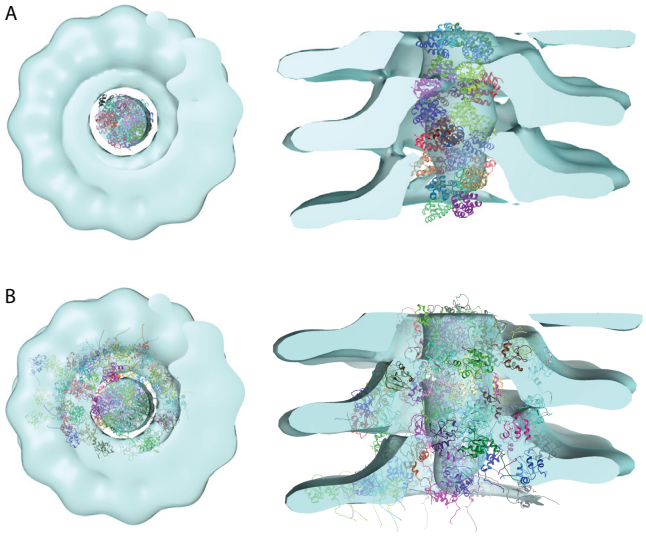

Supplementary Figure S4. Visualization of the fit of effector binding domains to the averaged density map. *A,B.* Top view and cross-section side view of the symmetrized density map showing an optimized fit of CARDs (A) or the BIR domains (B) to the central rod density. The CARD and BIR domains were fitted without imposing helical symmetry. While CARDs can be accommodated in the central rod density, BIR domains are placed outside the central rod. The figure was created using UCSF Chimera.

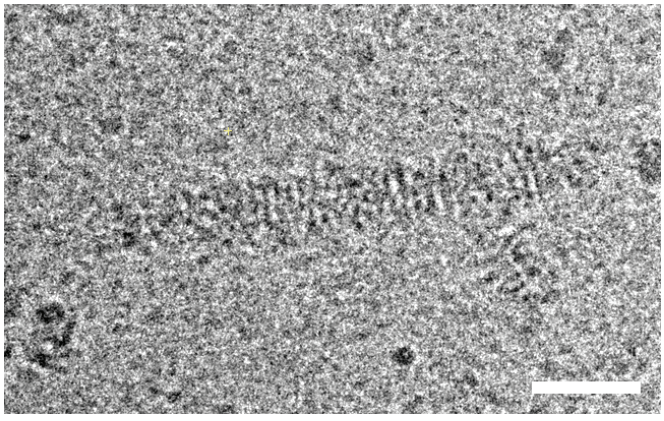

Supplementary Figure S5. Cryo-EM projection image of poly-NLRC4 rods. Representative image of poly-NLRC4 complexes imaged over a hole in the carbon support film. The white scale bar represents 50 nm.

Chapter **5**

General Discussion

Els F. Halff

Crystal and Structural Chemistry, Bijvoet Center for Biomolecular Research, Department of Chemistry, Faculty of Science, Utrecht University, The Netherlands

General Discussion

Summary of insights into NLR structure and function prior to this thesis

Our immune system faces the constant challenge of microbial invasion. This requires mechanisms for both recognition and clearance of infected cells and invading microorganisms. The family of Nod-like receptors (NLRs) plays an essential role in the intracellular recognition of pathogen and danger associated molecular patterns (PAMPs and DAMPs, respectively)[1]. PAMPs comprise conserved molecules derived from microorganisms that are essential for their survival but not present in the host; they include a wide range of molecules including peptidoglycans, proteins, and nucleic acids. DAMPs on the other hand are endogenous danger signals released by dying or injured cells, such as microcrystals, extracellular ATP and intracellular reactive oxygen species (ROS). Additionally, the NLR family member NLRP3 was shown to be able to recognize xenogenous compounds such as asbestos and silica[2-4].

NLR activation contributes to both the initiation of a rapid innate immune response as well as to the development of long-lasting adaptive immunity. The main signaling pathways induced by NLR activation entail the upregulation of the pro-inflammatory cytokines pro-IL-1β and pro-IL-18 via the NF-κB pathway as well as the proteolytic activation of procaspase-1[1]. Activated caspase-1 is required for the processing and subsequent secretion of pro-IL-1β and pro-IL-18[5]. Additionally, caspase-1 induces an inflammatory cell death called pyroptosis[6].

NLR activation requires tight regulation. On the one hand, a lack of activation at the appropriate time leads to a deficiency in pathogen clearance and uninhibited proliferation of the pathogen. On the other hand, failure to inhibit inappropriate activation in the absence of a stimulus causes constitutive inflammation and damage to the host[7].

An essential aspect of NLR activation is their oligomerization into a large complex called nodosome (for the NF-κB activating NLRs) or inflammasome (for the caspase-1 activating NLRs)[8-10]. NLR multimerization is thought to involve a series of conformational changes, induced by ligand recognition. Due to the lack of structural information on NLRs themselves, a model for their activation mechanism was mainly derived from homologous proteins. Biochemical studies on NLRs and homologous proteins suggested that, in the absence of a ligand, the C-terminal leucine rich repeat (LRR) sensor domain maintains the NLR in a monomeric, dormant conformation. The ligand presumably interacts with the LRR domain, thereby abrogating the dormant conformation and inducing a conformational change within the centrally located and highly conserved NAIP, CIITA, HET-E and THPI (NACHT) domain that allows nucleotide exchange and enables multimerization. These changes uncover the binding interface of the N-terminal effector binding domain (EBD) for interaction with downstream signaling molecules[11-12]. The structure of inflammasomes and nodosomes is thought to resemble that of the apoptosis-inducing complex called apoptosome, which is formed by the proteins Apaf-1, Dark, and CED-4 in mammals, *Drosophila*, and *C.elegans* respectively[13-15]. As for NLRs, signaling by these proteins is dependent on their multimerization via homotypic interactions between their NACHT domains. In the resulting complex the protomers are arranged in a ring, thereby forming a disk-shaped complex that exposes on one side a platform of

caspase activation and recruitment domains (CARDs) for the recruitment of downstream signaling molecules[16-17]. On the basis of a negative stain electron microscopy (EM) image of the NLRP1 inflammasome, which revealed complexes containing either 5 or 7 protomers[11], and the proposed resemblance to the heptameric and octameric apoptosomes[16-19], inflammasomes were generally expected to be ring-shaped oligomers consisting of 5-8 protomers.

Summary of recent developments and our contribution to understanding NLR structure and function

Although the above described hypothetical activation mechanism of inflammasome formation is supported by biochemical data on NLRs, primarily derived from cell-based experiments, for a long time it remained unknown whether NLRs directly interact with their ligands and how they transit from their inhibited to activated conformation. The difficulty to purify NLRs in sufficient amounts and to sufficient homogeneity for *in vitro* biochemical and structural studies has been one of the major reasons why these questions remained unanswered.

In this thesis we describe how we overcame challenges in NLR overexpression and purification and developed a successful protocol for obtaining small amounts of purified NLR from transiently transfected mammalian HEK293E cells (chapter 2). This method enabled us to study the activation mechanism of the NLRs NAIP5 and NLRC4. By means of cell-based assays in HEK293E cells as well as *in vitro* studies using the purified material we show for the first time that NAIP5 directly associates with the conserved D0 domain of *S.typhimurium* flagellin. Upon activation, NAIP5 recruits multiple copies of NLRC4 into a hetero-oligomeric inflammasome (chapter 3). Analysis of the purified NAIP5/NLRC4 inflammasomes by negative stain (chapter 3) and NAIP5-PKG/NLRC4 complexes by cryo-EM (chapter 4) provided initial structural insight into the hetero-oligomeric inflammasome structure. Our data is consistent with a model in which activated NAIP5 initiates and terminates helical multimerization of NLRC4.

The NLR field has been rapidly developing over the past few years. Since the start of this thesis research, many new interaction partners, ligands, and signaling pathways that involve NLRs have been described. Several NLRs have been shown to detect a variety of ligands, can be part of multiple signaling pathways, and can interact with a plethora of other intracellular proteins (for some examples, see refs. 20-22). These recent data challenge the original view of the NLRs being 'simple' detectors of invading microorganisms, each detecting a single and specific ligand, and being capable of passing on a single signal that sets the immune system to action.

In recent years, significant progress has also been made on the purification of NLRs. Recent studies now include *in vitro* analysis on the interaction of purified NLRs with their ligands. Of particular importance, shortly before the completion of this manuscript, and during the structural analysis of the NAIP5/NLRC4 complex as described in chapter 4, the crystal structure of the inactive conformation of CARD-deleted NLRC4 was published[76].

Below, the implications of our data are discussed in the light of these recent advances in the NLR field, focusing particularly on NLR expression and purification, interaction of NLRs with their ligands, and the formation and structure of hetero-oligomeric inflammasomes.

Overcoming Challenges in NLR Purification

For a long time biochemical studies on NLRs have been hampered by the inability to obtain sufficient amounts of purified protein. Isolated effector binding domains were the first NLR-domains to be successfully purified, and were obtained using bacterial expression systems (*e.g.* refs. 23-25). In many cases, however, these domains were reported to exhibit severe aggregation. The first full length NLRs reported to be purified were NLRP3, obtained from the human monocytic cell line THP1 at a yield of 10-20 µg/L of cell culture[26], and GST-fused NLRP1 obtained from the insect cell line Sf9 at 25 µg/L[11]. Both proteins were, however, reported to be unstable upon purification.

More recently, higher yields have been reported for NOD1 (1 mg/L HEK293 Freestyle cells after a single affinity purification step[27]) and NOD2 (100-300 µg/L Sf9 cells using dual affinity tag purification[28] or 1 mg/L Sf21 cells using single affinity tag purification[29]). Our yield of NLRC4 (100-200 µg/L HEK293E cells after dual tag purification and gelfiltration, chapter 2 and 3) thus falls within the same range. Notably, after the first affinity purification step by Ni-NTA we obtain a protein yield of about 1 mg NLRC4 per liter HEK293E cells (chapter 2). This yield is thus comparable to the published yields for NOD1 and NOD2 after a single affinity purification step[27,29]. In our hands, a large fraction of the NLRC4 protein is, however, lost upon further purification. SDS-PAGE gels of the purified NOD1 and NOD2 show that there is residual protein co-purifying. It remains to be seen what the protein yield will be upon further purification.

As was reported for the purification of NOD1 and NOD2[27-28], we also observe that a large fraction of the NLR protein that is present in the soluble lysate did either not bind the affinity column, or was only eluted at a high concentration of the elution agent. This suggests aggregation or misfolding of this fraction of the protein. We showed that NLRs aggregate over time already inside the cell, particularly at high expression levels (chapter 2). Possibly, NLRs continue to aggregate or multimerize even during purification.

We improved the solubility of NLRs inside the cell by plasmid titration, *i.e.* the reduction of expression levels by the replacement of expression plasmids with an empty vector (chapter 2). Even at these reduced expression levels we find that NLRC4 self-associates (chapter 3). This NLRC4 multimerization correlates with increased basal-level caspase-1 activation, suggesting that the NLRC4 multimers are at least partially functional. Potentially, spontaneous NLRC4-multimerization involves phosphorylation of residue Ser553, a process that was recently reported to be essential for NLRC4 oligomerization and downstream signaling[30]. Overexpression of NOD2 was also shown to increase the basal activation of NF-κB, and a significant reduction in expression plasmid used for transfection was necessary to prevent spontaneous activation of the downstream signaling pathway[31]. Possibly, overexpression of NLRs leads to their spontaneous multimerization inside the cell in a similarly ordered manner as we observed for purified NLRC4 at high concentration. This process might contribute to the difficulty of purifying NLRs as well as to protein loss during the purification procedure.

We find that a single-step affinity purification employing a triple StrepII tag yields relatively pure protein and is therefore a rapid and convenient method for purifying NLRs when high purity is not required. Similarly, a single-step purification protocol using a streptavidin-binding tag has recently been described for the successful purification of plant resistance proteins (R-proteins), the functional and structural homologues

of NLRs[32]. We applied purification via StrepTactin both for small scale purifications as a quick method to assess the effect of transfection methods or to find conditions in which the NAIP5/NLRC4 inflammasome is formed (chapter 2-4), as well as for the purification of NAIP5/NLRC4 complexes on larger scale for structural analysis (chapter 3-4).

Whereas the efficiency of *in vitro* formation of the NAIP5/NLRC4 complex was low, we successfully purified the NAIP5/NLRC4 complex that was formed in HEK293E cells by co-expression of NAIP5 and NLRC4 with the FliC-$D0_L$ domain (chapter 3). We found this complex to be significantly more stable than purified NLR monomers. The NAIP5/NLRC4 complex could be purified with a yield of 1-2 mg/L and could be concentrated to over 6 mg/ml with negligible loss of protein. Possibly, inflammasomes comprising other NLRs can also be obtained by formation *in vivo* and subsequent purification.

In this light, another reason why NLRs are so hard to purify and are instable upon purification, could be that they lack natural interaction partners that are required for their stabilization. Among the increasing number of putative NLR interaction partners reported in recent years, some are suggested to stabilize an inactive conformation of the NLR until it meets its ligand. We found HSP70, HSP90, and SGT1 to be associated with several NLRs (chapter 2), an interaction that has been described to be important for NLR stabilization in its dormant form[33-36]. Apart from these general regulators, NLR-specific binding partners have been described as well. NLRP1 was reported to associate with Bcl-2 and Bcl-X_L, an interaction that inhibited NLRP1 signaling until the effector MDP is encountered[37]. Bid, a family member of Bcl-2, associated with NOD1 and NOD2 in the absence of ligand[27,38]. This inhibition mechanism is reminiscent of the way in which CED-9, the *C.elegans* homologue of Bcl-2, inhibits CED-4 and maintains the protein in a signaling competent state prior to its activation[39-40]. In HEK293 cells and other expression systems, these natural binding partners may be missing, or they may not be present in sufficient amounts when overexpressing NLRs to prevent their aggregation inside the cell. Additionally, a lack of these stabilizing interaction partners may explain the instability of NLRs upon purification. This intrinsic instability may partially account for the contradicting outcomes of biochemical studies on the NLR activation mechanism. For instance, whereas NLRP1 only binds ATP in the presence of MDP, pre-incubation of NOD2 with ATPγS enhanced its association with MDP[11,28]. Co-purifying NLRs with their putatively stabilizing interaction partners may provide a solution to NLR instability during purification.

To bind or not to bind?

The question whether or not NLRs directly associate with their ligands has long remained unsolved. As mutations in the LRR linked to Crohn's disease renders the protein unresponsive to MDP[41-43], removal of the LRR domain renders NLRs auto-active[31,44-45], and a domain-swapping experiment between NLRs showed that ligand preference is determined by the LRR[46], the LRR domain is thought to be responsible for ligand binding. Homology modeling to map loss-of-function mutations in the NOD1 and NOD2 LRR domains showed that most of these mutations cluster to form a single patch on the concave side, suggesting but not proving a role in ligand binding for this region[46-48].

One early study failed to find an interaction between resin-bound MDP and NOD2 in cell lysates[49]. However, in this study MDP

was conjugated to sepharose via atoms that were later shown to be essential for NOD2 activation[50]; thus the lack of binding may be related to steric hindrance. The first study that indicated direct binding does occur was performed by Faustin et al.[11], who showed that reconstitution of a GST-NLRP1 inflammasome *in vitro* was greatly enhanced in the presence of MDP and ATP.

The recent developments in the ability to purify small amounts of NLRs also enabled *in vitro* studies on the interaction between NLRs and their ligands. Biochemical studies on the isolated LRR domain of NLRX1 give a strong indication for direct association with its ligands dsRNA and ssRNA, and its structure revealed a positive patch that was suggested to be involved in RNA binding[51]. Recently, it was shown by surface plasmon resonance and atomic force microscopy that purified NOD1 directly binds its ligand iE-DAP in an LRR-dependent way[52], and that this interaction induces NOD1 oligomerization[27]. Purified NOD2 appears to associate directly with MDP, and the presence of both ATPγS and MDP induces NOD2 homo-oligomerization[28-29]. Surprisingly, the study performed by Mo et al. suggested that the binding site for MDP resides within the NACHT domain[28]. The integrity of the purified protein and setup of the experiments used for these studies on NOD1 and NOD2 is, however, debated[53].

Our work provided the first evidence of direct interaction between the highly conserved D0 domain of *Salmonella* flagellin and murine NAIP5[54]. This is in agreement with the observation that the family of NAIP proteins determines the specificity of NLRC4-containing inflammasomes[55-56]. On the basis of structural and sequential homology between the D0 domain and the ligands that induce other NLRC4-containing inflammasomes[55-57], as well as the high conservation between NAIPs (>80% overall sequence identity), we hypothesize that formation of other NAIP/NLRC4 inflammasomes is likewise dependent on the direct interaction between the NAIP family member and the ligand, and that this interaction induces NAIP to recruit multiple molecules of NLRC4 into a hetero-oligomeric inflammasome.

Although these studies on purified NLRs favor a mechanism in which NLRs get activated by direct interaction with their specific ligand, the increasing number of NLR binding partners, ligands, and signaling pathways that involve NLRs suggest that the reality may be more complex. For instance, NLRP1 appears to be a general sensor for cellular stress caused by viral infection[58], and NOD2 also responds to viral ssRNA and dsRNA, which results in a downstream signaling pathway distinct from activation by MDP[22]. If different agonists can induce distinct signaling pathways via a single NLR, it is very likely that regulators are involved that determine the specificity and outcome of ligand recognition.

NLRP3 is notorious for responding to a wide variety of molecules (reviewed in refs. 59-62). It was suggested that NLRP3 must respond to a common endogenous cellular mechanism that is induced by the presence of these signals[63-64]. In recent years it has been described that several of the NLRP3 ligands induce the release of TXNIP from mitochondria, whereas others induce phosphorylation of double-stranded RNA-dependent protein kinase (PKR). Both TXNIP and PKR in turn bind NLRP3 and enhance formation of the NLRP3 inflammasome[65-66]. NLRP3 thus appears to function as secondary sensor that monitors danger signals. In a similar way, many plant R-proteins appear to be activated by microbe-induced alterations in endogenous proteins[67]. In the model that we propose for the formation of the NAIP5/NLRC4 inflammasome (chapter 3), NLRC4 does not associate with a microbial ligand itself but, instead, binds ligand-activated NAIP5 as

well as activated NLRC4. It may thus serve as a 'danger' receptor that recognizes and responds to a conformational change in these NLRs. It is still unclear whether other NLRs employ a similar indirect response to microbial invasion.

Hetero-oligomeric inflammasome formation

A central topic of this thesis is the formation and structure of the hetero-oligomeric NAIP5/NLRC4 inflammasome. Shortly after the discovery of NLRs, their central NACHT domain was proposed to be the region that mediates NLR self-association, essential for their functionality, as was also seen in the homologous apoptosome forming proteins Apaf-1 and CED-4[68]. For several of the NLRs it has by now been shown that they are able to homo-oligomerize via their NACHT domain. We find that NAIP5, despite the presence of a NACHT domain, does not homo-oligomerize, but instead recruits NLRC4 to form a caspase-1 activating hetero-oligomeric inflammasome (chapter 3). Heterotypic interaction between NLR NACHT domains has been observed as early as in 2004[69]. In this study, overexpressed NLRC4 was reported to inhibit NF-κB activation by associating via its NACHT domain with NOD2. Notably, the expression level observed for NLRC4 in this study was four times higher than that of NOD2. In chapter 3 we reported that co-expression of flagellin with NLRC4 leads to reduced NLRC4 expression levels. As the expression level of NOD2 in the absence of NLRC4 was not assessed, NLRC4 overexpression may have reduced NOD2 expression levels in this study, which could explain at least in part the reported inhibitory effect. In recent years, interference between NLR signaling pathways has also been observed in the endogenous context of immune cells: the NLRPs 2, 4, 6, 7, 10, and 12 appear to play a role not only in caspase-1 activation by the formation of a homo-oligomeric inflammasome, but are also capable of inhibiting the NF-κB pathway[70-72]. Whether this inhibition occurs via interaction with NOD1 and NOD2 remains to be investigated. It will be particularly interesting to see whether inhibitory interaction induces the formation of a large oligomeric complex similar to the inflammasome but incapable of signaling or, in contrast, the inhibitory effect is exerted by preventing multimerization.

In contrast to inhibitory effects, several NLRs have been found to employ hetero-oligomeric inflammasome formation to enhance their response. For instance, NLRP10, which in general is an inflammasome inhibitor, has been reported to enhance the effect of NOD1 activation[73]. NLRP1, which is capable of forming a homo-oligomeric inflammasome *in vitro* in response to MDP[11], was shown to form a complex with NOD2 in macrophages upon MDP stimulation, and exhibited decreased caspase-1 activation in a NOD2 knockout cell line[74].

The ability to form hetero-oligomeric inflammasomes is also exploited by pathogens to avoid immune detection. Kaposi's sarcoma-associated herpesvirus expresses the protein Orf63, a homolog of NLRP1. This protein interacts with NLRP1, NLRP3, and NOD2, and negatively regulates NLRP1 and NLRP3 inflammasomes, thus preventing death of the host cell and promoting viral persistence[75].

Little is currently known of how these various hetero-oligomeric inflammasomes are formed and how each NLR chooses its partner. It will be interesting to see whether other hetero-oligomeric inflammasomes also exhibit NACHT-NACHT interaction, as appears to be the case for the NAIP5/NLRC4 inflammasome (chapter 3-4). In this respect, it is interesting to note that

the NACHT domains of NLRC4 and NAIP5 are sequentially more related to each other than to other NLR family members[47]. Possibly, their ability to collaborate is related to common ancestry. Certain is that the ability of NLRs to associate with various family members adds another layer to the complexity of understanding the regulation of NLR activation.

Towards a structure based mechanism of inflammasome formation

Shortly before the completion of the manuscript for this thesis, the first NLR crystal structure appeared, namely that of the auto-inhibited conformation of CARD-deleted murine NLRC4[76]. The protein was produced in Sf21 cells, and the best crystals were obtained only after removal of a variable region (22 residues) at the start of the LRR domain. Most features of the NLRC4 structure are in accordance with what could be inferred from the structures of apoptosome forming proteins. The NACHT subdomains NBD (nucleotide binding domain), HD1 (helical domain 1), and WHD (winged helix domain) display a fold similar to the corresponding domains in Apaf-1 and CED-4, and, like in Apaf-1, an ADP molecule is coordinated by these three subdomains. The NACHT associated domain (NAD), which was predicted to be α-helical, indeed comprises six α-helices. This domain, also referred to as helical domain 2 (HD2), appears to have an essential role in stabilizing the dormant conformation through extensive interaction with the LRR domain, the WHD, and the NBD. Apart from its association with HD2, the LRR domain also contributes to stabilization of the dormant conformation by covering the interface of the NBD that is expected to interact with a neighboring NBD in the inflammasome. This mechanism of inhibition is similar to the way in which the WD40 domain in Apaf-1 stabilizes the inactive conformation by interacting with the NBD[77].

The model for inflammasome-incorporated NLRC4 that we constructed on the basis of cryo-EM studies on NAIP5-PKG/NLRC4 complexes (chapter 4) serves as a first insight into the mechanism of inflammasome formation. This model confirms that activation involves a rotation of the LRR away from the NBD to expose the multimerization interface. Notably, the arrangement of the NACHT subdomains in dormant NLRC4 is more similar to their arrangement in active than in inactive Apaf-1. This supports the conclusion based on our model that conformational changes in NLRC4 are less dramatic than those occurring during apoptosome formation. Interestingly, whereas one face of the NBD that interacts with a neighboring protomer in our model is covered by the LRR domain in dormant NLRC4, the surface for interaction with the other neighbor is available (Figure 5B in chapter 4). The NACHT N-terminus, which connects to the CARD, is located near the LRR C-terminus in the crystal structure of CARD-deleted NLRC4, far away from the exposed multimerization interface of the NBD (Figure 5A in chapter 4), suggesting that the CARD domain does not block this interface in the dormant conformation of the full length structure. In principle therefore, activated NLRC4 would be able to associate with an inactive monomer and induce the (relatively small) conformational change necessary for its incorporation into an NLRC4 complex. This mechanism is in agreement with the observation that NLRC4 is prone to self-association in the absence of a ligand, and would explain how incorporation of NLRC4 into a NAIP5/NLRC4 inflammasome without direct interaction with the bacterial ligand as proposed in chapter 3 is possible. However, this

mechanism is highly speculative.
Our model of a helical inflammasome was obtained from studying the rod-like NAIP5-PKG/NLRC4 complexes. This raises the question of what the native inflammasome looks like. In chapter 4 we argue that in the biologically relevant particle the effector binding domains must be sufficiently exposed for recruitment of downstream signaling partners, and therefore likely resembles or is identical to the smaller NAIP5/NLRC4 complexes that we purified from HEK293E cells. On the basis of our initial EM studies employing negative stain we suggested these complexes to be a flat disk-like particle, reminiscent of the apoptosome, albeit larger (chapter 3). Subsequent studies by cryo-electron tomography revealed these particles to be a heterogeneous mixture of various shapes and sizes, suggesting that both helical and disk-like NAIP5/NLRC4 inflammasomes may exist. A low resolution EM image of the NLRP1 inflammasome suggested that it is arranged in rings comprising either 5 or 7 protomers[11]. The differences between our NAIP5/NLRC4 complexes, the NLRP1 inflammasomes, and apoptosomes taken together imply that NACHT domains, despite their overall similarity, differ in the way they interact with neighboring molecules in the oligomeric complexes. Future structural studies may reveal how these different arrangements arise and may further our understanding of how each NLR displays unique properties in inflammasome formation.

Concluding remarks

The fact that the members of the NLR protein family are so similar and yet respond to such diverse ligands whilst participating in a variety of signaling pathways makes them an intriguing, if highly challenging, protein family to study. Recent data has only increased the complexity of understanding the role of NLRs. Instead of being the signal hubs that detect a signal and pass on a uniform message that they were originally considered to be, NLRs appear to be complex sensors that can detect multiple signals and, depending on their interaction partners, send out different signals. Additionally, results obtained from studies on different NLR family members are sometimes contradictory, suggesting that a mechanism that is true for one NLR may not necessarily apply for the others.
NLR activation should be under tight control to prevent detrimental effects to the cell. The increasing number of binding partners that is identified may serve an important role in regulating nodosome and inflammasome formation. Functions of these interaction partners include preventing inappropriate activation by maintaining the protein in its inactive conformation, regulating the sensitivity and selectivity of the NLR to its ligand, and selecting the downstream signaling pathway that is employed. In addition, the cooperation between different NLRs by hetero-oligomeric inflammasome formation may prove to be another important mechanism for regulating the activity and versatility of NLR activation.
As yet, many aspects related to NLR activation remain poorly understood. This work contributed to answering some of the intriguing questions in the NLR field by providing the first insight into their ability of direct ligand binding and into the structure and formation of a hetero-oligomeric inflammasome. However, many questions related to the activation mechanism of NLRs, and the differences that cause specificity of each family member, are yet to be answered. The tools that we developed during our studies, such as a straightforward method to improve NLR expression and purification,

in vivo formation of a hetero-oligomeric inflammasome, and its purification fur further *in vitro* characterization and structural analysis, may serve others in advancing the understanding of structural and functional aspects of NLR activation.

References

1. Chen, G., et al., *NOD-like receptors: role in innate immunity and inflammatory disease.* Annu Rev Pathol, 2009. **4**: p. 365-98.
2. Fritz, J.H., et al., *Nod-like proteins in immunity, inflammation and disease.* Nat Immunol, 2006. **7**(12): p. 1250-7.
3. Philpott, D.J. and S.E. Girardin, *The role of Toll-like receptors and Nod proteins in bacterial infection.* Mol Immunol, 2004. **41**(11): p. 1099-108.
4. Dostert, C., et al., *Innate immune activation through Nalp3 inflammasome sensing of asbestos and silica.* Science, 2008. **320**(5876): p. 674-7.
5. Dinarello, C.A., *Interleukin-1 beta, interleukin-18, and the interleukin-1 beta converting enzyme.* Ann N Y Acad Sci, 1998. **856**: p. 1-11.
6. Bergsbaken, T., S.L. Fink, and B.T. Cookson, *Pyroptosis: host cell death and inflammation.* Nat Rev Microbiol, 2009. **7**(2): p. 99-109.
7. Rosenstiel, P., A. Till, and S. Schreiber, *NOD-like receptors and human diseases.* Microbes Infect, 2007. **9**(5): p. 648-57.
8. Tattoli, I., et al., *The Nodosome: Nod1 and Nod2 control bacterial infections and inflammation.* Semin Immunopathol, 2007. **29**(3): p. 289-301.
9. Schroder, K. and J. Tschopp, *The inflammasomes.* Cell, 2010. **140**(6): p. 821-32.
10. Martinon, F., K. Burns, and J. Tschopp, *The inflammasome: a molecular platform triggering activation of inflammatory caspases and processing of proIL-beta.* Mol Cell, 2002. **10**(2): p. 417-26.
11. Faustin, B., et al., *Reconstituted NALP1 inflammasome reveals two-step mechanism of caspase-1 activation.* Mol Cell, 2007. **25**(5): p. 713-24.
12. Lukasik, E. and F.L. Takken, *STANDing strong, resistance proteins instigators of plant defence.* Curr Opin Plant Biol, 2009.
13. Chinnaiyan, A.M., et al., *Role of CED-4 in the activation of CED-3.* Nature, 1997. **388**(6644): p. 728-9.
14. Zou, H., et al., *Apaf-1, a human protein homologous to C. elegans CED-4, participates in cytochrome c-dependent activation of caspase-3.* Cell, 1997. **90**(3): p. 405-13.
15. Kanuka, H., et al., *Control of the cell death pathway by Dapaf-1, a Drosophila Apaf-1/CED-4-related caspase activator.* Mol Cell, 1999. **4**(5): p. 757-69.
16. Qi, S., et al., *Crystal structure of the Caenorhabditis elegans apoptosome reveals an octameric assembly of CED-4.* Cell, 2010. **141**(3): p. 446-57.
17. Yuan, S., et al., *Structure of an apoptosome-procaspase-9 CARD complex.* Structure, 2010. **18**(5): p. 571-83.
18. Acehan, D., et al., *Three-dimensional structure of the apoptosome: implications for assembly, procaspase-9 binding, and activation.* Mol Cell, 2002. **9**(2): p. 423-32.
19. Yu, X., et al., *Three-dimensional structure of a double apoptosome formed by the Drosophila Apaf-1 related killer.* J Mol Biol, 2006. **355**(3): p. 577-89.
20. Travassos, L.H., et al., *Nod proteins link bacterial sensing and autophagy.* Autophagy, 2010. **6**(3).
21. Ting, J.P., J.A. Duncan, and Y. Lei, *How the noninflammasome NLRs function in the innate immune system.* Science, 2010. **327**(5963): p. 286-90.
22. Murray, P.J., *Beyond peptidoglycan for Nod2.* Nat Immunol, 2009. **10**(10): p. 1053-4.
23. Coussens, N.P., et al., *Crystal structure of the Nod1 caspase activation and recruitment domain.* Biochem Biophys Res Commun, 2007. **353**(1): p. 1-5.
24. Fridh, V. and K. Rittinger, *The Tandem CARDs of NOD2: Intramolecular Interactions and Recognition of RIP2.* PLoS One, 2012. **7**(3): p. e34375.
25. Eibl, C., et al., *Structural and functional*

analysis of the NLRP4 pyrin domain. Biochemistry, 2012. **51**(37): p. 7330-41.
26. Duncan, J.A., et al., *Cryopyrin/NALP3 binds ATP/dATP, is an ATPase, and requires ATP binding to mediate inflammatory signaling.* Proc Natl Acad Sci U S A, 2007. **104**(19): p. 8041-6.
27. Askari, N., et al., *Expression, purification, and characterization of recombinant NOD1 (NLRC1): A NLR family member.* J Biotechnol, 2011.
28. Mo, J.Y., et al., *Pathogen sensing by nucleotide-binding oligomerization domain-containing protein 2 (NOD2) is mediated by direct binding to muramyl dipeptide and ATP.* J Biol Chem, 2012.
29. Grimes, C.L., et al., *The innate immune protein Nod2 binds directly to MDP, a bacterial cell wall fragment.* J Am Chem Soc, 2012. **134**(33): p. 13535-7.
30. Qu, Y., et al., *Phosphorylation of NLRC4 is critical for inflammasome activation.* Nature, 2012.
31. Ogura, Y., et al., *Nod2, a Nod1/Apaf-1 family member that is restricted to monocytes and activates NF-kappaB.* J Biol Chem, 2001. **276**(7): p. 4812-8.
32. Tameling, W.I., *A One-Step Affinity-Purification Protocol to Purify NB-LRR Immune Receptors from Plants That Mediate Resistance to Fungal Pathogens.* Methods Mol Biol, 2012. **835**: p. 585-90.
33. Kadota, Y., K. Shirasu, and R. Guerois, *NLR sensors meet at the SGT1-HSP90 crossroad.* Trends Biochem Sci, 2010.
34. Mayor, A., et al., *A crucial function of SGT1 and HSP90 in inflammasome activity links mammalian and plant innate immune responses.* Nat Immunol, 2007. **8**(5): p. 497-503.
35. da Silva Correia, J., et al., *SGT1 is essential for Nod1 activation.* Proc Natl Acad Sci U S A, 2007. **104**(16): p. 6764-9.
36. Lee, K.H., et al., *Proteasomal degradation of Nod2 mediates tolerance to bacterial cell wall components.* J Biol Chem, 2012.
37. Bruey, J.M., et al., *Bcl-2 and Bcl-XL regulate proinflammatory caspase-1 activation by interaction with NALP1.* Cell, 2007. **129**(1): p. 45-56.
38. Yeretssian, G., et al., *Non-apoptotic role of BID in inflammation and innate immunity.* Nature, 2011. **474**(7349): p. 96-9.
39. Chinnaiyan, A.M., et al., *Interaction of CED-4 with CED-3 and CED-9: a molecular framework for cell death.* Science, 1997. **275**(5303): p. 1122-6.
40. Yan, N., et al., *Structure of the CED-4-CED-9 complex provides insights into programmed cell death in Caenorhabditis elegans.* Nature, 2005. **437**(7060): p. 831-7.
41. Albrecht, M., et al., *Structural localization of disease-associated sequence variations in the NACHT and LRR domains of PYPAF1 and NOD2.* FEBS Lett, 2003. **554**(3): p. 520-8.
42. Hugot, J.P., et al., *Association of NOD2 leucine-rich repeat variants with susceptibility to Crohn's disease.* Nature, 2001. **411**(6837): p. 599-603.
43. Inohara, N., et al., *Host recognition of bacterial muramyl dipeptide mediated through NOD2. Implications for Crohn's disease.* J Biol Chem, 2003. **278**(8): p. 5509-12.
44. Chamaillard, M., et al., *An essential role for NOD1 in host recognition of bacterial peptidoglycan containing diaminopimelic acid.* Nat Immunol, 2003. **4**(7): p. 702-7.
45. Poyet, J.L., et al., *Identification of Ipaf, a human caspase-1-activating protein related to Apaf-1.* J Biol Chem, 2001. **276**(30): p. 28309-13.
46. Girardin, S.E., et al., *Identification of the critical residues involved in peptidoglycan detection by Nod1.* J Biol Chem, 2005. **280**(46): p. 38648-56.
47. Proell, M., et al., *The Nod-like receptor (NLR) family: a tale of similarities and differences.* PLoS One, 2008. **3**(4): p. e2119.
48. Tanabe, T., et al., *Regulatory regions and critical residues of NOD2 involved in muramyl dipeptide recognition.* Embo J, 2004. **23**(7): p. 1587-97.
49. Chen, D., et al., *Surface calreticulin mediates muramyl dipeptide-induced apoptosis in RK13 cells.* J Biol Chem, 2005. **280**(23): p. 22425-36.
50. Coulombe, F., et al., *Increased NOD2-mediated recognition of N-glycolyl muramyl dipeptide.* J Exp Med, 2009.
51. Hong, M., S.I. Yoon, and I.A. Wilson, *Structure and Functional Characterization of the RNA-Binding Element of the NLRX1*

Innate Immune Modulator. Immunity, 2012. **36**(3): p. 337-47.
52. Laroui, H., et al., *L-Ala-g-D-Glu-meso-DAP interacts directly with the leucine-rich region domain of nucleotide-binding oligomerization domain 1, increasing the phosphorylation activity of receptor-interacting serine/threonine-protein kinase 2 and its interaction with nucleotide-binding oligomerization domain 1.* J Biol Chem, 2011.
53. Monie, T.P., *NLR activation takes a direct route.* Trends Biochem Sci, 2013.
54. Halff, E.F., et al., *Formation and structure of a NAIP5-NLRC4 inflammasome induced by direct interactions with conserved N- and C-terminal regions of flagellin.* J Biol Chem, 2012.
55. Kofoed, E.M. and R.E. Vance, *Innate immune recognition of bacterial ligands by NAIPs determines inflammasome specificity.* Nature, 2011.
56. Zhao, Y., et al., *The NLRC4 inflammasome receptors for bacterial flagellin and type III secretion apparatus.* Nature, 2011. **477**(7366): p. 596-600.
57. Miao, E.A., et al., *Innate immune detection of the type III secretion apparatus through the NLRC4 inflammasome.* Proc Natl Acad Sci U S A, 2010. **107**(7): p. 3076-80.
58. Masters, S.L., et al., *NLRP1 Inflammasome Activation Induces Pyroptosis of Hematopoietic Progenitor Cells.* Immunity, 2012. **37**(6): p. 1009-23.
59. Benko, S., D.J. Philpott, and S.E. Girardin, *The microbial and danger signals that activate Nod-like receptors.* Cytokine, 2008. **43**(3): p. 368-73.
60. Schroder, K., R. Zhou, and J. Tschopp, *The NLRP3 inflammasome: a sensor for metabolic danger?* Science, 2010. **327**(5963): p. 296-300.
61. Franchi, L., R. Munoz-Planillo, and G. Nunez, *Sensing and reacting to microbes through the inflammasomes.* Nat Immunol, 2012. **13**(4): p. 325-32.
62. Davis, B.K., H. Wen, and J.P. Ting, *The Inflammasome NLRs in Immunity, Inflammation, and Associated Diseases.* Annu Rev Immunol, 2010.
63. Vladimer, G.I., et al., *Inflammasomes and host defenses against bacterial infections.* Curr Opin Microbiol, 2013.
64. Leemans, J.C., S.L. Cassel, and F.S. Sutterwala, *Sensing damage by the NLRP3 inflammasome.* Immunol Rev, 2011. **243**(1): p. 152-62.
65. Zhou, R., et al., *Thioredoxin-interacting protein links oxidative stress to inflammasome activation.* Nat Immunol, 2010. **11**(2): p. 136-40.
66. Lu, B., et al., *Novel role of PKR in inflammasome activation and HMGB1 release.* Nature, 2012.
67. DeYoung, B.J. and R.W. Innes, *Plant NBS-LRR proteins in pathogen sensing and host defense.* Nat Immunol, 2006. **7**(12): p. 1243-9.
68. Inohara, N. and G. Nunez, *The NOD: a signaling module that regulates apoptosis and host defense against pathogens.* Oncogene, 2001. **20**(44): p. 6473-81.
69. Damiano, J.S., et al., *Heterotypic interactions among NACHT domains: implications for regulation of innate immune responses.* Biochem J, 2004. **381**(Pt 1): p. 213-9.
70. Kufer, T.A. and P.J. Sansonetti, *NLR functions beyond pathogen recognition.* Nat Immunol, 2011. **12**(2): p. 121-8.
71. Damm, A., K. Lautz, and T.A. Kufer, *NLRP10 roles in innate and adaptive immunity.* Microbes Infect, 2013.
72. Ng, T.M., J. Kortmann, and D.M. Monack, *Policing the cytosol-bacterial-sensing inflammasome receptors and pathways.* Curr Opin Immunol, 2012.
73. Lautz, K., et al., *NLRP10 enhances Shigella-induced pro-inflammatory responses.* Cell Microbiol, 2012.
74. Hsu, L.C., et al., *A NOD2-NALP1 complex mediates caspase-1-dependent IL-1beta secretion in response to Bacillus anthracis infection and muramyl dipeptide.* Proc Natl Acad Sci U S A, 2008. **105**(22): p. 7803-8.
75. Gregory, S.M., et al., *Discovery of a viral NLR homolog that inhibits the inflammasome.* Science, 2011. **331**(6015): p. 330-4.
76. Hu, Z., et al., *Crystal Structure of NLRC4 Reveals Its Autoinhibition Mechanism.* Science, 2013.
77. Reubold, T.F., S. Wohlgemuth, and S. Eschenburg, *Crystal structure of full-length Apaf-1: how the death signal is relayed in the mitochondrial pathway of apoptosis.* Structure, 2011. **19**(8): p. 1074-83.

Summary

Our immune system faces the constant challenge of having to combat pathogens, such as bacteria and viruses, that have entered our body. To prevent and cure infection it is essential that the immune system is able to discern between potentially harmful invaders and infected cells on the one hand, and on the other hand the body's own molecules, healthy cells, and harmless microflora. Just over ten years ago a new family of proteins, the so-called Nod Like Receptors (NLRs), was discovered. They are located in the cytosol of selected cell types, and play an important role in the ability of the immune system to make this distinction. Some NLRs specifically recognize molecules that are derived from bacteria or viruses that have entered the cell, such as fragments of the bacterial cell wall or viral RNA. Other NLRs notice damage to the cell by recognizing molecules that only occur in damaged but not in healthy cells. An example of these molecules are proteins that leak from mitochondria into the cytosol when the cell is infected.

As soon as the NLR detects the presence of such a danger signal, it causes the cell to either secrete molecules that help the immune system to recognize and clear the infection, or they activate the protein caspase-1 that in turn induces a specific cell death mechanism called pyroptosis. The death and clearance of the infected cell ensures that the infection cannot spread any further. To prevent damage to the body it is essential that activation of NLRs occurs at the right moment. Several chronic disorders such as asthma, rheumatoid arthritis, and Crohn's disease are caused by a defect in NLRs which has the result that they are either not activated during infection, or get activated even in the absence of an invading microorganism. Detailed insight into the activation mechanism of NLRs is therefore important in the search for solutions to these disorders.

The human body contains 22 different NLRs, each specialized in the recognition of one or several specific signals, also called ligands. Upon recognition of these ligands, several activated NLRs of one kind together form a large complex, the inflammasome. This inflammasome induces the signaling route in the cell that eventually leads to cell death or the recruitment of specialized cleaner cells of the immune system. For a long time it has remained unknown how NLRs exactly recognize their ligand and form an inflammasome. The central questions in this thesis therefore are, firstly, whether NLRs recognize their ligand via direct interaction or that recognition requires other proteins as well, and, secondly, how the inflammasome is formed from individual NLRs and what this complex looks like. Specific focus is hereby on the two NLRs called NAIP5 and NLRC4. All taken together, the outcome of our research leads to the formulation of a model for the activation mechanism of NLRs.

In **chapter 1** the role of NLRs in the immune system is described more elaborately and, by comparison to proteins with a similar structure and function as NLRs, a hypothetical model is given for the activation of NLRs. Globally, NLRs comprise three parts, or domains. It is generally assumed that the first domain, the leucine rich repeat domain, is important for the recognition of the ligand. The NACHT domain, sometimes called NOD domain, enables formation of the inflammasome by binding NACHT domains of other activated NLR molecules. The last domain, the effector binding domain, interacts with downstream signaling proteins such as caspase-1. It is thought that during detection, activation, and

multimerization the conformation of these domains with respect to each other, and thus the shape of the protein, changes.

To study conformational changes in NLRs on a molecular level, and to investigate whether NLRs directly interact with their ligand without the interference of other cellular components, we wanted to isolate relatively large quantities of NLR from the cell. To this end we culture cells that, after addition of DNA that codes for a specific NLR, produce a large amount of this particular protein. Like several other researchers also reported, we found that Nod Like Receptors appear to be recalcitrant proteins that are not easily isolated. **Chapter 2** describes how we investigated what goes wrong during the production of NLRs, and how this can be improved. We discovered that, whereas a large amount of NLR protein is produced, the majority of the produced protein aggregates (forms clumps) in the cell, and moreover causes spontaneous cell death, thus making it useless for further study. We developed a novel method in which we replace part of the DNA that codes for the NLR by non-coding DNA, and show that although this significantly reduces the total protein production, the protein that is produced causes less cell death and aggregates less. Thus, with less production you end up with more useful material for further study, both for functional studies in the cell as well as to purify small amounts of NLR for structural investigation. We discovered that for each of the NLRs a different amount of coding DNA was optimal for maximal production of useful protein. Since proteins other than NLRs can potentially also be purified with higher yield using this so-called 'DNA titration method', and since every protein is unique, we present a systematic method that can be used to relatively quickly find the optimal conditions for protein production.

In **chapter 3** this production method is applied in the further investigation of the structure and function of two NLRs, namely NAIP5 and NLRC4, in closer detail. Both of these NLRs are activated by the protein flagellin, which forms the tail of amongst others *Salmonella* and *Legionella* bacteria, and subsequently cause activation of caspase-1. It was, however, unknown whether and how these two NLRs collaborate in the initiation of an immune response. By isolating one of the three proteins from the cell and investigating which of the other proteins co-purify, we show that NAIP5 and NLRC4, in the presence of flagellin, form a single inflammasome that contains both NLRs and induces cell death via caspase-1. A small but important fragment of flagellin, namely the part that prevents the bacterial tail from falling apart, is both indispensible and sufficient for the induction of inflammasome formation. This same fragment of flagellin co-purifies NAIP5 from the cell, suggesting that NAIP5 recognizes flagellin by binding to it directly and subsequently recruits NLRC4. Using purified NAIP5, NLRC4, and flagellin we show that even outside the cell flagellin can cause formation of the NAIP5-NLRC4 inflammasome. Hereby we provide the first evidence that these NLRs recognize their ligand by direct interaction without the requirement of other proteins from the cell. Finally, we studied the structure of the inflammasome by electron microscopy (EM) and show that it contains 11-12 individual NLR molecules. This makes the NAIP5-NLRC4 inflammasome far larger than was expected on the basis of multimers formed by similar proteins.

Since NAIP5 is responsible for the initial recognition of flagellin, and thereby has a special role in NAIP5-NLRC4 inflammasome formation, we investigated further by EM whether NAIP5 is also located on a special position within the inflammasome. The results of this investigation are described in **chapter 4**. In order to discern between both NLRs, we fused NAIP5 to the protein PKG, which resulted in the formation of helical NAIP5-PKG/NLRC4 complexes of variable length. Due to the regular buildup of these multimers we

were able to obtain more detailed insight into the shape of the protein in its activated conformation and to compare this with the dormant form. Our results confirm, at least for NLRC4, the hypothesis that an NLR undergoes conformational rearrangment upon activation, and suggest that this conformational change differs from what was observed in similar proteins.

Finally, **chapter 5** discusses how our results compare to other investigations on NLRs that have been published in recent years, and what our discoveries on a subset of NLRs potentially signify for the insight into the ligand recognition, activation mechanism, and structure of other NLRs and their inflammasomes.

Nederlandse samenvatting

Ons immuunsysteem staat voor de voortdurende uitdaging om ziekteverwekkers, zoals bacteriën en virussen, die ons lichaam binnengedrongen zijn onschadelijk te maken. Om infectie te voorkomen en bestrijden is het essentieel dat het immuunsysteem in staat is om onderscheid te maken tussen potentiële ziekteverwekkers en geïnfecteerde cellen enerzijds, en anderzijds lichaamseigen moleculen, gezonde cellen en onschuldige microflora. Ruim tien jaar geleden is een nieuwe familie van eiwitten ontdekt, de zogenaamde Nod Like Receptors (NLRs, oftewel: Nod gerelateerde receptoren). Deze bevinden zich in het cytosol van diverse celtypes en spelen een belangrijke rol bij het maken van dit onderscheid. Sommige NLRs herkennen moleculen die specifiek afkomstig zijn van bacteriën of virussen die de cel zijn binnengedrongen, zoals fragmenten van de bacteriecelwand of viraal RNA. Andere NLRs merken beschadiging aan de cel op doordat ze moleculen herkennen die alleen voorkomen in beschadigde maar niet in gezonde cellen. Dit zijn bijvoorbeeld eiwitten die uit mitochondriën in het cytosol lekken wanneer de cel geïnfecteerd is.

Zodra Nod receptoren de aanwezigheid van zo'n gevaarsignaal detecteren, zorgen ze dat de cel ofwel moleculen gaat secreteren die het immuunsysteem helpen om de infectie te herkennen en op te ruimen, of activeren ze het eiwit caspase-1 wat op zijn beurt een specifiek celdoodmechanisme, pyroptose genaamd, in gang zet. Celdood en afbraak van de afgestorven cel zorgt ervoor dat de infectie zich niet verder kan verspreiden. Om schade aan het lichaam te voorkomen is het essentieel dat de activatie van NLRs op het juiste moment gebeurt. Een aantal chronische aandoeningen zoals astma, reuma en de ziekte van Crohn wordt veroorzaakt door een defect in NLRs waardoor ze ofwel niet in actie komen tijdens infectie, of juist geactiveerd worden in afwezigheid van een ziekteverwekker. Gedetailleerd inzicht in het activatiemechanisme van NLRs is daarom van belang voor de zoektocht naar oplossingen voor deze ziektes.

Het menselijk lichaam bevat 22 verschillende NLRs die elk gespecialiseerd zijn in de herkenning van één of enkele specifieke signalen, ook wel liganden genoemd. Na herkenning van dit ligand vormen meerdere geactiveerde NLRs van één soort samen een groot complex, het inflammasoom. Dit inflammasoom brengt vervolgens de signaleringsroute op gang die uiteindelijk leidt tot celdood of de inschakeling van gespecialiseerde schoonmaakcellen van het immuunsysteem. Het is lang onbekend geweest hoe NLRs hun ligand precies herkennen en hoe ze vervolgens een inflammasoom vormen. De centrale vragen van dit proefschrift zijn dan ook ten eerste of NLRs hun ligand herkennen via directe interactie of dat hier nog andere eiwitten bij betrokken zijn, en ten tweede op welke manier het inflammasoom gevormd wordt uit individuele NLRs en hoe dit complex er uitziet. Hierbij wordt specifiek gekeken naar de twee NLRs NAIP5 en NLRC4. Alle resultaten samen leiden uiteindelijk tot de formulering van een model voor het activatiemechanisme van NLRs.

In **hoofdstuk 1** wordt uitgebreider beschreven welke rol NLRs spelen in het immuunsysteem en wordt, aan de hand van wat er bekend is over eiwitten met soortgelijke structuur en functie als NLRs, een hypothetisch model gegeven voor de activatie van NLRs. NLRs zijn globaal genomen opgebouwd uit drie onderdelen, of domeinen. Er wordt algemeen aangenomen dat het eerste domein, het leucine rich repeat domein, van belang is voor de herkenning van het ligand. Het NACHT domein, ook wel NOD domein genoemd, zorgt voor

inflammasoomvorming doordat het bindt aan het NACHT domein van andere geactiveerde NLR moleculen. Het laatste domein, het effector bindend domein, gaat interactie aan met downstream signaaleiwitten zoals caspase-1. Er wordt gedacht dat tijdens de stappen van detectie, activatie en multimerisatie de conformatie van deze domeinen ten opzichte van elkaar, en daarmee de vorm van het eiwit, verandert.

Om conformatieveranderingen in NLRs op moleculair niveau te bestuderen, en om te onderzoeken of NLRs directe interactie aangaan met hun ligand zonder daarbij gehinderd te worden door andere componenten uit de cel, wilden we relatief grote hoeveelheden NLRs uit cellen isoleren. Hiervoor kweken we cellen die, na toevoeging van DNA wat voor een specifieke NLR codeert, een grote hoeveelheid van het betreffende eiwit aanmaken. Zoals enkele andere onderzoekers ook al beschreven, kwamen we erachter dat Nod receptoren echter recalcitrante eiwitten zijn die zich niet makkelijk laten isoleren. In **hoofdstuk 2** is beschreven hoe we onderzocht hebben wat er misgaat tijdens de productie van NLRs, en hoe dit verbeterd kan worden. We ontdekten dat er weliswaar veel NLR eiwit geproduceerd wordt, maar dat het merendeel hiervan aggregeert (samenklontert) in de cel, en bovendien spontane celdood veroorzaakt, waardoor het niet bruikbaar is voor verdere studie. We ontwikkelden een nieuwe methode waarbij we een deel van het DNA wat voor de NLR codeert vervangen door niet-coderend DNA, en lieten zien dat terwijl hierdoor de totale eiwitproductie sterk vermindert, het eiwit wat geproduceerd wordt minder celdood veroorzaakt en minder aggregeert. Zo hou je dus met minder productie uiteindelijk meer bruikbaar materiaal over om mee te werken, zowel voor functionele studies in de cel als om kleine hoeveelheden NLR te kunnen zuiveren voor structuurgericht onderzoek. We ontdekten dat voor elk van de NLRs een andere hoeveelheid coderend DNA de optimale hoeveelheid bruikbaar eiwit opleverde. Omdat andere eiwitten dan NLRs wellicht ook beter gezuiverd kunnen worden met behulp van deze zogenheten 'DNA titratie methode', en omdat elk eiwit uniek is, presenteren we een systematische manier om relatief snel de optimale condities te vinden voor eiwitproductie.

In **hoofdstuk 3** wordt deze productiemethode toegepast om de structuur en functie van twee van de NLRs, namelijk NAIP5 en NLRC4, nader te onderzoeken. Deze beide NLRs worden geactiveerd door het eiwit flagelline, afkomstig uit de staart van o.a. *Salmonella* en *Legionella* bacteriën, en zorgen vervolgens voor activatie van caspase-1 en celdood. Het was echter onbekend of en hoe deze NLRs samenwerken bij het initiëren van de immuunreactie. Door steeds één van de drie eiwitten uit de cel te isoleren en te bekijken welke van de andere eiwitten meezuivert laten we zien dat NAIP5 en NLRC4 in aanwezigheid van flagelline samen één inflammasoom vormen wat celdood induceert via caspase-1. Een klein maar belangrijk fragment van flagelline, namelijk het gedeelte wat ervoor zorgt dat de bacteriestaart niet uit elkaar valt, is zowel onmisbaar als voldoende om inflammasoomvorming te induceren. Ditzelfde stukje flagelline kan NAIP5 uit de cel meezuiveren, wat suggereert dat NAIP5 flagelline herkent door er direct aan te binden om vervolgens NLRC4 te recruteren. Met behulp van gezuiverd NAIP5, NLRC4 en flagelline laten we zien dat flagelline ook buiten de cel ervoor kan zorgen dat het NAIP5-NLRC4 inflammasoom gevormd wordt, waarmee we voor het eerst aantonen dat deze NLRs hun ligand direct herkennen zonder dat daarvoor andere eiwitten uit de cel nodig zijn. Tenslotte hebben we met behulp van elektronenmicroscopie (EM) de structuur van het inflammasoom bestudeerd en laten we zien dat het bestaat uit 11-12 individuele NLR moleculen. Hiermee is het NAIP5-NLRC4 inflammasoom veel groter dan was verwacht aan de hand van multimeren van soortgelijke eiwitten.

Omdat NAIP5 als eerste flagelline herkent, en daarmee een bijzondere rol speelt in NAIP5-NLRC4 inflammasoomvorming, hebben we met behulp van EM verder onderzocht of NAIP5 ook een specifieke plek binnen het inflammasoom heeft. De resultaten van dit onderzoek zijn beschreven in **hoofdstuk 4**. Om onderscheid te kunnen maken tussen de beide NLRs hebben we NAIP5 aan het eiwit PKG gefuseerd, met als resultaat dat zich in aanwezigheid van flagelline spiraalvormige NAIP5-PKG/NLRC4 complexen van variabele lengte vormden. Dankzij de regelmatige opbouw van deze multimeren waren we in staat om een meer gedetailleerd beeld te krijgen van de vorm van het eiwit in geactiveerde conformatie en dit te vergelijken met de ongeactiveerde vorm. Onze resultaten bevestigen, in elk geval voor NLRC4, de hypothese dat een NLR vormverandering ondergaat tijdens activatie, en suggereren dat deze conformatieverandering anders is dan bij soortgelijke eiwitten.

Tot slot wordt in **hoofdstuk 5** bediscussieerd hoe onze resultaten zich verhouden tot andere onderzoeken aan NLRs die in de afgelopen jaren gepubliceerd zijn, en wat de ontdekkingen die wij aan een subset van NLRs hebben gedaan mogelijk betekenen voor het inzicht in de ligand-herkenning, het activeringsmechanisme en de structuur van andere NLRs en hun inflammasomen.

Dankwoord / Acknowledgements

Obtaining a PhD is something that cannot be accomplished on your own. Looking back on the past six years I count myself blessed for having been surrounded by many helpful, supportive, understanding, patient, and also fun people. I am thankful both for those who motivated me to become a scientist, either by being an inspiring teacher or by encouraging me to keep going even when things weren't running smoothly, as well as for those who managed to keep me away from the lab at times and forget about work for a while.

Eric, bedankt voor je begeleiding in al deze jaren en voor de leerzame en prettige samenwerking. Als ik soms de ongeduldige neiging had om te snel conclusies uit een experiment te willen trekken, leerde ik van jou om goed na te denken over de juiste controles en andere mogelijkheden om de resultaten te interpreteren. Ook van je nauwkeurigheid in het schrijven van artikelen heb ik geleerd hoe belangrijk het is om de tijd te nemen om alles precies goed te formuleren. Piet, we hebben diverse malen dankbaar gebruik gemaakt van jouw talent om knopen te hakken. Bedankt voor je bijdrage aan dit werk door je scherpe blik, je doortastendheid, het meedenken, en het vertrouwen wat je in me gesteld hebt. Christoph, the collaboration with you has been essential for this thesis. Thanks for all the effort you put into it, for the long days (and even nights) of measuring, running calculations, and working on figures, for your patience in explaining me how EM works, and for your humor and positive attitude that made me really enjoy collaborating with you. Roman, ook jij bedankt voor het meedenken, -meten en -interpreteren van de EM data. Arie, dankzij jouw ervaring in eiwitzuivering, en je doorzettingsvermogen daarin, zijn we uiteindelijk toch een heel eind gekomen in het zuiveren van de NLRs en het inflammasoom. Al vond ik het een prima taakverdeling dat jij zuiverde en ik de blots deed, dankzij jou ben ik toch ook over mijn Äkta-fobie heen geholpen. Tevens bedankt voor alle keren dat je me een hart onder de riem hebt gestoken als je doorhad dat ik het even niet meer zag zitten. Harma, ook jij hebt een belangrijke bijdrage aan dit project geleverd. Bedankt voor het meedenken en meeschrijven, je betrokkenheid, al je goede adviezen, en de gezellige babbels. Marian, bedankt voor de ca. 15.396 western blots en minizuiveringen die je voor me hebt gedaan (en die je zelfs nog eens wilde herhalen als ik het plaatje nóg mooier wilde hebben), en voor alle gezelligheid zowel in het lab als daarbuiten, ook nu nog. Eddie, je was een goede aanvulling op het TLR/NLR team; bedankt voor het delen van je ervaring in bioinformatica.

The great atmosphere in the K&S lab, and my roommates in N807, definitely contributed to the fact that I enjoyed going to work. Dennis en Arjen, met jullie als 'PhD-tijdgenoten' heb ik het langste opgetrokken in het lab. We konden frustraties delen, maar ik heb vooral ook veel gelachen met jullie in de buurt. En natuurlijk ook bedankt voor jullie geduldige pogingen om mij te leren squashen. Xiaoguang, I enjoyed chatting with you about science, movies, art, and chinese culture. It was a pleasure to have you as a roommate. Pramod, I'll always have a minute to translate something for you; hope you succeed in finding the perfect job soon. Coen en Stef, ook jullie voegden toe aan de gezelligheid in N807. Xinyi (ook eens kamergenoot geweest), Lucy en Harma, ik heb genoten van de musical-avonden, high-teas, en andere uitjes met jullie. Leuk dat we ook na onze gezamelijke labtijd contact zijn blijven houden! Louris, gelukkig nog een liefhebber op het lab van 'echte' muziek ;), ook

met jou en Marian heb ik gezellige en kwali-tijd doorgebracht zowel binnen als buiten het lab. Bedankt voor die waardevolle momenten! Joke, mijn 'buurvrouw' in het lab, bedankt voor alle opbeurende gesprekjes, gezellige praatjes, de 'labgoodies' die je altijd overal vandaan toverde, en je inzet voor leuke activiteiten met de groep. Tof dat je m'n paranimf wilde zijn en me hiermee ook geholpen hebt in de afronding van mijn tijd bij K&S. Federico, you are always ready to help out or give good advice. Thanks for all the practical help in the lab, for the amazing tiramisu and other Italian treats, and for bringing lots of fun to the lab. Good luck with setting up your own lab in Italy. Peng, will you be the next one to defend? You've definitely been working hard these years and can be proud of the result. Thanks for sharing your culture, food, and for your involvement. Bert, zowel als student als tijdens mijn promotie heb ik veel geleerd van jouw uitgebreide ervaring; bedankt voor al je goede adviezen! Michael and Jin, both of you were a few years ahead of me; thanks for sharing your experience and teaching me new skills. Rachel, it was great fun having you in the lab, and I really enjoyed our horse-riding adventures, especially racing on the beach in 'Western style'. Hopefully we can some day add a dude ranch holiday to that experience! Tom, thanks for sharing your valuable insights during lab meetings, for proofreading some parts of this book, and for useful insights in living in England and English culture. It will be nice to meet up once I also live on that side of the Channel. Deniz, Remco and Matti, glad you guys came back for your PhD; it's been a lot of fun having you around. Deniz, thanks for representing us among the other Bijvoet aio's and the amazing work you did for the video! Robbert and XinXuan, the Masterstudents that didn't return: thanks for your contribution to the good atmosphere in the lab and good luck with your PhDs elsewhere. Margerita, thanks for the useful work you did for the literature thesis. The 'youngest generation' Hedwich, Nadia, and Camilla, thanks for lots of fun and chit-chat in and around the lab. For you as well: good luck with your projects! I'm sure you will all do great. Martin, zoals je ziet is het toch echt mogelijk om een proefschrift bij elkaar te pipetteren. Bedankt voor het delen van je immer verfrissende blik op de Nederlanders met hun Bonuskaarten en andere rare gewoontes; zonder jou waren de koffiepauzes een stuk saaier geweest. Ton en Loes, samen met Martin altijd als eerste aan de koffietafel, bedankt voor jullie bijdrage aan de sfeer in de groep en voor de gesprekken bij de koffie. Pascal, thanks for all the delicious contributions to the coffeebreak and for the fun cake-baking afternoons. Toine, bedankt voor je hulp met al die (voor mij nog altijd) onbegrijpelijk ingewikkelde computerprogramma's. Alle secretaresses van de afgelopen jaren: Marjan, Kaoutar, Cécile en Caroline, bedankt voor alle pennen, labjournaals, enveloppen, declaraties, overige praktische hulp en gezelligheid. Marian, al hebben onze pogingen om de NOD2-MDP interactie te onderzoeken niet veel opgeleverd, het was toch gezellig om met je samen te werken! Roland, Wieger en Lucio, bedankt voor de vele transfecties, vectoren, en goede adviezen. Hebben jullie nog wel genoeg te doen nu ik niet meer minimaal 60 kleine-schaal transfecties per week bestel? ;) Bedankt ook voor de geweldige tijd bij UPE; ik heb er erg van genoten met jullie samen te werken en in die korte tijd een hoop geleerd. Smiriti, gelukkig is 'mijn'plekje binnen UPE bij jou in goede handen; ook jij bedankt voor de gezellige gesprekken tussen de bedrijven door.

I owe a lot of gratitude to my amazing friends and family, most of whom probably still don't have a clue about what I was actually doing with those bacteria and proteins I was always talking about. The time that I spent with all of you has been invaluable and equally important as the actual labwork to make it to the end of my PhD.

Willemieke, Aukje, Christine, Gert Jan en Esther, jullie hebben het van begin tot eind

meegemaakt; Hester, jij bent er wat later bijgekomen, maar ook jouw vriendschap is in de afgelopen jaren heel waardevol geweest. Jullie hebben me al die jaren geweldig gesteund. Bedankt voor alle goede gesprekken, leuke dagjes uit, concerten, avonturen in het bos en op de hei, therapeutische klusdagen, lieve kaartjes, smsjes, mailtjes, gebeden, en begrip als ik niet kon afspreken of toch weer moest afzeggen omdat ik m'n cellen moest voeren. Hanna en Emma, ik heb een toffe tijd gehad met jullie als huisgenoten. Dank voor alle gezelligheid, goede gesprekken, meidenfilms, chocola, en uiteraard heeeel veeeel thee. Lida en Leendert, bedankt voor jullie vriendschap en meedenken en meebidden in de vele uitdagende situaties van de afgelopen jaren. Olu, although we don't get to see each other regularly, I really value our friendship and all the things we can share; whenever we meet it's always as if no time has passed in between. Rio, Benedicta, and Tirza, in these last few years we've been sharing more and more life-events; thanks for the nice dinners, girl-talk, and your valuable friendship. Maryam joon, sepasgozaram ke dooste khubi mesle to dashtam, doosti ke hamishe be janbeye mosbate har etefaghi negah mikone, joda az inke natijeye oon etefagh chi bashe. Farhad, thanks for your support during the challenging start of this project. Guido, Hennie, Veeru, and Janine: it's only once in a while that we get to talk but it is a pleasure knowing you and sharing thoughts on life and science.

Everyone from the CU-team: Ian, Nicole, Catalin, Jethro, Hans-Peter: you guys taught me the meaning and importance of chilling. If it wasn't for you, it might have taken me a long time before I had learned how good it can be to spend a day or even a whole weekend not thinking of work. The same holds for the 'old' CLC group, Timo, Ian, Hester and Dorien, and later also Marjolein and the others from the girl-connect: I enjoyed the many relaxing Sundays of 'just hanging out' with you guys. En natuurlijk de CLC-band niet te vergeten; de bandrepetities waren vaak een prima ontlading aan het eind van de werkdag. Everyone who came and went in the Bible study group in the past years: Dorottya and Izaak, Vito and Santina, Josué, Nicole, Bart Jan, Ubaldo, Edyta, David and Yongking: thanks for a great time, for sharing your experiences and frustrations in getting a PhD, and for sharing life in general, both during our meetings, and with some of you also separately. In het laatste jaar zijn ook Carola, Peter, Frederike en Jiska aan het lijstje toegevoegd van mensen die hebben meegeleefd en ervoor gezorgd hebben dat ik ondanks de drukte ook af en toe iets anders deed dan me in het lab of achter de computer verstoppen; dank jullie wel daarvoor! De familie De Vries: Freek, Jing, Anna, Mayen, Josef en Gerco, bedankt voor jullie hartelijkheid en betrokkenheid.

Annerieke, Eelco en Matthijs, jullie hebben elk op je eigen manier een belangrijke bijdrage aan dit werk gehad. Bedankt voor de vele gezellige en ontspannende momenten, lekkere maaltijden, praktische (klus/verhuis)hulp, en adviezen over de kleine en grote zaken in het leven. Lieve papa en mama, bedankt voor al het meeleven, meedenken, bidden en luisteren, en vooral dat jullie altijd achter me hebben gestaan en zullen staan. Een grotere steun dan dat kan ik me niet bedenken. De laatste loodjes wegen het zwaarst. Lieve Joël, bedankt voor de manier waarop je me in de afgelopen anderhalf jaar steeds weer hebt aangemoedigd en ondersteund, en zo die loodjes hebt helpen dragen; dankzij jou waren ze een stuk lichter. Tot slot ben ik aan niemand meer dank verschuldigd dan aan mijn hemelse Vader, mijn Schepper en reden van zowel mijn bestaan als het bestaan van de wonderlijke wereld waarvan ik het voorrecht heb die te mogen bestuderen.

Curriculum vitae

Els Halff werd op 24 september 1983 geboren in Ede. Hier volgde zij zowel het basisonderwijs als het gymnasium, waar zij *cum laude* voor slaagde. Van 2001 tot 2004 volgde ze de Bacheloropleiding Scheikunde aan de Universiteit Utrecht. Voor haar Bachelorscriptie onderzocht ze de rol van de deubiquitinatie van Eps15 in EGFR internalisatie; dit onderzoek werd uitgevoerd in de vakgroep Cel Biologie van Dr. Paul van Bergen en Henegouwen. Eind 2004 begon ze aan de Masteropleiding Biomoleculaire Wetenschappen, eveneens aan de Universiteit Utrecht. Haar Masterscriptie bestond uit twee onderzoeksprojecten bij de vakgroep Kristal- en Structuurchemie, onder leiding van Prof. Dr. Piet Gros, waar zij eerst werkte aan de optimalisatie van expressie en zuivering van complement eiwitten C2, C8 en perforine, en vervolgens het complex van complement eiwit C3b met de inhibitor compstatine kristalliseerde en de structuur bepaalde. De kortere Masterstage van een half jaar werd in 2007 uitgevoerd aan het Karolinska Instituut in Stockholm, Zweden, onder leiding van Prof. Dr. Nico Dantuma. Hier onderzocht Els de invloed van cel stress, in het bijzonder de misvouwing van eiwitten, op de dynamica van het proteasoom. Zowel de Bachelor- als de Masteropleiding werden *cum laude* afgerond.

In november 2007 begon Els als promovendus bij de vakgroep Kristal- en Structuurchemie, ditmaal onder begeleiding van Dr. Eric Huizinga. Hier bestudeerde zij de functie en structuur van Nod Like Receptors zoals beschreven in dit proefschrift. In de tweede helft van 2012 werd dit onderzoek gecombineerd met een deeltijdaanstelling als wetenschappelijk medewerker bij U-Protein Express BV. Het promotieonderzoek werd in de zomer van 2013 afgesloten. Vanaf januari 2014 zal Els werkzaam zijn als postdoctoraal onderzoeker aan het University College London in de groep van Prof. Josef Kittler.

List of publications

Minde DP, **Halff EF**, Tans SJ, *Designing disorder : Tales of the unexpected tails.* Intrinsically Disordered Proteins, 2013; 1:e26790 (Review; in print)

Halff EF, Diebolder CA, Versteeg M, Schouten A, Brondijk TH, Huizinga EG, *Formation and structure of a NAIP5-NLRC4 inflammasome induced by direct interactions with conserved N- and C-terminal regions of flagellin.* J Biol Chem, 2012. 287(46): p. 38460-72

Verhoef LG, Heinen C, Selivanova A, **Halff EF**, Salomons FA, Dantuma NP, *Minimal length requirement for proteasomal degradation of ubiquitin-dependent substrates.* FASEB J, 2009. 23(1): p. 123-33.

Janssen BJ, **Halff EF**, Lambris JD, Gros P, *Structure of compstatin in complex with complement component C3c reveals a new mechanism of complement inhibition.* J Biol Chem, 2007. 282(40): p. 29241-7

Shortlist of frequently used abbreviations

AAA+	ATPases associated with various cellular activities
Apaf	apoptotic protease activating factor
ASC	apoptosis-associated speck-like protein containing a CARD
BIR	baculoviral inhibitor of apoptosis repeat
BS	Blau syndrome
CARD	caspase activation and recruitment domain
CD	Crohn's disease
CED	*Caenorhabditis elegans* cell-death protein
DAMP	danger associated molecular pattern
Dark	*Drosophila* Apaf-1 related killer
DD	death domain
EBD	effector binding domain
EOS	early onset sarcoidosis
FCAS	familial cold autoinflammatory syndrome
HD1/2	helical domain 1/2
HSP70/90	heat shock protein 70/90
IL	interleukin
LRR	leucine rich repeat
MDP	muramyl dipeptide
MHC-I/II	major histocompatibility complex I/II
MSU	monosodium urate crystals
MWS	Muckle-Wells syndrome
NACHT	NAIP, CIITA, HET-E, and TP-1
NAD	NACHT-associated domain
NAIP	neuronal apoptosis inhibitory protein
NBD	nucleotide binding domain
NLR	Nod-like receptor
NLRC	Nod-like receptor CARD containing
NLRP	Nod-like receptor Pyrin containing
NOD	nucleotide oligomerization domain
NOMID	neonatal onset multisystem inflammatory disease
PAMP	pathogen associated molecular pattern
PKG	cGMP dependent protein kinase I alpha
PRR	pattern recognition receptor
PYD	pyrin domain
RIP2	receptor-interacting protein 2
ROS	reactive oxygen species
R-protein	resistance protein
SGT1	suppressor of G2 allele of SKP1 homolog
STAND	signal transduction ATPases with numerous domains
TLR	Toll-like receptor
TXNIP	thioredoxin-interacting protein
T3/4SS	type III/IV secretion system
WHD	winged-helix domain